BAJECE

e-mail: editor@bajece.com

Balkan Journal of Electrical & Computer Engineering

An International Peer Reviewed, Indexed and Open Access Journal

www.bajece.com

Vol : 4
No : 1
Year : 2016
ISSN : 2147-284X

Sponsored by the

- Istanbul Technical University
- Klaipeda University

This journal is accredited by the Istanbul Technical University subsidy purposes. It is abstracted and indexed in, Index Google Scholarship, the PSCR, DOAJ, Research Bible, Indian Open Access Journals (OAJ), Institutional Repositories (IR), J-Gate (Informatics India), Ulrich's, ResearchGate, International Society of Universal Research in Sciences, DRJI, EyeSource.

Aim & Scope

The journal publishes original papers in the extensive field of Electrical-Electronics and Computer engineering. It accepts contributions which are fundamental for the development of electrical engineering, computer engineering and its applications, including overlaps to physics. Manuscripts on both theoretical and experimental work are welcome. Review articles and letters to the editors are also included.

Application areas include (but are not limited to): Electrical & Electronics Engineering, Computer Engineering, Software Engineering, Biomedical Engineering, Electrical Power Engineering, Control Engineering, Signal and Image Processing, Communications & Networking, Sensors, Actuators, Remote Sensing, Consumer Electronics, Fiber-Optics, Radar and Sonar Systems, Artificial Intelligence and its applications, Expert Systems, Medical Imaging, Biomedical Analysis and its applications, Computer Vision, Pattern Recognition, Robotics, Industrial Automation.

BAJECE

Balkan Journal of Electrical & Computer Engineering

An International Peer Reviewed, Indexed and Open Access Journal

ISSN: 2147- 284X
Vol: 4
No : 1
Year: March 2016

CONTENTS

K.Lenin, B.RavindhranathReddy, and M.Suryakalavathi; Reduction of Real Power Loss by Nature Inspired Algorithm, ……..….. **1-4**

A. Ates, and C. Yeroglu; Online Tuning of Two Degrees of Freedom Fractional Order Control Loops, ……..……..... **5-11**

T. Pala and A.Y. Camurcu; Design of Decision Support System in the Metastatic Colorectal Cancer Data Set and Its Application, ……..…… **12-16**

A. Darwish, I. Morsi, and A. El Zawawi; Complete Combustion Control for a Steam Boiler Plant,..... **17-23**

S. Roy and Dr. P.S. Babu; An Advanced Fault Locating Technique with WAMS based Backup Protection Scheme for Power System with Simultaneous Faults, ……..……. **24-36**

Sridhar. S, K. Uma Rao and Sukrutha Jade; Detection and Classification of Power Quality Disturbances in the Supply to Induction Motor Using Wavelet Transform and Neural Networks, ……. **37-45**

H. Boztoprak; An alternative image quality assessment method for blurred images,…….... **46-50**

BALKAN
JOURNAL OF
ELECTRICAL & COMPUTER ENGINEERING
(An International Peer Reviewed, Indexed and Open Access Journal**)**

Contact
Istanbul Technical University
Department of Electrical Engineering
Ayazaga Campus, Maslak, Istanbul-Turkey

Web: https://www.bajece.com
http://dergipark.ulakbim.gov.tr/bajece/
e-mail: editor@bajece.com

Reduction of Real Power Loss by Nature Inspired Algorithm

K.Lenin, B.RavindhranathReddy, and M.Suryakalavathi

***Abstract*- This paper presents American Buffalo algorithm (AB) to solve reactive power dispatch problem. AB algorithm imitates the American buffalo behaviour and their exploration techniques they utilize in the American forests and grasslands. The American buffalo employs its special intellectual, cooperative and independent approach in its exploration for the optimal path to reach the grassland. This endows it to get results faster than some other exploration agents. Proposed AB algorithm has been verified in standard IEEE 30 bus test system. Simulation results show evidently about the improved performance of the proposed algorithm in reducing the real power loss with control variables within the limits.**

Index Terms— **American buffalo, Optimization, Optimal reactive power, Transmission loss.**

I.INTRODUCTION

UP to now various methodologies have been applied to solve the Optimal Reactive Power problem. The vital aspect of solving Reactive Power problem is to decrease the real power loss. Earlier several types of mathematical approaches like linear programming, gradient method (Alsac et al., 1973; Lee et al., 1985; Monticelli et al., 1987; Deeb et al., 1990; Hobson, 1980; Lee et al., 1993; Mangoli et al., 1993; Canizares et al., 1996) [1-8] has been used to solve the reactive power problem, but they lack in handling the constraints to reach a global optimization solution.

In the following level several types of evolutionary algorithms (Berizzi et al., 2012; Roy et al., 2012; Hu et al., 2010; Eleftherios et al., 2010) [9-12] has been applied to solve the reactive power problem. In this paper American Buffalo (AB) algorithm has been used to solve reactive power problem. American Buffalo algorithm is comprehensible, stout, operative, and proficient however simple to implement.

K. Lenin is with Department of Electrical & Electronics Engineering, Jawaharlal Nehru Technological University Kukatpally, Hyderabad, India (e-mail:gklenin@gmail.com)

B. Ravindhranathreddy is with Department of Electrical & Electronics Eng., Jawaharlal Nehru Tech. University Kukatpally, Hyderabad, India (email:bumanapallibrreddy@yahoo.co.in)

M. Suryakalavathi is with Department of Electrical & Electronics Engineering, Jawaharlal Nehru Technological University Kukatpally, Hyderabad, India (e-mail: munagala12@yahoo.co.in)

It has noble ability in the exploitation and exploration of the search space. Efficiency of Proposed american buffalo (AB) algorithm has been verified by testing it in standard IEEE 30 bus test system. The simulation results reveals about the best performance of proposed algorithm in minimization of real power loss, when compared to other standard reported algorithms.

II.OBJECTIVE FUNCTION

A.Real power loss

The main objective of the reactive power dispatch problem is to reduce the real power loss and can be written in mathematically as follows:

$$F = P_L = \sum_{k\in Nbr} g_k \left(V_i^2 + V_j^2 - 2V_iV_j\cos\theta_{ij}\right) \quad (1)$$

Where F- objective function, P_L – power loss, g_k - conductance of branch, V_i and V_j are voltages at buses i,j, Nbr- total number of transmission lines in power systems.

B. Voltage profile augmentation

To decrease the voltage variation in PQ buses, the objective function (F) can be written mathematically as follows:

$$F = P_L + \omega_v \times VD \quad (2)$$

Where VD - voltage deviation, ω_v- is a weighting factor of voltage deviation.

And the Voltage deviation given by:

$$VD = \sum_{i=1}^{Npq} |V_i - 1| \quad (3)$$

Where N_{pq}- number of load buses.

C. Equality Constraint

The equality constraint of the problem is given as power balance equation as follows:

$$P_G = P_D + P_L \quad (4)$$

Where P_G- total power generation, P_D - total power demand.

D. Inequality Constraints

Upper and lower bounds on the active power of slack bus (Pg), and reactive power of generators (Q_g) are written in mathematically as follows:

$$P_{gslack}^{min} \le P_{gslack} \le P_{gslack}^{max} \quad (5)$$

$$Q_{gi}^{min} \le Q_{gi} \le Q_{gi}^{max}, i \in N_g \quad (6)$$

Upper and lower bounds of the bus voltage magnitudes (V_i) is written by:

$$V_i^{min} \le V_i \le V_i^{max}, i \in N \quad (7)$$

Upper and lower bounds of the transformers tap ratios (T_i) is written by:

$$T_i^{min} \le T_i \le T_i^{max}, i \in N_T \quad (8)$$

Upper and lower bounds of the compensators (Q_c) is written by:

$$Q_c^{min} \le Q_c \le Q_C^{max}, i \in N_C \quad (9)$$

Where N is the total number of buses, N_g is the total number of generators, N_T is the total number of Transformers, N_c is the total number of shunt reactive compensators.

III. American Buffalo Algorithm

American Buffalo (AB) algorithm pretends the vigilant sound and anxiety sound - behaviour of American buffalos in its scavenging endeavours. These vigilant and anxiety are the two elementary sounds of the american buffalos with which they are able to organize themselves to explore for food and guard themselves whenever they are attacked. The anxiety sound is used to rally the buffalos to travel on to explore the search space while the vigilant sound expresses the buffalos to stay on to exploit their environment since it is safe and has sufficient pastures. With these sounds, the buffalos are able to optimize their search for food source (Julius Beneoluchi Odili et al., 2015) [13]. The AB is a population-based algorithm in which individual buffalos work together to solve reactive power problem. Each buffalo within the AB algorithm epitomises an aggregate object containing a number of elements. The American Buffalo algorithm identifies the independent nature of the buffalos and integrates this into the algorithm. This is represented by Equation (10).

$$c_{k+1} = c_k + r_{g1}a_1(lo_{max} - d_k) + r_{g2}a_2(lf_{max} - d_k) \quad (10)$$

Where c_k and d_k represents the exploration and exploitation moves respectively of the kth buffalo (k =1,2,……..N) ; $r_{g1}$and r_{g2} are learning factors; a_1 and a_2 are arbitrary numbers between [0,1]; lo_{max} is the herd's best fitness and lf_{max} *is* the individual buffalo's best one.

In the above equation (10), there is an interface of the numerous buffalos with the prominent (best) buffalo at a specific iteration, a comparison with each buffalos best ever location in relative to the target solution as well as a memory of each animals immediate past location. Depending on the result of the equation (10), the animals move on to explore other locations as expressed in equation (11),

$$d_{k+1} = \lambda(c_k + d_k) \quad (11)$$

Where λ is a unit of time. The algorithm starts by initializing the population of animals through sensible distribution of arbitrary locations to each buffalo within the N-dimensional space. After this, the algorithm modernizes each buffalo's fitness and determines the lf_{max} (individual buffalo's location) and lo_{max} (the herd's best location) in specific iteration in relation to the optimal solution. If the existing fitness is superior to the individual's maximum fitness (lf_{max}), it protects the location vector for the particular buffalo. If the fitness is superior than the herd's overall extreme, it protects it as the herd's maximum (lo_{max}). Lastly it modernizes the buffalo's position and looks at the subsequent buffalo in the population. At this point, if our global best fitness meets our exit criteria, it ends the run and delivers the location vector as the solution to the given problem. Twofold key equations control the movement of buffalos within the search space and these are Equations (10) and (11). The equation (10) provides the decision to either stay on to exploit the environment further or to travel on to search other areas based on the collective intelligence of the herd after intermingling with each other in a communal decision-making process.

The equation (11) pushes the buffalos to travel on to search other areas based on the consequence of (10) after due consideration of the two competing forces (lo_{max}, lf_{max}). The λ parameter which outlines the discrete time interval over which the buffalo must move is usually set to 1.0. The application of these two Equations results in a new location for the buffalos. It should be observed that equation (10) aside from the memory part (c_k), have two other controlling features, namely, the global maximum (lo_{max}) and the individual maximum positions (lf_{max}): each defining the representative influence over the animal's location.

The algorithm subtracts the dimensional element d_k from the maximum vector and then multiplies this by an arbitrary number (a_1,a_2) usually between 0.0 and 0.6 a learning/acceleration parameter (r_{g1}, r_{g2}) .Using the arbitrary numbers between 0.0 and 0.6 has been effective in obtaining fast convergence. It should be emphasized that the arbitrary numbers give an amount of arbitrariness in the path to help the animals move throughout the search space. It does this by arbitrarily giving more or less emphasis to the global (lo_{max}) or individual maximum solutions depending on the need for more exploration or exploitation respectively as the algorithm developments.

AB algorithm for solving reactive power problem.

a. Objective function of the problem
b. Initialization: arbitrarily place buffalos to nodes at the solution space
c. Update the buffalo's fitness values using Equation (10)
d. Update the location of buffalo using equation (11)
e. Is lo_{max} updating if yes, go to next step or else go to b
f. If the ending criterion is not met, then go back to algorithm step c
g. Output finest solution.

IV. Simulation Results

Legitimacy of proposed AB algorithm has been confirmed by testing it in IEEE 30-bus, 41 branch system and it has 6 generator-bus voltage magnitudes, 4 transformer-tap settings, and 2 bus shunt reactive compensators.

Bus 1 is taken as slack bus and 2, 5, 8, 11 and 13 are considered as PV generator buses and others are PQ load buses. Control variables limits are given in Table I. In Table II the power limits of generators buses are enumerated.

TABLE I
PRIME VARIABLE LIMITS (PU)

List of Variables	Minimum	Maximum	Type
Generator Bus	0.95	1.1	Continuous
Load Bus	0.95	1.05	Continuous
Transformer-Tap	0.90	1.1	Discrete
Shunt Reactive Compensator	-0.10	0.30	Discrete

TABLE II
GENERATORS POWER LIMITS

Bus	P_g	$P_g$min	$P_g$max	$Q_g$min
1	96.00	49	200	-19
2	79.00	18	79	-19
5	49.00	14	49	-11
8	21.00	11	31	-14
11	21.00	11	28	-12
13	21.00	11	39	-14

Table III shows the proposed AB methodology efficiently kept the control variables within limits. Table IV list out the overall comparison of the results of optimal solution obtained by various methods. AB is an attempt to develop a user-friendly, effective, efficient, simple-to-application algorithm that will demonstrate exceptional capacity in the exploitation and exploration of the search.

TABLE III
AFTER OPTIMIZATION VALUES OF CONTROL VARIABLES

Control Variables	AB
V1	1.0231
V2	1.0179
V5	1.0186
V8	1.0541
V11	1.0699
V13	1.0387
T4,12	0.00
T6,9	0.01
T6,10	0.90
T28,27	0.91
Q10	0.10
Q24	0.10
Real power loss	4.2879
Voltage deviation	0.9081

TABLE IV COMPARISON OF RESULTS

Techniques	Real power loss (MW)
SGA(Wu et al., 1998) [14]	4.98
PSO(Zhao et al., 2005) [15]	4.9262
LP(Mahadevan et al., 2010) [16]	5.988
EP(Mahadevan et al., 2010) [16]	4.963
CGA(Mahadevan et al., 2010) [16]	4.980
AGA(Mahadevan et al., 2010) [16]	4.926
CLPSO(Mahadevan et al., 2010) [16]	4.7208
HSA (Khazali et al., 2011) [17]	4.7624
BB-BC (Sakthivel et al., 2013) [18]	4.690
Proposed AB	4.2879

V. Conclusion

In this paper, (AB) algorithm has been successfully applied to solve optimal reactive power dispatch problem. Proposed AB algorithm has been verified in the standard IEEE 30 bus system. Simulation results show the vigour of proposed AB algorithm in reducing the real power loss. Detailed comparison of results given in table 4 and our proposed approach outperforms all other reported standard algorithm in reduction of real power loss The control variables obtained after the optimization by (AB) methodology are well within the limits. So by keeping the voltage profile within the stipulated limits the real power loss has been reduced by our projected American Buffalo Algorithm.

References

[1] O. Alsac, and B. Scott, "Optimal load flow with steady state security", IEEE Transaction. Vol.PAS-93, No.3, pp.745-751, 1974.

[2] K.Y. Lee, Y.M. Park, J.L. Oritz, "A united Approach to Optimal Real and Reactive Power Dispatch", IEEE Transactions on power Apparatus and systems, Vol.PAS-104, No.5, pp.1147-1153, 1985.

[3] A.Monticelli , M .V.F Pereira, and S. Granville, "Security constrained optimal power flow with post contingency corrective rescheduling" , IEEE Transactions on Power Systems, Vol.PWRS-2, No.1, pp.175-182,1987.

[4] DeebN ,Shahidehpur S.M ,Linear reactive power optimization in a large power network using the decomposition approach. IEEE Transactions on power system, Vol.5, No.2, pp.428-435, 1990.

[5] E. Hobson,"Network Consrained Reactive Power Control Using Linear Programming", IEEE Transactions on Power Systems, Vol.PAS-99, No.4, pp.868-877, 1980.

[6] K.Y. Lee, Y.M Park, and J.L Oritz, "Fuel –cost optimization for both real and reactive power dispatches", IEE Proc. Vol.131, No.3, pp.85-93, 1984.

[7] M.K. Mangoli, and K.Y. Lee, "Optimal real and reactive power control using linear programming", Electr.Power System Research, Vol.26, No.1, pp.1-10, 1993.

[8] C.A. Canizares, A.C.Z.de Souza and V.H. Quintana, "Comparison of Performance Indices for Detection of Proximity to Voltage Collapse", Vol.11, No.3, pp.1441-1450, Aug 1996 .

[9] A.Berizzi, C. Bovo, M. Merlo, and M. Delfanti, "A GA Approach to Compare orpf Objective Functions Including Secondary Voltage Regulation", Electric Power Systems Research, Vol.84, No.1, pp.187- 194, 2012.

[10] P. Roy, S. Ghoshal, and S. Thakur, "Optimal VAR Control for Improvements in Voltage Profiles and for Real Power Loss Minimization Using Biogeography Based Optimization," International Journal of Electrical Power and Energy Systems, Vol.43, No.1, pp.830-838, 2012.

[11] Z. Hu, X. Wang, and G. Taylor, "Stochastic Optimal Reactive Power Dispatch: Formulation and solution method", International Journal of Electrical Power and Energy Systems, Vol.32, No.6, pp.615-621, 2010.

[12] I.A. Eleftherios, P.S. Georgilakis, M.A. Tsili, G.K. Antonios, "Ant Colony Optimisation Solution to Distribution Transformer Planning Problem", Internationl Journal of Advanced Intelligence Paradigms , Vol.2, No.4 , pp.316-335, 2010.

[13] J.B. Odili, M.N.M. Kahar, "Numerical Function Optimization Solutions Using the African Buffalo Optimization Algorithm", British Journal of Mathematics & Computer Science, Vol.10, No.1, pp.1-12, 2015.

[14] Q.H. Wu, Y.J.Cao, and J.Y. Wen. "Optimal Reactive Power Dispatch Using an Adaptive Genetic Algorithm", International Journal of Elect. Power Energy Systems, Vol.20. pp.563-569, Aug 1998.

[15] B. Zhao, C. X. Guo, and Y.J. CAO, "Multiagent-based Particle Swarm Optimization Approach for Optimal Reactive Power Dispatch", IEEE Trans. Power Syst. Vol.20, No.2, pp.1070-1078, May 2005.

[16] Mahadevan. K, Kannan P. S. "Comprehensive Learning Particle Swarm Optimization for Reactive Power Dispatch", Applied Soft Computing, Vol.10, No.2, pp.641–52, March 2010.

[17] A.H. Khazali, M. Kalantar, "Optimal Reactive Power Dispatch based on Harmony Search Algorithm", Electrical Power and Energy Systems, vol.33, no.3, pp.684-692, March 2011.

[18] S. Sakthivel, M. Gayathri, V. Manimozhi, "A Nature Inspired Optimization Algorithm for Reactive Power Control in a Power System", International Journal of Recent Technology and Engineering (IJRTE) , vol.2, no.1, pp.29-33, March 2013.

BIOGRAPHIES

Kanagasabai Lenin has received his B.E., Degree, electrical and electronics engineering in 1999 from university of madras, Chennai, India and M.E., Degree in power systems in 2000 from Annamalai University, TamilNadu, India. Presently pursuing Ph.D., degree at JNTU, Hyderabad, India.

Bhumanapally RavindhranathReddy, Born on 3rd September, 1969. Got his B.Tech in Electrical & Electronics Engineering from the J.N.T.U. College of Eng., Anantapur in the year 1991. Completed his M. Tech in Energy Systems in IPGSR of J.N.T. University Hyderabad in the year 1997. Obtained his doctoral degree from JNTUA, Anantapur University in the field of Electrical Power Systems. Published 12 Research Papers and presently guiding 6 Ph.D. Scholars. He was specialized in Power Systems, High Voltage Engineering and Control Systems. His research interests include Simulation studies on Transients of different power system equipment.

M. Surya Kalavathi has received her B.Tech. Electrical and Electronics Engineering from SVU, Andhra Pradesh, India and M.Tech, power system operation and control from SVU, Andhra Pradesh, India. she received her Ph.D. Degree from JNTU, Hyderabad and Post doc. From CMU – USA. Currently she is Professor and Head of the electrical and electronics engineering department in JNTU, Hyderabad, India and she has Published 16 Research Papers and presently guiding 5 Ph.D. Scholars. She has specialised in Power Systems, High Voltage Engineering and Control Systems. Her research interests include Simulation studies on Transients of different power system equipment. She has 18 years of experience. She has invited for various lectures in institutes.

Online Tuning of Two Degrees of Freedom Fractional Order Control Loops

A. Ates, and C. Yeroglu

***Abstract*—This paper presents online tuning of Two Degrees of Freedom control loops with fractional order proportional-integral-derivative controller. Since, simultaneous system objectives can be achieved by these types of control loops it can be used for challenging control problems. Thus, five various control loops are reconfigured with fractional order integral and derivative expressions for real time controller tuning problem. Seven parameters of the modified control loops are optimized via stochastic multi parameter divergence optimization algorithm. The optimization algorithm employs good performance for online tuning. The performance of the five various structures are compared using simulation model and real time experimental study on a prototype flight control simulator.**

Index Terms—**Control design, Closed loop systems, Position control, Design optimization, Stochastic processes.**

I. Introduction

ONE Degree of Freedom (1DOF) control configuration generally unable to solve problems of achieving desired system response and sufficient feedback performance simultaneously. Two Degrees of Freedom (2DOF) control loop emerges as a necessary control tool to attain these two simultaneous system objectives. Research on 2DOF control structure reaches back to Horowitzh's study [1]. The major advantage of the 2DOF control structure is that the steady state error to the unit step change of the set-point variable and steady state error to the unit step disturbance become robustly zero [2,3]. Araki and Taguchi have presented important results about 2DOF structure with proportional-integral-derivative (PID) controller for tutorial purpose, including equivalent transformations and various explanations [4]. Many design studies of 2DOF control loop with PID (2DOF-PID) were already studied in the literature [5-7].

Thus, researches on control performance of 2DOF structure are still promising subject. In this respect, a fractional integral and differentiation may increase the possibility of fine tuning on controller parameters that yield better control performance on 2DOF structure [8-11]. Fractional order controllers are used with 2DOF in recent studies [12,13]. Being a keystone study on the fractional order controller researches, Podlubny has proposed Fractional Order PID (FOPID) controller in [14]. Then, many analytical design procedures were studied [15,16]. On the other hand, several numerical tuning methods were also proposed for FOPID controllers tuning [17-19].

Nowadays, Stochastic Multi-parameter Divergence Optimization (SMDO) algorithm has been used as an effective numerical tuning method for FOPID controller tuning [20], [21,22]. The SMDO algorithm may provide effective results for 2DOF with FOPID (2DOF-FOPID) control loops.

In the proposed study, five different types of 2DOF structure, namely FeedBack (FB), Feed-Forward (FF), Component Separated (CS), Set-Point Filter type (SPF) Filter Preceded-Derivative (FPD) types in [3] are modified using FOPID controller. Then, five parameters of the FOPID controller and two parameters of 2DOF control structures were optimized simultaneously using SMDO algorithm for simulation model and real time experimental setup of Twin Rotor MIMO (Multi Input Multi Output) System (TRMS). Then the performances of each 2DOF-FOPID control loops are compared.

The TRMS experimental setup provides a nonlinear and complex helicopter flight control test platform to simulate complex mechanisms of aircrafts [23]. The adaptive control skill based on online controller tuning is required to maintain control performance under the variable conditions found in real-time flight applications. The novelty of the paper lies in introducing SMDO method for 2DOF-FOPID control loop optimization for real time flight control simulator.

Following sections provides two degree of freedom FOPID control structure, brief introduction to the TRMS and SMDO method, simulation and experimental results, respectively.

II. 2DOF Control Structure

2DOF control system in Fig.1 consists of serial compensator $C(s)$ and feedforward compensator $C_f(s)$. Let disturbance input be $P_d(s)$ and plant transfer function be $P(s)$ [2,3]. The closed-loop transfer functions from set point variable (r) to output (y) and form disturbance input (d) to (y) are given, respectively as,

$$G_{yr2} = \frac{P(s)\{C(s)+C_f(s)\}}{1+P(s)C(s)H(s)} \quad (1)$$

$$G_{yd2} = \frac{P_d(s)}{1+P(s)C(s)H(s)} \quad (2)$$

A. ATES and **C. YEROGLU** are with Computer Engineering Department, Inonu University, 44280, Malatya, TURKEY
(e-mail: abdullah.ates@inonu.edu.tr; c.yeroglu@inonu.edu.tr).

It can be shown that the steady-state error to the unit step change of the set point variable $\varepsilon_{r,step}$ and the steady-state error to unit step disturbance, $\varepsilon_{d,step}$ become robustly zero if conditions $\lim_{s\to 0} C(s)=\infty$, $\lim_{s\to 0}\frac{C_f(s)}{C(s)}=0$, $\lim_{s\to 0} H(s)=1$, $\lim_{s\to 0} P(s)\neq 0$, $\lim_{s\to 0}\left|\frac{P_d(s)}{P(s)}\right|<\infty$ are satisfied [2,3].

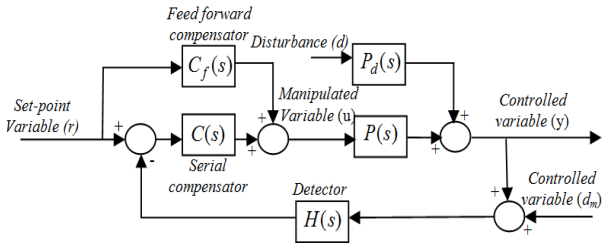

Fig. 1. 2DOF Control Structure

III. 2DOF Fractional Control Loop Optimization

In order to improve system performance, the system sensitivity and transmission function can be realized independently by 2DOF configuration [1]. The performance of the 2DOF control loop can be further improved by using fractional order controller for new control loop design.

Some recent studies present the advantage of the following FOPID controller [14] over conventional PID in control system design,

$$C(s)=PI^{\lambda}D^{\mu}=k_p+\frac{k_i}{s^{\lambda}}+k_d s^{\mu} \tag{3}$$

FOPID controller in Eq. 3 can be used to improve the performance of 2DOF control structure. Motivation of the present study is to improve the performance of 2DOF configuration with FOPID via a recent optimization algorithm. In this study, the fundamental 2DOF structures in [1,3,12] have been modified with FOPID to obtain effective control loops as in Figs. 2-6. Fig. 2 shows that FF type 2DOF-FOPID control loop can be obtained by adding feed forward path to the output of the FOPID control signal.

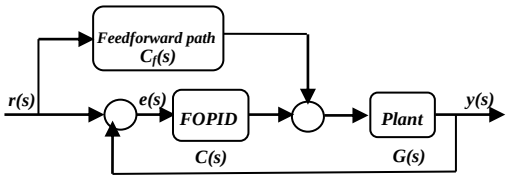

Fig. 2. FF type 2DOF-FOPID Control Structure

One can compute the following transfer function for the feedforward path using proportional and differential parameters of the FOPID controller.

$$C_f(s)=-k_p\alpha-\beta k_d s^{\mu} \tag{4}$$

where, α is the coefficient of the proportional gain $(0<\alpha<1)$, β is coefficient of the differentiation gain $(1<\beta<2)$. Fig. 3 gives FB type 2DOF-FOPID control loop, where C_b is called feedback compensator. Following transfer function for the feedback path can be obtained using proportional and fractional integro-differential parameters of the FOPID controller,

$$C'(s)=(1-\alpha)k_p+\frac{k_i}{s^{\lambda}}+(1-\beta)k_d s^{\mu} \tag{5}$$

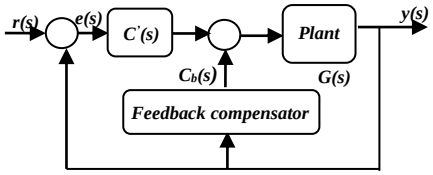

Fig. 3. FB type 2DOF-FOPID Control Structure

The transfer function for the feedback compensator C_b is also computed using proportional and differential parameters as follows,

$$C_b(s)=k_p\alpha+k_d\beta s^{\mu} \tag{6}$$

CS, SPF and FPD type 2DOF PID control loops in [3] is modified using FOPID controller as given in Figs. 4, 5 and 6, respectively. The transfer functions $F_{SPF}(s)$ in Fig. 5 and $F_{FPD}(s)$ in Fig. 6 can be obtained as in Eqs. 7 and 8.

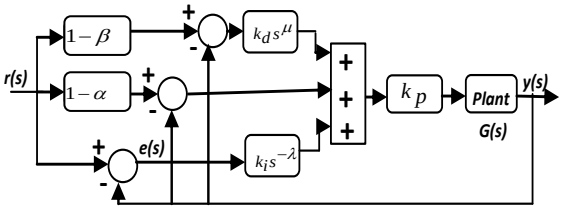

Fig. 4. CS type 2DOF-FOPID Control Structure

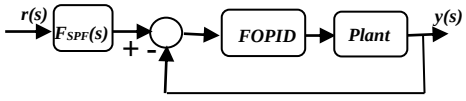

Fig. 5. SPF type 2DOF-FOPID Control Structure

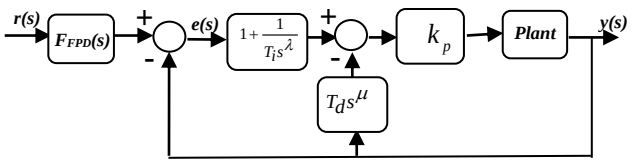

Fig. 6. FPD type 2DOF-FOPID Control Structure

$$F_{SPF}(s)=\frac{1+(1-\alpha)T_i s^{\lambda}+(1-\beta)T_i T_d s^{\mu}}{1+T_i s^{\lambda}+T_i T_d s^{\mu}} \tag{7}$$

$$F_{FPD}(s)=\frac{1+(1-\alpha)T_i s^{\lambda}+(1-\beta)T_i T_d s^{\mu}}{1+T_i s^{\lambda}} \tag{8}$$

Totally, seven parameters of the FF, FB, CS, SPF and FPD type 2DOF-FOPID control loops should be optimized to provide best control performance. However, SMDO emerges as an effective optimization tool to obtain optimum parameters for the proposed control loops in Figs. 2-6. Practical implementation of FOPID controller has some difficulties for realization of the fractional-order derivative and integrator terms. Several methods are used for realization of the FOPID controller in literature [24]. Valerio proposed a non-integer toolbox for realization of the FOPID controller by combining following three approximation methods [25]; i) The Crone, ii) Carlson's and iii) Matsuda's methods can be summarized as following [24,26];

$$C(s) = \tilde{k}\prod_{n=1}^{N}\frac{1+s/w_{zn}}{1+s/w_{pn}} \tag{9}$$

$$C_n(s) = C_{n-1}(s)\frac{\alpha-(1)C_{n-1}{}^{\alpha}(s)+(\alpha+1)g(s)}{(\alpha+1)C^{\alpha}{}_{n-1}+(\alpha-1)g(s)} \tag{10}$$

$$C(s) = a_0 + \frac{s-s_0}{a_1+}\frac{s-s_1}{a_2+}\frac{s-s_2}{a_3+} \tag{11}$$

Thus the Valerio's toolbox benefits from these three methods to implement approximate solutions for FOPID. In this study, we used Valerio's toolbox to implement FOPID in our experimental setup.

Optimal performance of 2DOF-FOPID control loops in Figs. 2-6 can be reached using SMDO algorithm, which can optimize two parameters of the 2DOF structure and five parameters of FOPID controller simultaneously. SMDO algorithm in [20-22] is modified for 2DOF-FOPID control loop.

Let us denote coefficients of the 2DOF-FOPID control loop at time instance $t = nh$ by the vector $X^n = [k_p^n\ k_i^n\ k_d^n\ \lambda^n\ \mu^n \alpha^n \beta^n]$ in a parameter space X. Here, parameters h represent the sampling period of discrete state sampling, and $n = \{1,2,3,...\}$ is the discrete time increment. In order to adapt a 2DOF-FOPID control loop to the system, X^n turns into X^m to satisfy the following adaptation condition,

$$E(X^m) - E(X^n) < 0 \tag{12}$$

where E is a positive real-valued error function that is used to evaluate the performance of the parameter optimization. SMDO uses consecutive set and trial tasks for optimization of parameter vectors. The objective of SMDO is to transform initial X^0 parameter vector to the optimal vector X_{opt}. The optimization ends when the following equation is satisfied,

$$E(X_{opt}) = \min_{X^n \in X_s}\left\{E(X^n)\right\} \tag{13}$$

The pseudo code of the modified SMDO algorithm in Fig. 7 is given to optimize seven parameters of 2DOF-FOPID control loop. Main step of the algorithm is to generate a divergence vector. Let a divergence vector be,

$$\Delta X^n = \varphi_v^n[\Delta k_p^n\ \Delta k_i^n\ \Delta k_d^n\ \Delta\lambda^n\ \Delta\mu^n \Delta\alpha^n \Delta\beta^n] \tag{14}$$

Forward and backward steps can be obtained according to divergence vector. The modified SMDO algorithm can search optimum solution in parameter space.

Components of forward divergence and arithmetic expression to test convenient divergence can be written respectively as,

$$X^{n+1} = X^n + \varphi_v^n[\Delta k_p^n\ \Delta k_i^n\ \Delta k_d^n\ \Delta\lambda^n\ \Delta\mu^n \Delta\alpha^n \Delta\beta^n] \tag{15}$$

$$E(X^n + \Delta X^n) - E(X^n) < 0 \tag{16}$$

Similarly, components of backward divergence and related test expressions can be written respectively as,

$$X^{n+1} = X^n - \varphi_v^n[\Delta k_p^n\ \Delta k_i^n\ \Delta k_d^n\ \Delta\lambda^n\ \Delta\mu^n \Delta\alpha^n \Delta\beta^n] \tag{17}$$

$$E(X^n - \Delta X^n) - E(X^n) < 0 \tag{18}$$

where, φ_v is the divergence rate vector.

```
Start
Parameter Initialization
Starting point:
  If E(X^n) > E_min
Adaptation;Goto Adapted
v = v + 1
    if v > 7
      v = 0
    end
        Compose ΔX^n
Forward test:
    if E(X^n + ΔX^n) − E(X^n) < 0
    X^{n+1} = X^n + ΔX^n
    Go to Starting Point
    end
      Backward test:
    if E(X^n + ΔX^n) − E(X^n) < 0
        X^{n+1} = X^n − ΔX^n
      Go to Starting Point
    end
Go to Starting Point
Adopted
end
 end
```

Fig. 7. Draft code of the SMDO algorithm for tuning 2DOF-FOPID control structure.

IV. 2DOF-FOPID CONTROL LOOP FOR TRMS

This section presents five types of 2DOF-FOPID control loops for simulation and real time models of a TRMS. Performance of the control loops are tested for simulation model, than applied to the real time experimental setup.

A. Twin Rotor MIMO Systems (TRMS)

The TRMS in Fig. 8 is widely used for flight control experiments. TRMS is a two-rotor system that maneuvers by vertical and horizontal rotors. The TRMS control problem is characterized a highly nonlinear multi-input multi-output problem [27-29]. Fig. 8 shows the experimental system developed for 2DOF-FOPID control loop tuning. The vertical and horizontal angle controls were tested in our experiment. The objective of this study is to make the TRMS move accurately and quickly to the desired attitudes and directions, by controlling the horizontal and vertical angles.

Fig. 8. TRMS Experimental Setup

In this paper, a mathematical model of TRMS main pitch rotor was obtained for simulation studies. Firstly multi-sinusoidal signal was applied to TRMS main pitch rotor to obtain relation vector that is between TRMS output and multi-sinusoidal signal. The system run during *100 sec* with *0.1 sec* sampling time. Then the data is transferred to MATLAB "system identification toolbox". Second order mathematical model in Eq. 19 for TRMS main pitch rotor was obtained according to "output error", linear parametric model structure with MATLAB system identification toolbox. This mathematical model is used for TRMS simulation setup.

$$G_{TRMS}(s)\frac{0.06725+1.359}{s^2+0.7906s+3.666} \tag{19}$$

Five different 2DOF-FOPID control loops, namely FF, FB, CS, SPF and FPD types, are used with second order mathematical model of TRMS main rotor in Eq. 19 for the simulation study. The control performances of these control structures are compared to point out the more suitable 2DOF-FOPID control loop. Simulation and experimental result are obtained according to TRMS optimization setup in Fig. 9. Real time experimental study takes initial values from the results of simulation.

B. Simulation Study

The second order mathematical model in Eq. 19 is used to represent TRMS main rotor. FF, FB, CS, SPF and FPD type 2DOF-FOPID control loops in Figs. 2-6 are used in simulation setup in Fig. 9 respectively. The "integer" block in [25] is used to realize fractional order integral and derivative. The parameters of control loops are obtained using SMDO algorithm in Fig. 7. The best cost function for optimum values is obtained during the simulation study by operating the simulation for 15 seconds using ode45 Matlab Simulink Solver with variable-steps [30], for all iterations. The cost function for the SMDO algorithm is defined as,

$$J(\theta)=\min\frac{1}{N}\sum E^2 \tag{20}$$

where E in real valued error function (cost function). Then, seven optimum parameters of FF, FB, CS, SPF and FPD type 2DOF-FOPID control loops are obtained as given in Table 1. Fig. 10 demonstrates the step responses of the system for the proposed FF, FB, CS, SPF and FPD type 2DOF-FOPID control loops in Table 1. The best step response is obtained for FB type 2DOF-FOPID control loop. Figs. 11 and 12 present the behavior of the cost function and parameters variation for the FB type 2DOF-FOPID, respectively that demonstrates the effectiveness of the optimization. Fig. 13 compares values of cost functions for control loops. The best cost function is also obtained for FB type 2DOF-FOPID control loop.

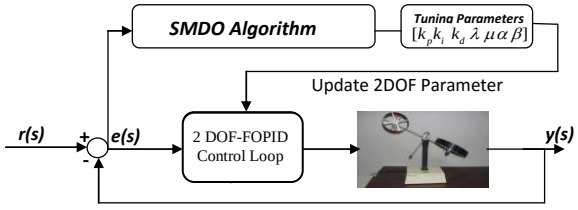

Fig. 9. Optimization process for simulation and experimental setup.

TABLE 1: PARAMETERS OF THE FIVE VARIOUS 2DOF-FOPID CONTROL STRUCTURES THAT ARE GENERATED BY THE SMDO ALGORITHM FOR SIMULATION STUDY

	FF	**FB**	**CS**	**SPF**	**FPD**
k_p	7.9888	10.8318	15.9728	79.8708	63.0741
k_i	3.9993	3.3221	3.9337	31.8713	48.3935
k_d	13.3757	12.5241	12.2003	24.4112	33.1517
λ	0.9698	0.9374	0.5690	0.9334	0.5323
μ	1.2454	1.2845	0.7529	0.9722	0.5953
α	0.3169	0.3077	0.1356	2.1217	0.9906
β	0.5422	0.1300	0.6106	0.7555	0.3057
e)	0.0037	$5.03*10^{-5}$	0.0119	0.0082	$1.62*10^{-4}$

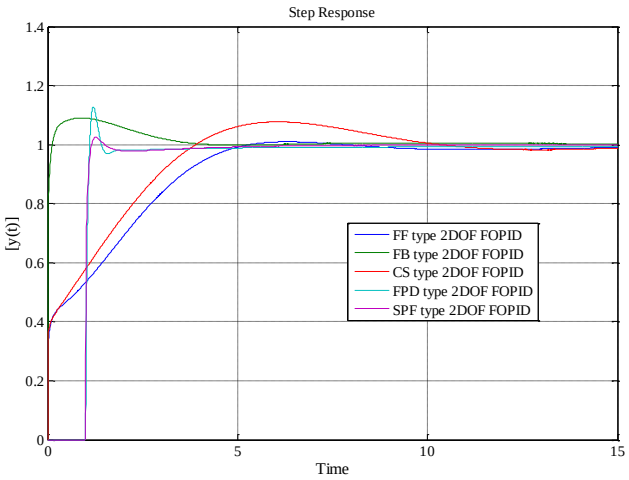

Fig. 10. Step Responses of FF, FB, CS, SPF, FPD types control loops.

C. *Experimental Study*

This section tests the proposed SMDO method experimentally on TRMS system in the optimization setup in Fig. 9. SMDO algorithm in Fig. 7 is employed for this system. "Advantech PCI 1711" interface card is equipped to control TRMS and data acquisition. The real time experimental study is carried on experimental setup in Fig. 9 for FF, FB, CS, SPF and FPD types 2DOF-FOPID control loops respectively. Results of the optimization algorithm are provided in Table 2. Fig. 14 shows the step responses of SMDO for FF, FB, CS, SPF and FPD type 2DOF-FOPID control loops. The best performance is obtained for FF type 2DOF-FOPID control loop in real time application. Fig. 15 provide the variation the cost function during the optimization process.

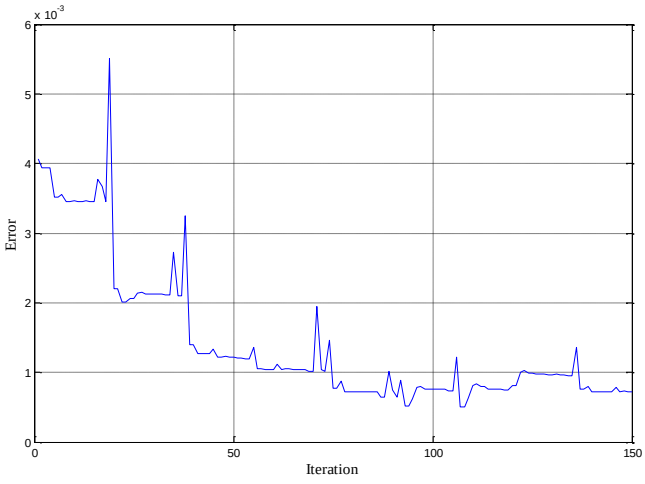

Fig. 11. Variation of the cost function for FB type 2DOF-FOPID during the optimization process.

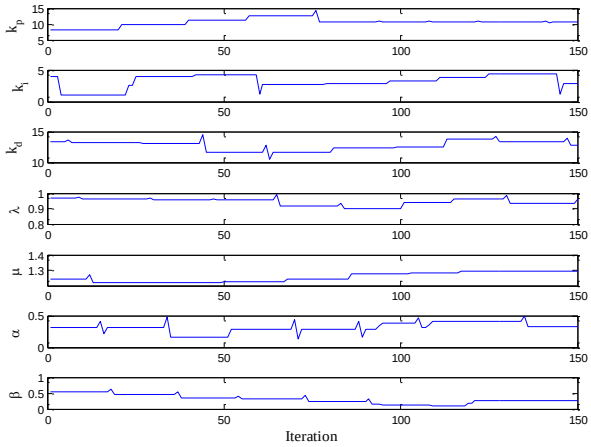

Fig. 12. Parameter variation of FB type 2DOF-FOPID during the optimization process.

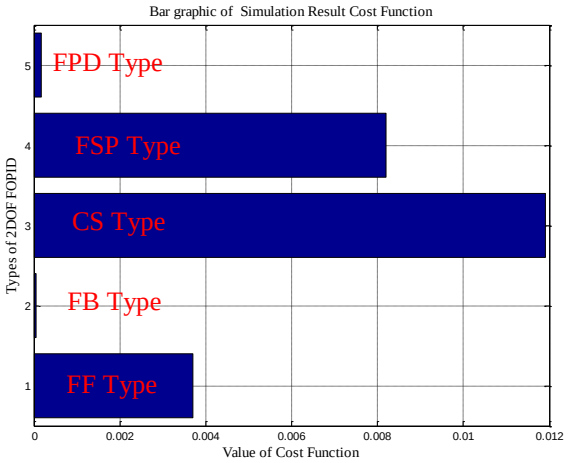

Fig. 13. Simulation result of cost function value (E).

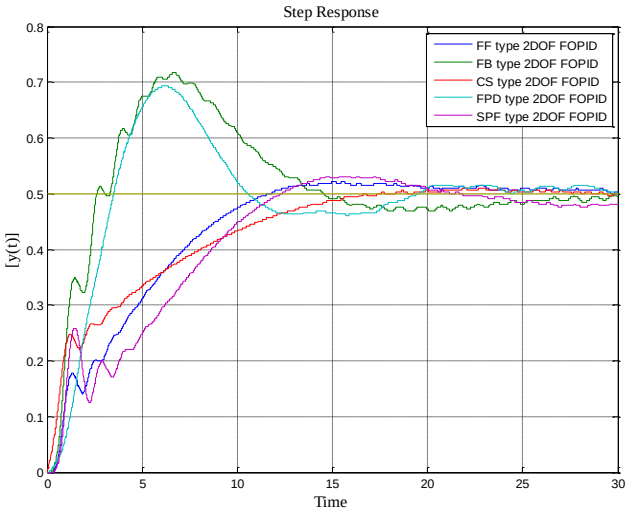

Fig. 14. Comparison of five various 2DOF-FOPID control structures.

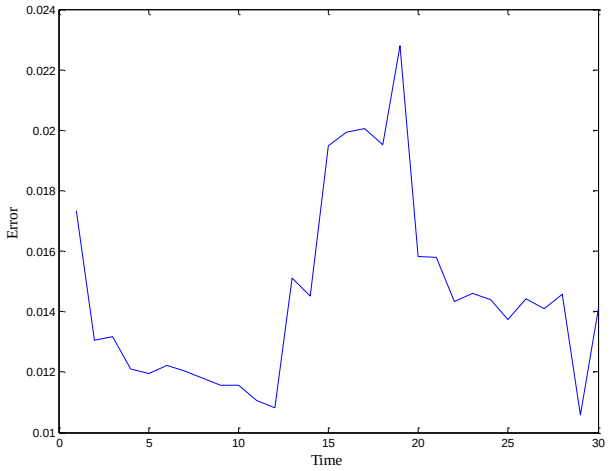

Fig. 15. Variation of the cost function for FF type 2DOF-FOPID during the optimization process.

TABLE 2: PARAMETERS OF THE FIVE VARIOUS 2DOF-FOPID CONTROL STRUCTURES THAT ARE GENERATED BY THE SMDO ALGORITHM FOR EXPERIMENTAL STUDY.

	FF	**FB**	**CS**	**SPF**	**FPD**
k_p	5.4582	8.9189	0.9593	1.8147	0.9514
k_i	1.3239	1.7707	1.6041	0.8000	0.8714
k_d	18.8850	18.0714	16.6405	13.2539	3.1982
λ	1.1456	1.0646	1.1244	1.0464	1.0322
μ	1.1273	1.0505	1.0938	1.0716	1.1513
α	0.8303	0.8662	0.5292	0.5195	0.8168
β	5.0000	5.0000	4.9290	4.9721	4.9040
e)	0.0106	0.0232	0.0132	0.1196	0.0125

V. CONCLUSION

This paper presents the optimization of FF, FB, CS, SPF and FPD types 2DOF-FOPID control loops for simulation and real time TRMS experimental setup using SMDO algorithm. Generally, 2DOF controller design procedures were given in two steps; First step is to optimize controller and second step is to optimize 2DOF structure according to fixed controller value. But, SMDO algorithm gives opportunity to optimize the fractional order controller parameters and 2DOF structure parameters simultaneously to achieve better control performance. This study illustrates the advantage of 2DOF-FOPID control structures and performance of SMDO algorithm.

REFERENCES

[1] I. M. Horowitz, *Synthesis of Feedback Systems*, Academic Press, New York, The University of Michigan, pp.1-726, 1963.

[2] M. Araki, "PID control system with reference feedforward (PID-FF control systems)", *Proc 23rd SICE (Society of Instrument and Control Engineers) Annual Conference*, pp.31-32, 1984.

[3] M. Araki, H. Taguchi, "Two-degree-of-freedom PID controllers", *International Journal of Control Automation and Systems*, Vol.1, pp. 401-411, 2003.

[4] T. Nagashio, T. Kida, Y. Hamada, T. Ohtani, "Robust Two-Degrees-of-Freedom Attitude Controller Design and Flight Test Result for Engineering Test Satellite-VIII Spacecraft", *Control Systems Technology*, Vol. 22, No.1, pp.157-168, 2014.

[5] M. Ajmeri, A. Ali, "Two degree of freedom control scheme for unstable processes with small time delay", *ISA Transactions*, Vol.56, pp.308-326, 2015.

[6] B. B. Ghosh, B. K. Sarkar, R. Saha, "Realtime performance analysis of different combinations of fuzzy–PID and bias controllers for a two degree of freedom electro hydraulic parallel manipulator", *Robotics and Computer-Integrated Manufacturing*, Vol. 34, pp. 62-69, 2014.

[7] G. H. Choi, K. Park, J. H. Jung, "An optimal H_2 decoupling design for non-square plant systems based on the two-degree-of-freedom standard model", *International Journal of Control, Automation and Systems*, Vol.7, No.2, pp.193-202, 2009.

[8] R. E. Gutierrez, J. M. Rosario, J. A. T. Machado, "Fractional Order Calculus: Basic Concepts and Engineering Applications", *Mathematical Problems in engineering*, Hindawi Publishing Corporation, Vol.2010, pp.1-9, 2010.

[9] I. Podlubny, *Fractional Differential Equations*, Mathematics in Science and Engineering, Academic Press, USA, 1999.

[10] B. Ross, *Fractional Calculus and its Applications*, Springer, Verlag, Berlin, New York, 1975.

[11] F. Merrikh-Bayat, N. Mirebrahimi, M. R. Khalili, "Discrete-time fractional-order PID controller: Definition, tuning, digital realization and some applications", *International Journal of Control Automation and Systems*, Vol.13, No.1, 81-90, 2015.

[12] G. Feng, Z. Xiao-ping, "Research on fractional order two-degrees-of-freedom flight control technology of unmanned air vehicle", *Computer Science and Information Processing*, pp. 807–812, 2012.

[13] S. Debbarma, L. C. Saikia, N. Sinha, "Automatic generation control using two degree of freedom fractional order PID controller", *International Journal of Electrical Power & Energy Systems*, Vol.58, pp. 120-129, 2014.

[14] I. Podlubny, "Fractional order systems and $PI^{\lambda}D^{\mu}$ controller", *Proc. IEEE Trans. Automatic Control*, Vol. 44, pp. 208–214, 1999.

[15] C. Yeroglu, N. Tan, "Note on fractional-order proportional-integral-differential controller design", *IET Control Theory and Applications*, Vol. 5, No.17, pp.1978-1989, 2011.

[16] C. Yeroglu, N. Tan, "Classical controller design techniques for fractional order case", *ISA Transactions*, Vol.50, No.3, pp.461-472, 2011.

[17] R. El-Khazali, "Fractional-order controller design", *Computers & Mathematics with Applications*, Vol. 66, No.5, pp.639-646, 2013.

[18] L. H. Sheng, Y. Luo, Y. Q. Chen, "A fractional order proportional and derivative (FOPD) motion controller: tuning rule and experiments", *Control Systems Technology*, Vol.18, No.2, pp. 516-520, 2010.

[19] A. Ates, C. Yeroglu, "Tabu Search Algorithm for Fractional Order PID via Non-linear Multi Objective Function", *International Conference on Fractional Differentiation and Its Applications*, Italy, 2014.

[20] C. Yeroglu, A. Ates, "A stochastic multi-parameters divergence method for online auto-tuning of fractional order PID controllers", *Journal of the Frankline Institue*, Vol.351, No.5, pp.2411-2429, 2014.

[21] B. B. Alagoz, A. Ates, C. Yeroglu, "Auto-tuning of PID controller according to fractional order reference model approximation for DC rotor control", *Journal of the Mechatronics*, Vol.23. No.7, pp.789-797, 2013.

[22] A. Ates C. Yeroglu, B. B. Alagoz, B. Senol, "Tuning of Fractional Order PID with Master Slave Stochastic Multi-Parameter Divergence Optimization Method", International Conference on Fractional Differentiation and Its Applications, Italy, 2014.

[23] D. Song, J. Han, G. Liu, "Active Model-Based Predictive Control and Experimental Investigation on Unmanned Helicopters in Full Flight Envelope", *IEEE Transactions on Control System Technology*, Vol.99, pp.1-8, 2012.

[24] A. Oustaloup, *La commande CRONE: commanderobusted'ordre non entire*, Hermès, Paris, 1991.

[25] D.Valerio, *Ninteger v. 2.3 Fractional Control Toolbox for MATLAB*, 2005. [Online]. Available: http://web.ist.utl.pt/~duarte.vale

[26] K. Matsuda, H. Fujii, "H_∞–optimized wave-absorbing control: analytical and experimental results", *Journal of Guidance Control and Dynamics*, Vol.16, No.6, pp.1146–1153, 1993.

[27] S. F. Ahammad, S. Purwar, "A nonlinear state observer design for 2-dof twin rotor system using neural networks", *Advances in Computing, International Conference on Control, & Telecommunication Technologies*, Trivandrum, Kerala, India, 2009.

[28] C. L. Shih, M. L. Chen, J. Y. Wang, "Mathematical Model and Set-point Stabilizing Controller Design of a Twin Rotor MIMO System", *Asian Journal of Control*, Vol.10, No.1, pp.107-114, 2008.
[29] J. J. Gau, W. K. Liu, C. Y. Tsai, "Intelligent control scheme for twin rotor MIMO system", *IEEE International Conference on Mechatronics*, Taipei, Taiwan, 2005.
[30] C. Xie, A. Mark, "Turnquist Lane-based evacuation network optimization: An integrated Lagrangian relaxation and tabu search approach", *Transportation Research-Elseiver*, Vol.19, No.1, pp.40–63, 2011.

BIOGRAPHIES

ABDULLAH ATES received his B. Sc. Degree in Electrical and Electronics Engineering from Erciyes University in 2011. He received his master degree in Computer Engineering from Inonu University in 2013. His research interests include optimization algorithm, analytical and numerical optimization method, fractional order control systems, fractional order calculus and its application, linear and nonlinear optimization algorithm and flight control.

CELALEDDIN YEROĞLU received his B.Sc. degree in Electrical and Electronics Engineering from Hacettepe University in 1990. He received his first Ph.D. degree in Computer Engineering from Trakya University in 2000 and his second Ph.D. degree in Electrical and Electronics Engineering from Inonu University in 2011. His research interests include fractional order control systems, robust control, nonlinear control, modeling and simulation, optimization algorithm, flight control.

Design of Decision Support System in the Metastatic Colorectal Cancer Data Set and Its Application

T. Pala and A.Y. Camurcu

***Abstract*— Developing the system which will help doctors with the result to be obtained from the medical data sets by realizing the design of the medical decision support system in which data mining methods are used is the primary objective of this study.**

The survivability condition of metastatic colorectal cancer disease has been predicted using data mining methods in the developed system. In the process of data mining, after the phase of data preprocessing, Support Vector Machines, Naive Bayes, Decision Trees, Artificial Neural Networks, Multilayer Perceptron, Logistic Regression algorithms have been used.

In the study, two different medical decision support system models, classifying prediction and hybrid models, have been developed, and the results obtained from the two models have been compared after being examined. While the most successful algorithm is Support Vector Machines in Classifying Prediction Model in which only classification algorithms are applied, it is Decision Trees and Artificial Neural Networks which are the most successful algorithms with an accuracy rate of 100 per cent in Hybrid Prediction Model. In consequence of the classifying processes, when the accuracy rates of the models are examined, it is seen that while the accuracy rate of Classifying Prediction Model is 65-70%, this rate reaches 95-100% in Hybrid Prediction Model. It has been seen that accuracy rates have elicited very high and very close values for all of the algorithms with the realized hybrid structure, that is, with clustering, in the applications of the classifying algorithms combined.

Index Terms— ***Medical Decision Support System, Data Mining, Classification, K-Means Clustering, Metastatic Colorectal Cancer Disease Data Set***

I. INTRODUCTION

THE large intestine that forms some of the digestive system is composed of two parts named as colon and rectum. Colon is the name for the most of the large intestine; rectum is the about 10-cm part before anus. Cancer cells can spread out of the large intestine after colorectal cancer is formed, and can make the other organs metastasis.

T. PALA, works in University of Duzce, Duzce, Turkey, (e-mail: palatuba@gmail.com , tubapala@duzce.edu.tr).

A.Y. CAMURCU, is with Department of Computer Engineering University of Fatih Sultan Mehmet Vakif University, Istanbul, Turkey, (e-mail: ycamurcu@fsm.edu.tr).

The cancers that appear in the large intestine (colon + rectum) are named as colorectal cancers. Every year, colorectal cancer develops in over 1 million people in the World. Mortality rate is around 33% [1]. In the case of that the cancer cells spread out of the tissue from which they take their roots to another tissue, the tumor cells that are formed in the new tissue show the former tissue cells properties and are named identically. For example; the colorectal cancer cells which make the liver metastasis are actually the large intestine cancer cells settled in the liver tissue. In this case, the disease is named as "metastatic colorectal cancer", not "liver cancer", and the treatment of these cancer cells is done considering not liver cancer but colorectal cancer [1].

According to Bijan and Safaee, although survivability length has increased in recent years, mortality rate is still high. Studies done in this field have determined a couple of factors for patients' survivability prediction; however, survivability length hasn't increased significantly. Among these factors, those which are related to cancer early diagnosis are taken as the most important ones [2].

Grumett and his friends have done the study of survival prediction using artificial neural networks and logistic regression analysis on colorectal cancer patients' data. In this study, data that belong to 403 patients are analyzed. Results obtained from the logistic regression analysis and artificial neural network models have been evaluated concerning characteristically drawings, and the compatibility of the models have been compared. Logistic regression model has resulted in 66%, artificial neural network model in about 78%. It has been seen that neural network model is superior to logistic regression analysis model according to these results [3].

Biglarian and his friends collected the data of this study in which they aimed to make distant metastasis prediction on colorectal cancer patients using artificial neural networks as 1219 records from a hospital in Iran between the years 2002 and 2007. In the metastasis prediction, artificial neural networks and logistic regression models C_index (concordance _index) and AUROC (Area Under Receive Operating Characteristic) parameters have been compared. In the application which has been done using R2.14.1 statistical software, C_index has obtained ANN 0.82 Logistic Regression 0.77 results for ANN 0.812 Logistic Regression 0.779 AUROC. These results have demonstrated that the prediction accuracy of ANN is better than Logistic

Regression. This study shows that ANN is an appropriate method which can be used in metastasis prediction [4].
Shenbaga and Vijayalakshmi have searched the subtraction of survival rate with the help of feedback networks from the SEER colorectal cancer data. When Multilayer Perceptron and Feedback networks are compared through classical statistical algorithms, the use of data mining algorithms have been seen to be acceptable in survival prediction [5].

Fathy has analyzed the data of over 100000 colorectal cancer patients taken from SEER through artificial neural networks for colorectal cancer survival prediction. In SEER data set, there are over 70 inputs. Out of these inputs, 20 inputs which are not related to other variables have been selected. The best prediction accuracy rate has been sought to be reached with the most appropriate ANN architecture. For survival prediction, two models have been formed. In the first model, the experimental results have demonstrated that the highest prediction rate is 84.73% with 19 inputs. In the second model, it has been sought to reach the highest accuracy value with the smallest number of inputs. The number of inputs has been decreased to 14, and the number of latent neurons from 11 to 8. As a result of these measurements, it has been seen that 73.68% of the number of the inputs and 72.72% of the number of the latent neurons are sufficient to form an appropriate ANN architecture [6].

In this study, cancer data collected by the Oncology Department at Erciyes University Medical Faculty. These data are the data of 200 patients from 27 fields, and they include demographic information and biochemical and pathological results of the patients. The rapid and substantial technological development has enabled database systems to develop, too. Developments in database systems have enabled collecting data, creating databases, managing data and data to be transferred to electronic environment more easily and to be stored more safely and cheaply. Developments in database systems have increased the use of data mining. The purpose of data mining is to analyze the data collected in databases examining them with mathematical and statistical methods, and to reveal the available rules, relationships, structures or different unfamiliar information. The application has been done using RapidMiner data mining program. RapidMiner has been developed using Java code by Yale University. For categorization and regression, there are many characteristics such as a variety of algorithms, decision tress, Bayesian, logical clusters, association rules and clustering algorithms, data preprocessing, normalizing, filtering properties, genetic algorithm, artificial neural networks, data analysis in 3D. RapidMiner can import data from the databases Oracle, Microsoft SQL Server, PostgreSQL, MySQL [7]. Two models have been designed: Classifying Prediction Model and Hybrid Prediction Model. Predicting success rate of the models have been evaluated by applying the designed models on the data set, and their effects on the predicting results have been observed.

II. Data Mining Models

A. Data Mining Classification Models

Human mentality tends to categorize and classify the objects, events, situations around. Thus, he can understand and talk about the objects and events better. Categorization process in data mining is the process of categorizing the available data according to the determined features and of predicting this data category when some new data are added.

Decision Tree: Decision Tree is one of the most frequently used classification models to analyze data. A decision tree is composed of root, trunk and leaf joints. Considering that the structure of a tree develops from root to leaves, it's formed from top to bottom. The most outer joint is the root joint. Each inner joint of the tree is separated to make the best decision with the help of algorithms [8]. Tree leaves form the category tags, namely, categorical characteristics, making the data in the data set groups.

Artificial Neural Networks: Artificial Neural Networks (ANN) normally enable people to learn from similar or different events they experience, face, observe, to get new knowledge, to generalize those events, relating them with each other, to learn from their mistakes if they make any, and to make decision using all of these in an event they come across. ANN is inspired from human's problem solving with the abilities of thinking, observing, learning from mistakes, trial-error, that is, in a more general speaking, learning. An artificial neural network is an information processing system based on human cognition simulation. It is composed of plenty of calculating neural units attached together. These units are called neurons. The neurons in the nervous system form the network getting attached. ANN is a model developed on layers.

The neurons in the network are arranged all along the layers. A neuron in a layer is connected to all of the neurons in the next layer. Every neuron in the layers takes informative signals from all of the neurons in the former layer, and multiplies every informative signal with their massive values. Process is done with the activation function to get the output, collecting weighted inputs. The output of this function is transmitted to all of the neurons in the next layer. This process is completed after done by the neuron in the output layer, too [9].

Multilayer Perceptron: MLP (Multilayer Perceptron) is an artificial neural network model which is mostly used and learns best [10]. It is known that Multilayer Perceptron has a very strong function in classifying prediction problems [10]. The purpose of this model is to minimize the difference between the target result (output) of the network and the attained result. This model is expressed as propagation algorithm since it makes the mistake spreading it over the network, or as backpropagation since it uses backpropagation learning algorithm in the process of that the multilayer perceptron is getting trained.

Naive Bayes: Bayes classifiers are statistical classifiers. Bayes predicts the membership probabilities of the data, that is, their probability about belonging to a specific category. Bayes classifier is based on the Bayes theorem explained below:

A sample in a data set is composed of the input values X = {x1,x2,xm}. If it is pretended that the total number of the categories is m, the probability calculations are done with Equation 1 for the sample whose category is to be determined [11].

$$P(Ci/X)\frac{P(X/Ci)P(Ci)}{P(X)} \quad (1)$$

p(x|Ci) : the probability for a sample from Category *i* to be *x*
P(Ci) : the first probability of Category *i*
p(x) : the probability for any sample to be *x*
P(Ci|x) : the probability for sample x to be from Category i (last probability)

Support Vector Machines: Support vector machines is a popular method for binary categorization. SVMs can be seen as a perceptron which tries to find a hyper plane that separates the data. The perceptron simply tries to find a hyper plane. It does this process in a way that it separates the data of the hyper plane best. However, it is preferred for the hyper plane to separate the categories as much as possible because it is sought that the hyper plane generalizes the invisible data best with this way of separation. The structure that technically best calculates the separation of data is geometric boundaries. The distance of the hyper plane means the largest boundary which will separate the closest points in the data set, saying in general, means the largest boundary which will categorize the data best [12]. It is not enough for the data in the data set to be in the right side, in the right category of the hyper plane in SVM. Also, they should be in some distance to the hyper plane for a good generalization. Determination of the most appropriate hyper plane directly affects the success of the categorization.

Logistic Regression: The statistical analysis method which is used to express the relationship between a dependent variable and one or more than one independent variables numerically is called Regression Analysis. The purpose in Regression Analysis is to calculate to what extent the independent variables affect the dependent variable, that is, to predict the value of the dependent variable starting out of predicted variables. Logistic Regression is primarily used to predict binary or multi-category dependent variable categories; because response variable is separate, and cannot be directly modeled with linear regression. Therefore, instead of prediction of the point, prediction model of the event occurring is built. In case of the ratio to be more than 50% in the binary categorization problem, category '1' is meant to be assigned to the category determined as category '0' for other cases [13]. The purpose of Logistic Regression Analysis is to calculate to what extent independent variables affect dependent variables.

B. Data Mining Clustering Model

K-Means: It is the best and mostly used clustering algorithm. It is used to divide into k number of categories which have been determined according to quality and characteristics of the records in the data set beforehand. Categorization is done by locating the records in the data set in the closest cluster centers. The success of the clustering process is determined by intra-cluster similarity to be maximum, inter-cluster to be minimum. In other words, objects in the cluster are to be located in the closest way, clusters in the most distant way.

III. APPLICATION

A. Data Set Preprocessing Procedure

In the quality of data analysis results, data quality is very important. Data should be meticulously selected, analyzed, synthesized and prepared for data mining analysis. In this study, quality values have been placed into certain intervals with their mean and standard deviation values by applying data transformation with Z-score normalization in the Metastatic Colorectal Cancer data set. For the qualities in the cancer data set to be equal, z-sore normalization equation has been applied like this:

$$NewQualityValue(i)\frac{QualityValue(i)-Mean(i)}{S\tan dard\ Deviation(i)} \quad (2)$$

B. Design of the Models Applied on the Data Set

In the study, to predict the survival condition of Metastatic Colorectal Cancer patients, two models, Classifying Prediction Model and Hybrid Prediction Model, have been designed. Prediction success ratio has been evaluated by applying the designed models on the data set and the effects of the models on predicting results have been observed.

While applying algorithms on the data set, "10-times cross correction" method has been used as testing method. With this method, the data set is divided into ten parts, and every part is used as test data for one time, as training data for the other nine times. When evaluating the success of the created models, accuracy value has been used.

C. Classifying Prediction Model

Block diagram belonging to the first model, Classifying Prediction Model as we call it, is seen in Figure 1.

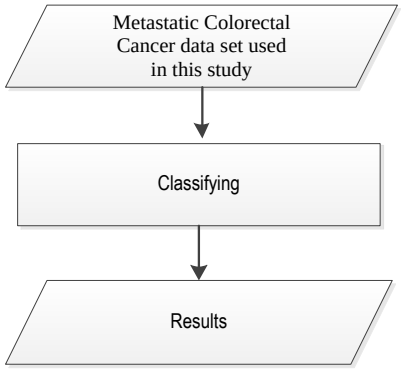

Fig.1. Block Diagram of Classifying Prediction Model

In Classifying prediction model, Metastatic Colorectal Data Set which has been ready for data analysis passing through pre-processing is categorized with selected categorization algorithms. Later, categorization results are compared according to accuracy percentage value which is from the algorithm evaluation criteria. Classifying algorithms have been applied in the data set, and their accuracy values have been compared in Table 1.

TABLE I
ACCURACY VALUES OF CLASSIFYING PREDICTION MODEL

Classifying Algorithms	Accuracy (%)
ANN	62,50
Naive Bayes	64,00
Decision Trees	64,00
MLP	65,00
LR	66,00
DVM	71,00

In Table 1, algorithms and accuracy percentages are seen. When the values are examined, it is seen that the algorithm of artificial neural network has an accuracy percentage of 62,50%, Bayes and decision trees algorithms 64%. MLP with an accuracy ratio of 65%, Logistic Regression with 66%, have very close values to other algorithms. On these data, the algorithm with maximum accuracy ratio is SVM algorithm with 71%.

D. Hybrid Prediction Model

The model applied in Hybrid Prediction Model is for K-Means clustering algorithm to be applied on the data set which has been pre-processed, and for the classifying algorithms of the data (patient records) whose categories have been mispredicted as a result of clustering to be tested on the new data set by clearing the data. Thus, Hybrid Prediction Model is a hybrid model which is formed with clustering+classifying techniques. In Figure 2, the block diagram of Hybrid Prediction Model is seen.

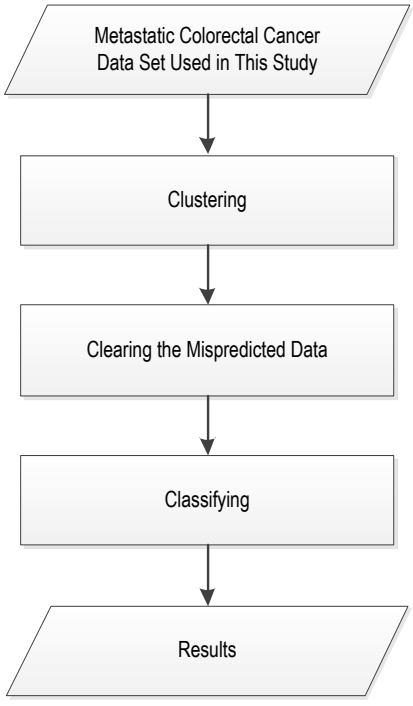

Fig.2. Block Diagram of Hybrid Prediction Model When K-Means clustering algorithm is applied on the data set, emerging results are seen.

TABLE II
K-MEANS CLUSTERING ALGORITHMS CLUSTERING CATEGORIES

Cluster attribute (clusters)	Number of the samples	Number of the data whose categories are mispredicted
Cluster 1 → alive Cluster 0 → dead	200	90

90 misclassified data seen in Table 2 are deleted, and when classifying algorithms are applied on the new data set, the results are as below:

TABLE III
ACCURACY VALUES OF HYBRID PREDICTION MODEL

Classifying Algorithms	Accuracy (%)
LR	96,36
Naive Bayes	97,27
MLP	98,18
SVM	99,09
ANN	100,00
Decision Trees	100,00

Accuracy values of classifying of this model give pretty good results. The algorithm which has the lowest accuracy value is Logistic Regression algorithm with 96,36%. Bayes has an accuracy percentage of 97,27%, MLP 98,18%. It is seen that artificial neural networks and decision trees are the best algorithms with a 100% classifying success in Hybrid Prediction Model. SVM is the second best algorithm with a high success percentage of 99,09%.

IV. RESULTS AND SUGGESTIONS

In this study, survival conditions of Metastatic Colorectal Cancer patients have been predicted by benefitting from data mining algorithms. Predicting process has been done by classifying the data with RapidMiner. In RapidMiner, also the mispredicted data have been detected.

For predicting survival condition, two different models, Classifying Prediction Model and Hybrid Prediction Model, have been created.

In conducted studies, processes have been done on the data composed of 20 qualities of 200 Metastatic Colorectal Cancer patients. Pre-processing, classifying and clustering processes have been applied on the data. The data have been classified according to 6 classifying algorithms which give the best results.

Decision trees and artificial neural networks have been the most successful algorithms with an accuracy percentage of 100% in Hybrid Prediction Model, while the best algorithm in the classifying model in which only classifying algorithms are applied is SVM.

When the accuracy values of the models are examined as a result of the classifying processes, while accuracy percentages of Classifying Prediction Model are 65-70%, this ratio is seen to have reached 95-100% in Hybrid Prediction Model. With the realized hybrid structure, that is, with clustering, accuracy

percentages have been seen to reveal very high and very close values in applying classifying algorithms by combining them. In predicting survival condition, a very successful predicting model with very high success percentages has been realized in the model formed using clustering and classifying algorithms. New hybrids models can be developed by changing the algorithms used here. On future dates, better results than data mining can be obtained by increasing the number of the data used in this study and creating more extensive patterns. In the future, this application can be developed on other cancer types, too.

Doctors can be provided convenience in the progress of the disease and treatment for patients whose death is predicted by making survival or death prediction of colorectal cancer disease which is seen on many people in the world and in our country beforehand. Also, survival length of patients can be extended or their treatment can be procured by trying some other new treatment methods and taking other precautions.

ACKNOWLEDGEMENT

I would like to thank Assist. Prof. Dr. Veli Berk, academic member in Oncology Department at Erciyes University Medical Faculty, for providing the data of this study, and Assist. Prof. Dr. Çiğdem Pala, academic member in Hematology Department at Erciyes University Medical Faculty, for her help in medical matters.

REFERENCES

[1] http://kolonkanseri.blogspot.com/p/kolorektal-kanser-nedir.html: Kolorektal Kanser Nedir ? (Son erişim: 06.10.2012).

[2] B. Moghimi-Dehkordi, A. Safaee, “An overview of colorectal cancer survival rates and prognosis in Asia”, World J Gastrointest Oncol Vol.4, No.4, pp.71-75, 2012.

[3] S. Grumett, P. Snow, and D. Kerr”, Neural Networks in the Prediction of Survival in Patients with Colorectal Cancer”, Clinical Colorectal Cancer, Vol.2, No.4, 239-244, 2003.

[4] A. Biglarian, E. Bakhshi, M.R. Gohari, R. Khodabakhshi, “Artificial Neural Network for Prediction of Distant Metastasis in Colorectal Cancer”, Asian Pacific Journal of Cancer Prevention, Vol.13, pp.927-930, 2012.

[5] S. Shenbaga Ezhil, and C. Vijayalakshmi, “Prediction Of Colon-Rectum Cancer Survivability Using Artificial Neural Network”, International Journal of Computer Engineering and Technology (IJCET), Vol.3, No.1, January- June 2012.

[6] S.K. Fathy, “A Predication Survival Model for Colorectal Cancer”, proceeding AMERICAN-MATH’11/CEA’11 Proceedings of the 2011 American conference on applied mathematics and the 5th WSEAS international conference on Computer engineering and applications, pp.36-42, 2011.

[7] M. Dener, M. Dorterler, and A. Orman, "Açık Kaynak Kodlu Veri Madenciliği Programları: WEKA’da Örnek Uygulama", Akademik Bilişim’09 - XI. Akademik Bilişim Konferansı, Harran University, 11-13 February 2009 Şanlıurfa. (in Turkish).

[8] J.R. Quinlan, C4.5: Programs for Machine Learning, Morgan Kaufmann, San Mateo, California, 1993.

[9] C. Beh Boon, M.Z.M. Jafri, S. Lim Hwee, "Mangrove Mapping in Penang Island by Using Artificial Neural Network Technique", Open Systems (ICOS), 2011 IEEE Conference on, pp.245-249, 2011.

[10] D. Delen, G. Walker, A. Kadam, “Predicting breast cancer survivability: a comparison of three data mining methods”, Artificial Intelligence in Medicine, Vol 34, pp.113-127, June 2005.

[11] R. Jiangtao, L. Sau Dan, C. Xianlu, K. Ben, R. Cheng, and D. Cheung, "Naive Bayes Classification of Uncertain Data", Data Mining, 2009. ICDM '09. Ninth IEEE International Conference on, pp.944-949.

[12] A. Menon Krishna, “Large-Scale Support Vector Machines: Algorithms and Theory”, Research Exam, University of California, San Diego, 2009.

[13] H. Arslan, “Web Mining and Data Analysis of a Web Site, Sakarya University, Master Thesis, Sakarya, Turkey, 2008. (in Turkish).

BIOGRAPHIES

TUBA PALA was born in Konya, Turkey. She received the B.S. and M.S degrees from the University of Marmara, Istanbul, Turkey. Since 2011, she is a Lecturer with the Duzce University. Her research interests are in Data Mining and Biomedical Data Processing, Artificial Intelligence.

.

ALI YILMAZ CAMURCU has been a Professor with the Computer Engineering Department, University of Fatih Sultan Mehmet Vakif University, Istanbul, Turkey. He received his Ph.D. from University of Marmara, Istanbul, Turkey in 1996. His research interests include: Computer Architecture, Data Mining, Artificial Intelligence

Complete Combustion Control for a Steam Boiler Plant

A. Darwish, I. Morsi, and A. El Zawawi

***Abstract*— Steam boiler is one of the most widely used industrial systems. The boiler is used in many industrial applications. It produces steam and is used for many purposes, for example as a heat exchanger used in the refining and separation of oil and is used in electricity production also. Like any combustion system, boilers burn fossil fuels to generate steam. Emissions from fuel include carbon monoxide and nitrogen oxides. Incomplete combustion increases these emissions. The way to reduce these emissions is the control of combustion to make complete combustion by monitoring exhaust components like (NOx, CO2, CO and O2). Steam boilers are usually controlled for steam pressure only without including the exhaust components in the control loop. In this paper, a limiter for exhaust components will be included in the control loop beside the steam pressure control. This paper outlines the various stages of operation involved in the conversion of a manually operated boiler towards a fully automated one. Over the years, the demand for high quality, greater efficiency and automated machines has increased. The first part of the paper focuses on passing the inputs to the boiler at a required temperature, so as to constantly maintain a particular temperature in the boiler. The air preheater and economizer help in this process. The paper mainly focuses on level, pressure and flow control at the various stages of the boiler plant. The temperature in the boiler is constantly monitored. The automation is further enhanced by constant monitoring using a Supervisory Control and Data Acquisition system (SCADA) screen which is connected to the PLC by means of a communication cable. This paper describes the construction of SCADA and the corresponding Human Machine Interface (HMI) for a steam boiler plant. This last consists of the water drum, the air heaters and the main boiler. The control system of the plant is implemented using Siemens SIMATIC S7 PLC with ladder programming and WINCC to create the SCADA/ HMI system.**

Index Terms— **Boiler, PLC, SCADA.**

I. Introduction

LATELY Egypt has been trying to expand in the industrial field, especially in the sectors of electricity generation, oil refining, and petrochemicals production [1]. Over the years, the demand for high quality, greater efficiency, and automated machines has increased in the industrial sector.

Ahmed Darwish, is with Department of Electronics and Communication Engineering Arab Academy for Science and Technology, Alexandria, Egypt, (e-mail: fairejeune@gmail.com).

Iman Morsi, is with Department of Electronics and Communication Engineering Arab Academy for Science and Technology, Alexandria, Egypt, (e-mail: drimanmorsi@yahoo.com).

Amr El Zawawi, is with Department of Electrical Engineering University of Alexandria, Alexandria, Egypt, (e-mail: amr.elzawawi@yahoo.com).

Huge plants require continuous monitoring and inspection at frequent intervals. There are possibilities of errors at measuring and at various stages involved with human workers and the lack of few features of microcontrollers [2]. SCADA and the corresponding HMI are used in many large and medium systems. The SCADA development programs are proprietary and PLC dependent [3, 4].

The steam boiler plant is a large application which needs a large PLC. S7 300 is chosen to operate the plant which consists of a water drum, feed water pumps, air heater and condenser.

A boiler is defined as a closed vessel in which steam is produced from water by the combustion of fuel. Generally, in boilers steam is produced by the interaction of hot flue gases which is coming out from the fuel, mainly coal or coke, with water pipes. In boilers, the chemical energy of stored fuel is converted into heat energy which is absorbed of water that converts it to steam. Due to poor understand of working principles boilers have many serious flaws. Low water level may overheat boiler tubes and damage them. Various controlling mechanism are used to control the boiler system so that it works properly [5].

II. Instrumentation

To detect the level of different parameters several samples have been taken from Alexandria Petroleum Company from January 2014 to June 2014 and the new boiler at Middle East Oil Refinery MEDOR with new CEMS (Continuous Emission Monitoring System) from September 2014 to March 2015.

A. Oxygen Measurement

Yokogawa Model ZR22G separate type zirconia oxygen analyzer is used to measure the quantity of oxygen in the boiler exhaust. A solid electrolyte such as zirconia measures the conductivity of oxygen ions at high temperatures. Therefore, a zirconia-plated element with platinum electrodes on both sides is heated up in contact with gases having different oxygen partial pressures on each side is stable as a concentration cell. As the gas comes in contact with the zirconia element in the negative electrode, oxygen molecules in the gas acquire electrons and become ions. Moving in the zirconia element, electrons arrive at the positive electrode on the opposite side. There, the electrons are released and the ions return to the oxygen molecules. This reaction is indicated as follows [6]:

$$\text{Negative electrode: } O_2 + 4e \rightarrow 2O_2^- \qquad (1)$$

$$\text{Positive electrode:} \quad 2O_2^- \rightarrow O_2 + 4e \qquad (2)$$

The induced voltage E (mV) between the two electrodes, generated by the reaction, is governed by Nernst's equation as follows:

$$E = -(RT/nF) \ln (Px / Pa) \qquad (3)$$

Where:
R: Gas constant
T: Absolute temperature
n: Number of electrons transferred per ion exchanged
F: Faraday's constant
Px: Oxygen concentration in a gas in contact with the positive zirconia electrode
Pa: Oxygen concentration in a gas in contact with the negative zirconia electrode

B. *CO Analyzer*

Teledyne API Model 300 CO Analyzer measures low ranges of carbon monoxide by comparing infrared energy absorbed by a sample to that absorbed by a reference gas. This is accomplished by a Gas Filter wheel, which alternately allows a high energy light source to pass through a CO-filled chamber and a chamber with no CO present. The light path then travels through the sample cell, which has a folded optical path of 14 meters. The energy loss through the sample cell is compared with the zero reference signal provided by the gas filter to produce a signal proportional to concentration, with little effect from interfering gases within the sample. This design produces excellent zero and span stability and a high signal-to-noise ratio allowing extreme sensitivity [7].

C. *Oxides of Nitrogen*

Emerson Model 951C which uses chemiluminescence detection technique, is based on the principle that nitric oxide (NO) reacts with ozone (O3) to produce nitrogen dioxide (NO2), 10% electronically excited nitrogen dioxide (NO2*) and oxygen. Following the NO-O3 reaction, the NO2 molecules immediately revert to NO2. This process creates a light emission directly propor¬tional to the NO concentration in the sample. The intensity of the resulting light emission is then measured by a pho¬tomultiplier tube and associated electronics. An NO2 to NO converter is used for NOX (NO +NO2) analysis [8].

$$NO + O_2 \rightarrow No2^* + O_2 \qquad (4)$$

$$No_2^* \rightarrow NO + h\nu \qquad (5)$$

D. *Pressure Measurement*

A common electrical pressure sensor design works on the principle of differential capacitance. In this design, the sensing element is a taut metal diaphragm located equidistantly between two stationary metal surfaces, comprising three plates for a complementary pair of capacitors. As shown in figure (1) an electrically insulating fill fluid transfers motion from the isolating diaphragms to the sensing diaphragm, and acts as an effective dielectric for the two capacitors [9].

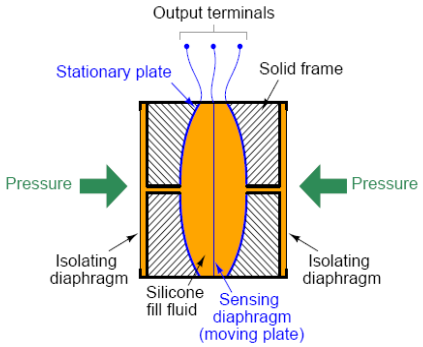

Fig.1. Differential capacitance sensors [9]

E. *Temperature Measurement*

Thermocouples generate their own electric potential. In some ways, this makes thermocouple systems simpler because the device receiving the thermocouple signal does not have to supply electric power to the it. Thermocouples exist in many different types, each with its own color codes for the dissimilar-metal wires. Type (E) can measure from 0 ˚C to 1000 ˚C. It is suitable to use in this process [9].

F. *Level Measurement*

Ultrasonic level instruments measure the distance from the transmitter to the surface of a process material located farther below using reflected sound waves. The frequency of these waves extends beyond the range of human hearing. This is why they are called ultrasonic. The time of flight for a sound pulse indicates this distance, and is interpreted by the transmitter electronics as process level. These transmitters may output a signal corresponding either to the fullness of the vessel (fillage) or the amount of empty space remaining at the top of a vessel (ullage) and the actual level can be calculated as shown in the figure (2).

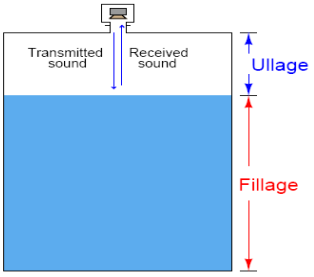

Fig.2. Ultrasonic level measurement [9]

III. PRINCIPLE OF COMBUSTION

To attain a clear understanding of the combustion control methods, a simple fuel like methane (CH4) is used. The chemical equation for the reaction of methane with oxygen is presented below. Methane will react with oxygen to release energy and form carbon dioxide as well as water. Each molecule of fuel would find the exact amount of oxygen to cause complete combustion. In case of methane, one molecule

of methane must find two molecules of oxygen to produce a complete reaction [10].

$$CH_4+2O_2 \rightarrow CO2+2H_2O \quad (6)$$

The combustion process does not proceed in a perfect manner. A fuel molecule may encounter less oxygen than is required for complete combustion. The result will be partial combustion. The exhaust gases will then contain some un-reacted fuel and some partially reacted fuel. Generally, these unburned fuel components are in the form of carbon monoxide (CO), hydrogen (H2), and other fuel components that may include the fully un-reacted fuel source, which is methane (CH4) in this case [10].

$$CH_4+2O_2 \rightarrow \alpha CO_2+\beta H_2O+\gamma CO+\theta H_2+ \varepsilon CH_4+ \zeta O_2 \quad (7)$$

Unburned fuel presents negative safety, health, environmental, and economic impacts on the boiler operation. As a result, it is imperative to manage the combustion process to maintain these components to minimum levels. So combustion management requires that extra oxygen be provided to the combustion zone to ensure all the fuel is reacted. But, the amount of extra oxygen must be minimized to reduce energy loss.

The measurements required to manage the combustion loss are the flue gas oxygen content and the flue gas combustible concentration. The flue gas oxygen content is measured to allow the combustion air flow to be controlled to meet a set point. Combustibles concentrations are measured to identify the minimum practical oxygen concentration.

There are many measurements required to obtain a boiler tuning. There are several critical measurements required to ensure good combustion. The critical measurements are oxygen concentration and flue gas combustibles concentration [11].

IV. SCADA System

SCADA is an acronym for Supervisory Control and Data Acquisition. SCADA systems are used to monitor and control a plant or equipment in industries such as water and waste control, energy, oil and gas refining and transportation. These systems encompass the transfer of data between a SCADA central host computer and Programmable Logic Controllers (PLCs), and the operator terminals [12].

A SCADA system gathers information, transfers the information back to a central site, then alerts the home station if anything occurred. These systems can be relatively simple, such as one that monitors environmental conditions of a small office building, or very complex, such as a system that monitors all the activities in a nuclear power plant or the activity of a municipal water system.

Many systems are monitored using the infrastructure of the corporate Local Area Network (LAN)/Wide Area Network (WAN). Wireless technologies are now being widely deployed for purposes of monitoring. WinCC is a powerful HMI system for use under Windows XP or Windows 7 to simulate a steam boiler plant. HMI stands for "Human Machine Interface", i.e. the interface between the human (the operator) and the machine (the process) [13].

V. Steam Boiler System Description

Steam required for the plants needs to be dry and at high temperature. Feed water coming to the economizer is evenly distributed in the drum by the feed water distribution pipe. Boiler water leaves the drum through the down comers to the water wall. The steam/water mixture coming from the water wall enters the drum in the primary steam separator, where water and steam are separated. Steam leaves the drum via the saturated steam line.

The drum contains a hold-up volume of water to produce steam for at least three minutes during failure of feed water supply. The drum is able to contain the swell of water volume of the water wall during start-up, when the start level is taken into account [14].

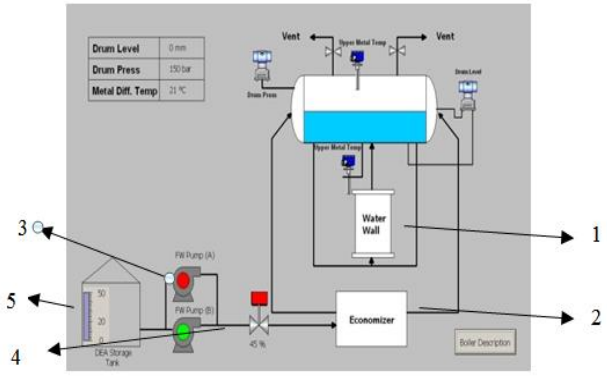

Fig.3. The Graphical User Interface (GUI) of the drum

Where:
1. Water wall
2. Economizer
3. Feed water pumps
4. Feed water valve
5. Dearator storage tank

VI. Steam Boiler Main Components

Actually, a small amount of excess air is needed to ensure complete combustion. Air enters the furnace at different locations depending on the size. Boilers are usually equipped with chimneys to produce the draft necessary to move combustion air into the furnace and to discharge the combustion products, or flue gas to atmosphere. The draft must be produced high enough to provide enough air to burn the fuel without causing it to smoke and move the flue gas up to the chimney.

Large boilers that use heat recovery equipment and air pollution control devices must use fans to move air through the system as shown in the figure (4) below; because of high draft losses produced by this add on equipment [15].

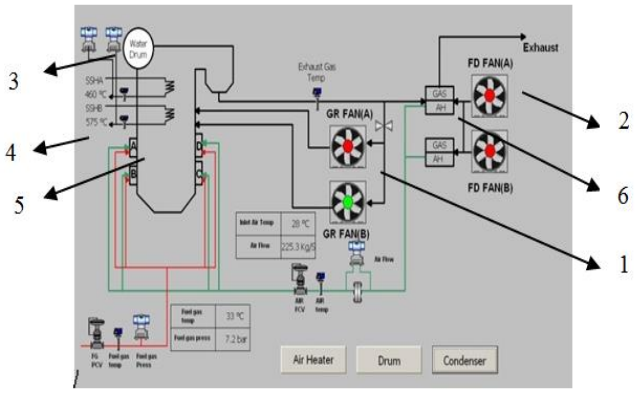

Fig.4. The Graphical User Interface (GUI) of the boiler

Where:
1. Gas Recirculation (GR) fans
2. Forced Draft (FD) fans
3. Water drum
4. Super heat coils
5. Main boiler
6. Air heater

A. *Air Heater*

Boilers are provided with air pre-heaters to recover heat from the flue gases. An increase of about 12% in boiler efficiency is achieved by providing air pre-heaters. Air pre-heaters are provided in boilers to preheat the combustion air before supplying it to the boiler as shown in the figure (5).

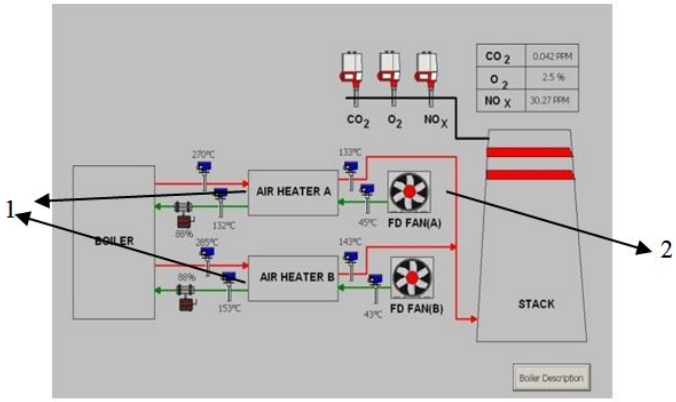

Fig.5. The graphical user interface of the air heaters

Where:
1. Air heaters
2. FD fans

B. *Steam Condenser*

The object of the condensate system is to condense the steam and circulate the water back to the drum. Steam is condensed in the condenser. The condensate is then pumped to the condensate preheater. In the preheater, the condensate is heated with heat from the returned stream. Part of the water from the preheater outlet is recirculated to the condensate preheater inlet as shown in the figure (6). This way, the minimum inlet temperature of the preheater is controlled above the water dew point of the flue gas. From the preheater, the condensate is directed to the deaerator.

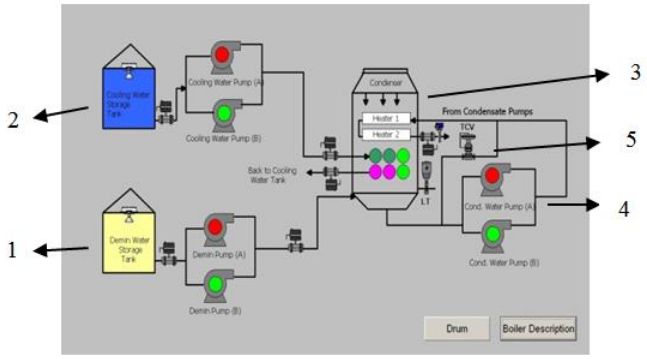

Fig.6. The Graphical User Interface (GUI) for the Condenser

Where:
1. Demineralised water storage tank
2. Cooling water storage tank
3. Condenser
4. Condensate water pumps
5. Condensate water temperature control valve

IX. RESULT

The steam boiler plant, with a SCADA system is designed as well as the interface of this SCADA with the PLC .The HMI is programmed to interface with the field to achieve the different control tasks. Therefore at anytime, the valve can be opened or closed, and any pump can be started or stopped using the HMI according to the operation instructions. Face plates are used to open and close fans as shown in figure (7).

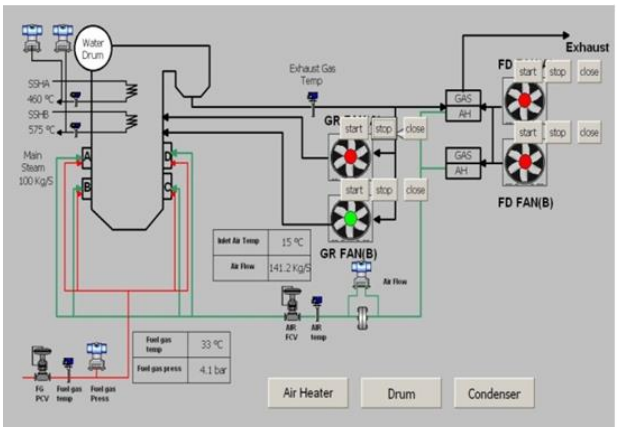

Fig.7. GUI of the boiler showing starts and stops for all fans

The combustion process should proceed in a perfect manner. A fuel molecule needs a limited quantity of air for complete combustion. In figures (8) and (9) fuel to air ratio changes as steam flow changes.

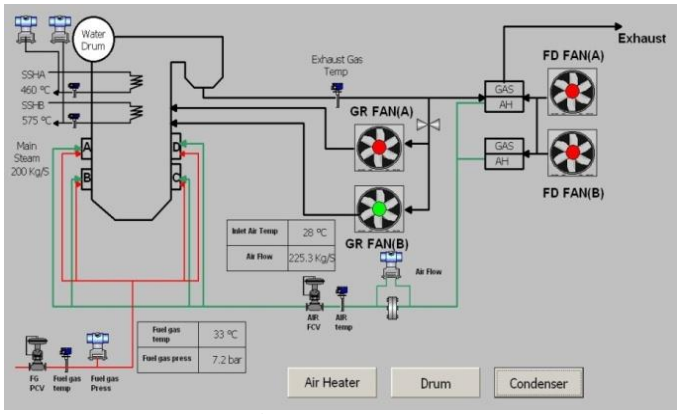

Fig.8. GUI of the boiler showing changing in the fuel to air ratio as steam flow changes

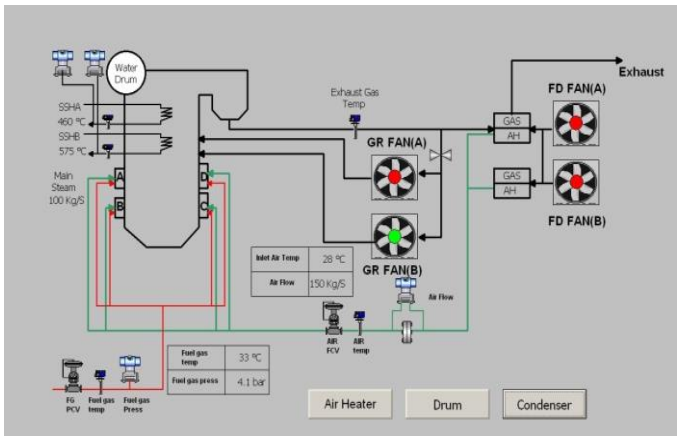

Fig.9. The GUI of the boiler showing fuel to air ratio at half load

At same steam flow demand, if combustion parameters change, like air temperature, it will lead to change the air density and fuel to air ratio. To avoid this case, the air flow control valve will change his value to compensate changing in fuel to air ratio as shown in figure (10) .The air flow will be 141.2 kg/s.

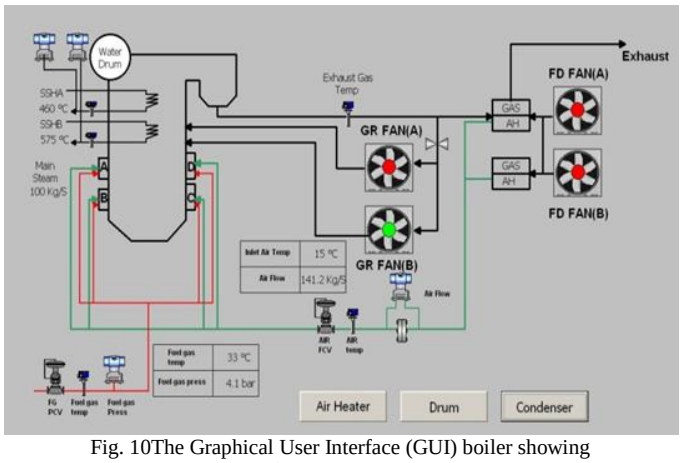

Fig. 10The Graphical User Interface (GUI) boiler showing changing in air flow as air temperature changes

Any large boiler burns a huge amount of fuel. Operating a plant without measuring its performance it will lead to decreasing its efficiency. By using Yokogawa Model ZR22G, described before, oxygen concentration can be detected as show in the figure (11).

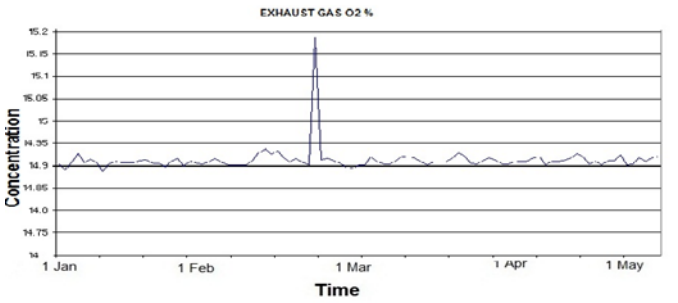

Fig.11. Oxygen concentration %

By using CO analyzer, Model 6300E CO concentration can be detected as shown in figure (12).

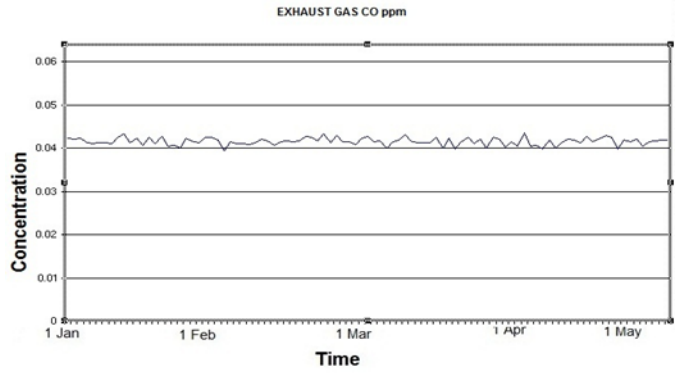

Fig.12. CO concentration (ppm)

By using Emerson Model 951C, NO concentration can be detected as shown in figure (13).

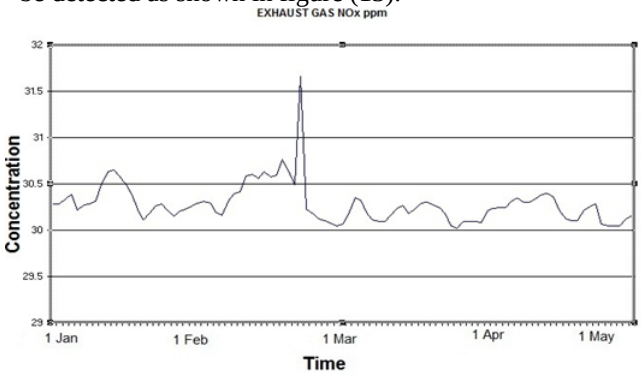

Fig.13. NO concentration (ppm)

Figure (14) shows the ambient temperature during 36 hours of continuous measurement using type (E) thermocouple.

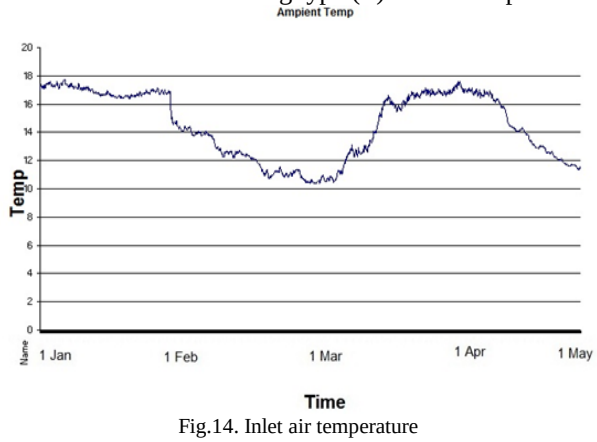

Fig.14. Inlet air temperature

Figure (15) shows degradation of demineralized water level during 36 hours of continuous measurement showing maximum level and minimum levels.

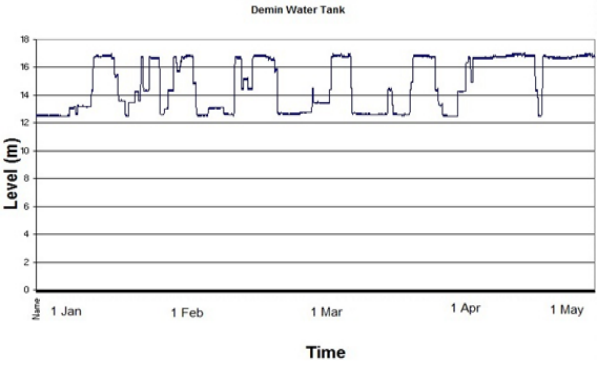

Fig.15. Inlet Demin water level

Any automatic control system should have instrument air to operate pneumatic valves. Its pressure should be within range as shown in figure (16).

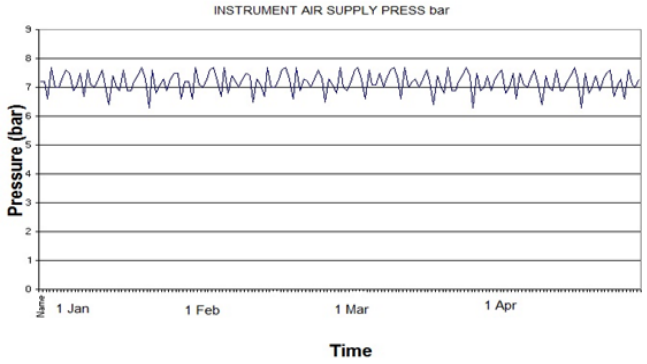

Fig.16. Instrument air pressure (bar)

X. CONCLUSIONS

An important aspect of any power plant is the boiler control. Several techniques can be implemented, but the used method relies on many objectives like: superior quality, increased efficiency, and high profit. SCADA system is used to collect data from the steam boiler plant and control it by sending and receiving control signals from and to this system [16,17]. In this system, WinCC is used to create graphics that is used to interface the operator to all the demineralization plant equipment. The most important benefits from using a SCADA system is decreasing man power and operating time by allowing the operator to control all equipment, take all instruments readings continually, allowing designing control functions, operate all equipment and store plant historical data to create graphic trends which allow the operator to monitor any change in the measured values and to allow more efficient operation. The advantage of using SCADA/PLC system is that the scan time needed to monitor the system, detect the problems, and executing the actions swiftly.

REFERENCES

[1] I. Morsi, A. El Zawawi and M. Amin, "Statistical Analysis Techniques for High Quality Water", Global Climat Change Conference, Alexandria, Egypt, 2013.

[2] I. Morsi, M. El Deeb, and A. El Zawawi, "SCADA/HMI Development for a Multi Stage Desalination Plant", Computation World Future Computing, Athens, Greece, pp. 67–71, 2009.

[3] K. Barnes and B. Johnson; "Introduction to SCADA Protection and Vulnerabilities", IEEE Transactions on Instrumentation and Measurement, Vol. 56, No. 1, February 2007. Electromagnetic Fields (300 Hz to 300 GHz), Environmental Health Criteria 137, World Health Organization, Geneva, Switzerland, 1993.

[4] Iman Morsi, Loay Mohy El-Din,"SCADA System for Oil Refinery Control", Elsevier Measurement Journal, Vol.47, 2014.

[5] K. Gowri Shankar, "Control of Boiler Operation using PLC – SCADA", International MultiConference of Engineers and Computer Scientists 2008 Vol II, Hong Kong.

[6] Yokogawa Zirconia Oxygen Analyzer, Model ZR22G, Datasheet, 8th Edition, 2012.

[7] Teledyne API Model 300 CO Analyzer Instruction Manual, 2006.

[8] Rosemount NOx Analyzer, Model 951C, Product Data Sheet, May, 2009.

[9] Tony R. Kuphaldt; "Lessons In Industrial Instrumentation, Version 1.12", September 20, 2010.ISBN (1009217397803).

[10] Partha S. Sarathi; "Combustion Handbook Principles and Practice", 1999. DOElPC l91008-0374, Distribution Category UC-122.

[11] Weber, Roman; "Combustion Fundamentals with Elements of Chemical Thermodynamics", Clausthal-Zellerfeld, Papierflieger 2008, ISBN 978–3–89720–921–3.

[12] Hjalti Kristinsson, "Boiler Control", Coden :Lutedx /(TEIE-5278)/1-89 (2011)

[13] Ken Heselton, "Boiler operator's handbook", ISBN 0-88173-434-9, 2004.

[14] Simatic HMI WinCC flexible 2008 Compact/Standard/Advanced, user's manual.

[15] Zhao li-ming and Zhang bing", Large Scale Motor Group Integrative Management and Control Network System Based on PLC-SCADA Under Complex Environment", Applied Mechanics and Materials Vol. 742 (2015) pp 698-707.

[16] S. Lishev, R. Popov, and A. Georgiev "Laboratory SCADA systems – the state of art and the challenges". Balkan journal of electrical & computer engineering, ISSN 2147-284X, Vol.3, 2015.

BIOGRAPHIES

AHMED DARWISH Alexandria, in 1987. He received the B.S. in electronics and communication engineering from Arab Academy for engineering and technology, in 2010. He was I&C engineer since 2011, His research interests include high-pressure boilers and high-accuracy instruments and its applications.

IMAN MORSI Morsi was born in 1969 at Alexandria. B.Sc. in Electrical Engineering (Electronics and Communications) from Alexandria University,Egypt,1991 .M.Sc. in Electrical Engineering (Electronics and Communications) "An Integrated Energy Management System for Intelligent Buildings" from the Faculty of Engineering, Alexandria University, Egypt,1969. PhD in Electrical Engineering (Electronics and Communications),"Photovoltaic Systems Management Using Artificial Intelligence Techniques" from the Faculty of Engineering, Alexandria University, Egypt, 2002.
Currently: Vice-Dean of Training Affairs and Community Service of Arab Academy for Science and Technology and Maritime Transport (AASTMT), Abo-Qir Campus, Alexandria. Professor in Electronics and Communications Department in Faculty of Engineering (AASTMT). Field of interests are: Sensors fabrication and applications. Application using microcontroller and PLC. Data fusion system using artificial intelligence techniques. IEEE Senior member in measurements society. I got Marquis' Who's Who Award for outstanding achievement in my own field and Socity,2007. I contributed in many community services and charities.

Amr M. O. El ZAWAWI Born on 1950 in Alexandria, Egypt. He obtained his BSc and MSc in Electrical Engineering from the University of Alexandria on 1972 and 1976 receptively. He obtained the DEA and PhD degree from the INPG, France on 1977and 1980 respectively. His fields of interest are Electric Machines and Power Electronics. He served as a teaching assistant, assistant lecturer, lecturer and associate professor in the department of Electrical Engineering, Faculty of Engineering, the University of Alexandria

An Advanced Fault Locating Technique with WAMS based Backup Protection Scheme for Power System with Simultaneous Faults

S. Roy and Dr. P.S. Babu

***Abstract*—Protection of power systems is important for stable and uninterrupted operation of power network. Maloperation of traditional back up protection schemes (e.g-Zone3 maloperation) causes many catastrophic phenomenon like cascaded tripping in power systems. So, some defensive mechanism are needed for taking care of such failures in power systems and to increase their security and reliability. Due to hugeness and complexity of Modern power systems, they are controlled, monitored and protected by Wide Area Measurement systems (WAMS). WAMS increases the efficiency and reliability of power networks and prevent the chance of blackouts and cascading failures in tandem. A synchronized phasor measurement-based wide-area backup protection scheme is presented in the paper where the magnitude of sequence voltages of buses at a system protection centre are used to identify the faulted area, bus closest to the fault and faulted line. The proposed method is tested for several faults including simultaneous faults in power systems with interconnections also. This technique is found to be Reliable, accurate and fast with contemporary synchronized measurement based technology. It is expected that numerous disastrous blackouts, cascaded tripping of power networks can be avoided and reliability and security of the power systems can be improved by the scheme. The study of new and improved back up protection scheme is done on a WSCC-3 machine-9 bus system. The data is simulated through EMTDC/PSCAD and MATLAB /SIMULINK software.**

Index Terms—**Distance Protection, Simultaneous Faults, Series Compensation, Faulted bus Identification, Backup protection, faulted Line identification, Sequence Components of Voltage, Balanced Fault, Unbalanced Fault.**

Symbols

$Ø_{1s}$, $Ø_{1s}^1$- Phase angle between positive sequence Voltage and before and after placement of series capacitor.

$Ø_{2s}$, $Ø_{2s}^1$- Phase angle between negative sequence Voltage and current before and after placement of series capacitor.

$Ø_{1R}$ - Phase angle between positive Sequence Voltage and current at the other end of the protected line.

$Ø_{2R}$ - Phase angle between negative Sequence Voltage and current at the other end of the protected line.

$Ø_{2R}$ - Phase angle between negative Sequence Voltage and current at the other end of the protected line.

S. ROY, Research Scholar, Department of Electrical Engineering, NIT Warangal, India, (email: saptarshi.roy.ju@gmail.com).

Dr.P.S. BABU, Assistant Professor, Department of Electrical Engineering, NIT Warangal, India, (email: drsureshperli@nitw.ac.in).

$g_{1s} = \cos(Ø_{1s})$
$g_{1s}^1 = \cos(Ø_{1s}^1)$
$g_{1R} = \cos(Ø_{1R})$
$g_{2s} = \cos(Ø_{2s})$
$g_{2s}^1 = \cos(Ø_{2s}^1)$
$g_{1R} = \cos(Ø_{1R})$

I. INTRODUCTION

IN GENERAL local voltage or current measurements are used in conventional back up protection schemes used for power networks which find obstacle in distinguishing the fault from heavy loading conditions [1]. Maloperation of back up protection during stressed conditions causes the cascaded tripping. Wide area interconnection leads to huge number of blackouts throughout the world.

Recent advancements in technology draws significant attention for the utilization of the synchronized phasor measurement unit (PMU) based wide-area measurement system (WAMS) for power system protection [2,3]. Emergence of new technologies like smart electric grid increased the safety and reliability power networks and mitigates the more serious consequences like blackouts, cascaded tripping of power networks and other power outages. Thus they help to continue safe, reliable and continuous power supply.

The largest power outage in history happened in India on 30th and 31st July 2012. The outage affected 22 states in Northern, Eastern and Northeast India. About 32000MW of generating capacity was taken offline in the outage. Several factors responsible for the blackout were:

i) Weak inter-regional power transmission due to multiple existing outages.
ii) Drastically increase in loading on 400 kV Binna-Gwalior-Agra power link.
iii) Inadequate response by State Load Dispatch Centres (SLDCs). This outage affects most of the population of India (about 620 million).
iv) Loss of 400 kV Binna-Gwalior link due to mal-operation of the protection system [12].

The wide-area backup protection (WABP) based on faulted line identification (FLI) is an interesting topic of research in recent days due to several reasons. First of all a good backup protection can increase the security and reliability of power system. Second of all, a good back up protection can ensure a stable and uninterrupted flow of power. Thus, it reduces power

outage and loss of production in plants. The proposed technique can overcome the limitations of conventional backup protection and allows faster operation since it does not need coordination among different zones.

Different WABP schemes for FLI are discussed [4-8]. In [4], a WABP is proposed that compares the positive-sequence voltage magnitude at each bus during the fault to identify the closest bus to the fault. Positive-sequence current angles of all lines connecting the selected bus are used to detect the line having fault. In [5] the residual vector of a Synchro-phasor based state estimator, used in a supervisory system, is proposed to improve security of an existing remote backup protection scheme. A supervisory and an agent-based ad-hoc backup relay protection scheme based on a network infrastructure and communication are proposed in [6].

A WABP scheme based on the fault steady-state component of voltages and currents is proposed for Faulted line identification in [7]. In that method, subsets of buses, called protection correlation regions (PCRs), are formed on the basis of network topology and PMU placement. The steady-state component of differential currents in each region is used to identify the PCR with the fault. A WABP algorithm based on the fault component voltage distribution is proposed in [8]. In this scheme, the faulted voltage at one terminal of the line is estimated by the measured values of faulted voltage and current at other terminals, and the faulted line is identified based on the ratio of estimated values to measured values. A faulted area detection technique is also used to accelerate the faulted line identification task. In [12,13], synchronized phasor measurement based back up protections are suggested but those schemes deal with only one fault at a time occurred in a power network. But faults or contingencies in a power network is not an isolated issue. In fact, more than one fault or contingencies can occur in a power network, especially in a Wide area network, at a time or simultaneously. But nothing is discussed about power systems behaviour if more than one fault or contgencies occurred in power network simultaneously, in any of the above methods. In this paper, the method discussed is an advanced version of the method discussed in [12,13], which is modified and extended up to describing the behaviour of power systems during simultaneous faults.

A series capacitor with Metal Oxide Varistor creates problems to distance relaying based transmission-line protection. Typical problems associated with relays have been addressed in [9-10] which include several critical phenomena like voltage/current inversion, sub harmonic oscillations, and additional transients caused by the air-gap operation [19]. Performances of available WABP schemes [4-8] have not been evaluated for series-compensated lines and may find limitation for such lines. This paper proposes a WABP scheme where angle information between voltage and current at both ends of a line is used for faulted line identification. The scheme is found to be accurate for the compensated and uncompensated line from the evaluation for a 400-kV, 9-bus system with simultaneous faults also. In this paper several cases have been studied to justify the proposed technique.

II. WIDE AREA SYNCHROPHASOR SYSTEM WITH PHASORS OF NOMINAL FREQUENCY SIGNALS

Nominal frequency means desired central frequency. In case of a signal, the desired central frequency is the same as source or generation frequency. If it deviates from desired central frequency, then it is called off-nominal.

Let us consider a constant input signal $x(t)$, with nominal frequency f_0 [5].It is sampled at a sampling frequency Nf_0.The sampling angle $ø = 2\pi/N$, and the phasor estimation is done below :

$$X(t) = X_m \text{ Cos } (2\pi f_0 t + ø)$$

The data samples of this input X_n :{n=0,1,2,….,N-1) are

$$X_n = X_m \text{Cos } (nø + \delta)$$

$$X_c^{n-1} = \sqrt{2}/N \sum_{n=0}^{N-1} X_n \text{ Cos}(nø + \delta)$$
$$= \sqrt{2}/N \sum_{n=0}^{N-1} X_m \text{Cos}(nø + \delta).\text{Cos}(nø)$$
$$= (\sqrt{2}/N) X_m \sum_{n=0}^{N-1} [Cos\delta.\text{Cos}^2 nø - ½ \text{Sin}\delta.\text{Sin } (2nø)]$$
$$= X_m/\sqrt{2} \text{ Cos}\delta \quad (1)$$

Similarly

$$X_s^{N-1} = \sqrt{2}/N \sum_{n=0}^{N-1} X_n \text{ Sin}(n \delta)$$
$$= - X_m/\sqrt{2} \text{ Sin } \delta \quad (2)$$

The Phasor $X^{N-1} = X_c^{n-1} - j\, X_s^{n-1}$

$$= X_m/\sqrt{2} [Cos\delta + j\, Sin\delta]$$
$$= X_m/\sqrt{2} e^{j\delta} \quad (3)$$

A synchro-phasor based system having several components .e.g- Phasor measurement unit (PMU), phasor data concentrator (PDC), GPS satellite system, super PDC (SPDC) as shown in Fig.1(a) & Fig.1(b). The real time data from the various remote areas are collected by PMUs and sent to local data concentrator called phasor data concentrator through communication system. This system is same as the backup protection system for Wide Area Protection System (WAPS) and it is capable of acting as the substitution of conventional backup protection in power system [12]. The relay decision is taken based on collected data via communication network. The suggested technique increases the accuracy, reliability and stability of the system.

Usually the data collection activity follows the below hierarchy. Level 1 being the lowest and level 4 is the highest position as indicated in Fig.1(a). In case of a power network level 1 can be compared as feeder level data, level 2 can be compared as substation level data, level 3 can be compared with a State board or grid data and level 4 can be compared with a load dispatch centre data (e.g – Northern Regional Load dispatch centre or Southern Region Load dispatch centre in context to India).

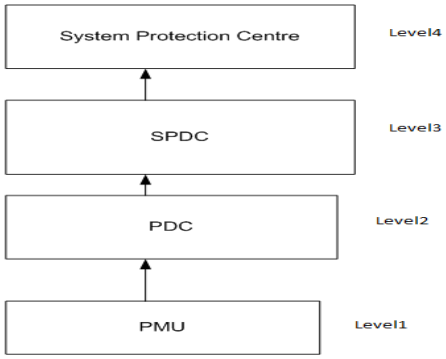

Fig.1(a). Collection of Data Hierarchy

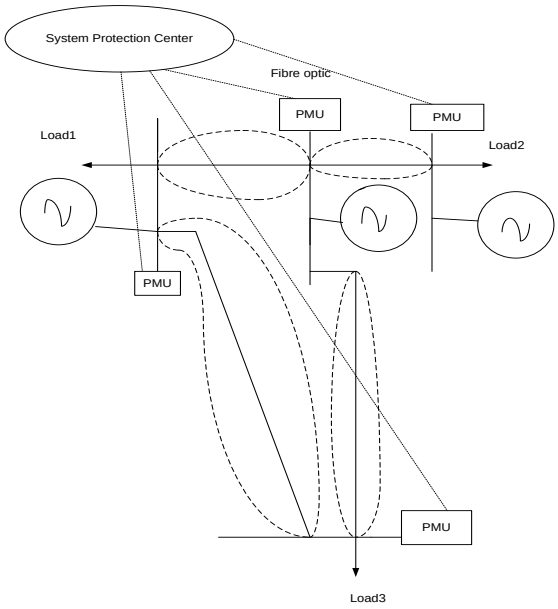

Fig.1(b). Wide Area Measurement Back Up Protection

III. PROPOSED METHOD

The main purpose of this proposed technique is to improve wide area monitoring and system event analysis. The proposed technique is useful for monitoring and control of large power networks like plants, transmission lines and significant control points of the grid [13]. Synchro-phasor using phasor measurement unit provides all significant measurements required for the operation including voltage magnitudes, phase angles and frequency. The rate of data sampling is maintained at 4 kHz . Channel plot step in project settings of EMTDC/PSCAD is kept at 250 micro-seconds.

The Proposed Technique is follows:

Algorithm:

***Step1*:** Start

Step2: Collect all data from all PMUs and PDCs in real time.

***Step 3*:** Obtain minimum positive sequence voltage magnitude or maximum negative or zero sequence magnitude (v_k)

Step4: Compare with the threshold value. If it is less than minimum positive sequence voltage magnitude or more than maximum negative or zero sequence magnitude value, then there is no fault in the system. Otherwise, area or bus *k* is the nearest to the fault go to Step5 and Proceed

***Step5* :** Check whether it is a balanced fault or unbalanced fault.

The negative- and zero-sequence voltages are used to identify unbalanced faults [13]. For these faults, the pickup criterion is defined as,

$$V_{m2} \geq K_2 V_n \; U \; V_{m0} \geq K_0 V_n \quad (4)$$

Where V_{m2} & V_{m0} are the negative and Zero sequence components of the waveform of m^{th} bus and V_n is the rated voltage of the bus. K_2 and K_0 are the constants. In this paper, the thresholds of K_2 and K_0 and set at 0.1 for an unbalanced fault. The reason of choosing low threshold settings are that the combined information of negative and zero-sequence voltage magnitudes could improve the sensitivity of pickup criterion during a high-resistance earth fault.

If unbalanced fault condition is not satisfied, then the substation will check for balanced fault criterion:

$$V_{m1} \leq K_1 V_n \quad (5)$$

K_1 is a constant whose value is kept 0.6 in this paper. Higher threshold for the balanced fault is chosen in order to avoid frequent pickup of the WABP system under normal switching condition of the power Network.

***Step6*:** Compute absolute angle difference of all lines connected to bus or area k.
Step7: Obtain highest value line of phase angle.

***Step8*:** The j^{th} line connected to area k is faulted line.

***Step9*:** Authentication if series capacitor compensation involved in the faulted line: Check g_{2s} , g_{2s}' , g_{2R} all >0 (6) for an unbalanced fault.

Check,

$$g_{1s} \; , g_{1s}' , \quad g_{1R} \text{all} \; > 0 \quad (7)$$

for a balanced fault.

Step10 : Relaying algorithm

Step11 : Stop

IV. CASE STUDIES

The proposed Wide Area Measurement Back up protection (WABP) algorithm is tested for a WSCC 3-Machine-9 bus system (same as Fig 2). Using EMTDC/PSCAD and MATLAB/SIMULINK software simulations are carried out for different types of fault and even simultaneous faults in different branches of the system (both balanced and unbalanced faults). The data sampling rate is maintained at 4 KHz throughout. Solution time step is kept at 50 microsecond and channel plot step is kept 250 micro seconds in project settings of EMTDC / PSCAD for capturing data (in case used EMTDC/PSCAD for WSCC-3-Machine-9 bus system

simulation). In figure 6, Simulink implementation of WSCC-3-Machine-9 bus system is shown.

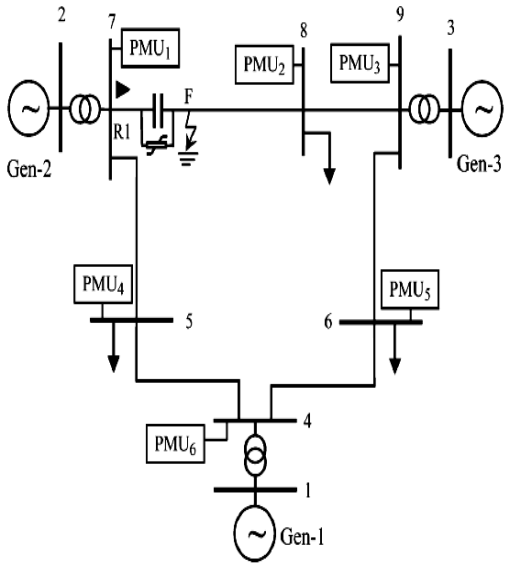

Fig.2. Single Line Diagram of WSCC-3Machine-9bus system with PMUs.

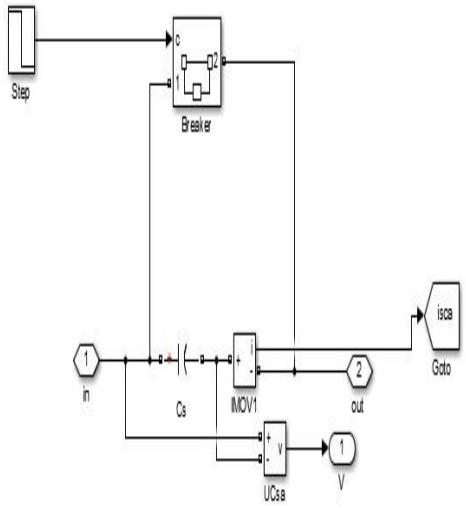

Fig.3. Simulink Design of MOV Circuit with different protections.

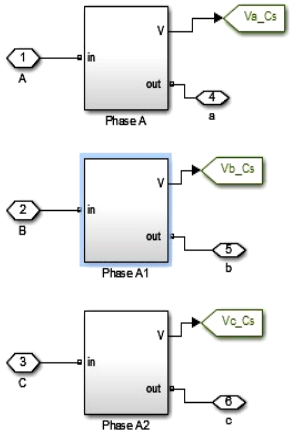

Fig.4. Simulink Design of Data Acquisition system

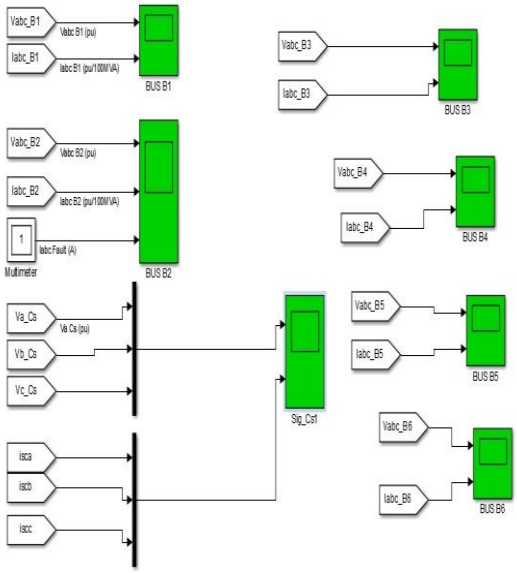

Fig. 5. Design of Data Acquisition with Simulink.

Fig.6 is showing Simulink implementation of WSCC-3-Machine-9 bus system. Fig.3, Fig.4 and Fig.5 are showing different internal protections and arrangement of data acquisition by Simulink software required for the work.

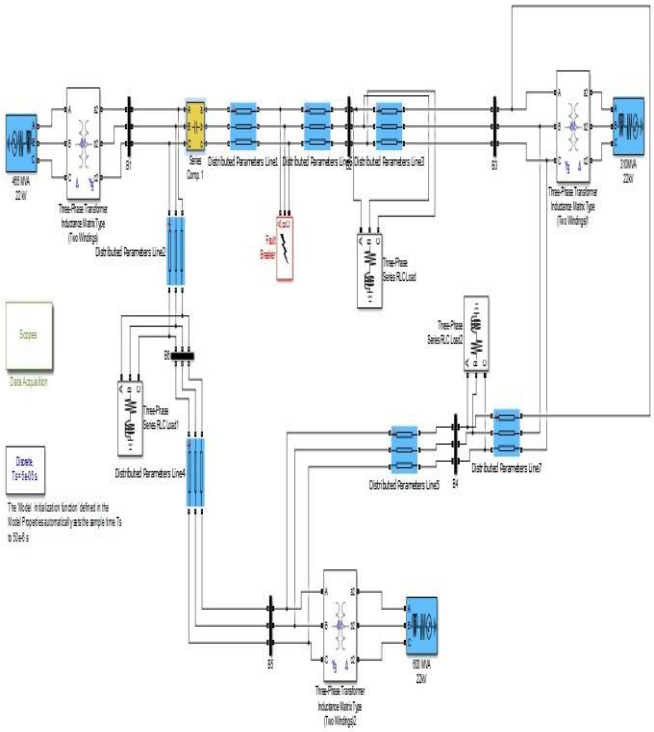

Fig.6. Simulink Implementation of 9 bus system

A. *Case-i : LG fault :*

An LG fault (AG-type) is created at 0.34 sec. on line 5-7 at a distance of 30 km from bus-5 for 0.04 sec. A capacitor is used in Line 5-7 with 40% compensation. The waveform got from different buses are studied below:

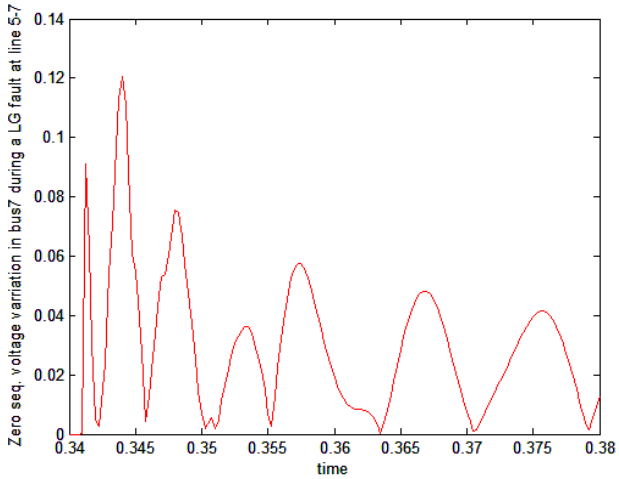

Fig.7(a). Zero Sequence Voltage Profile at bus7.

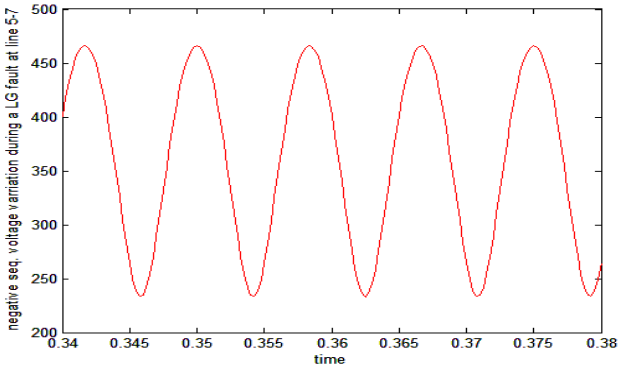

Fig7(b):Negative Sequence Voltage Profile at bus5.

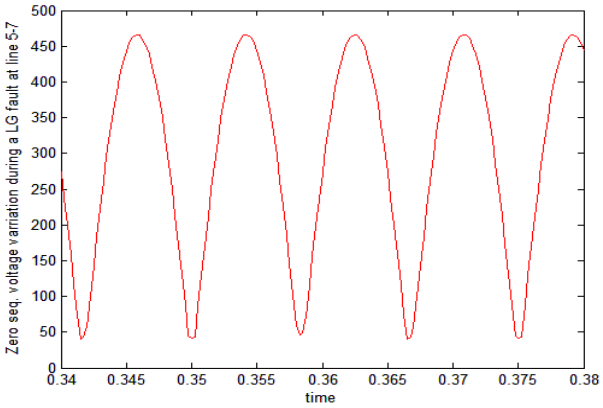

Fig.7(c). Zero Sequence Voltage Profile at bus5.

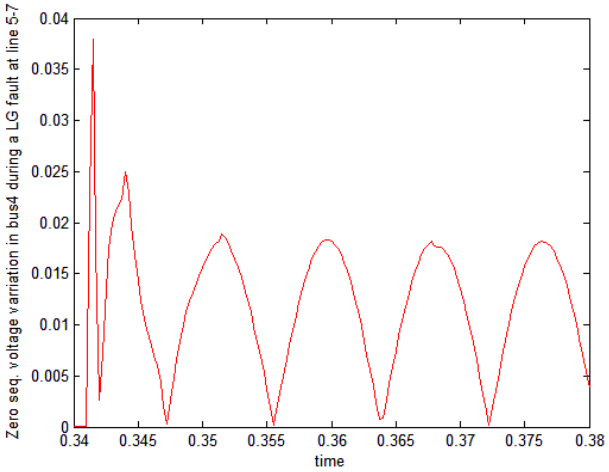

Fig.7(d). Zero Sequence Voltage Profile at bus4.

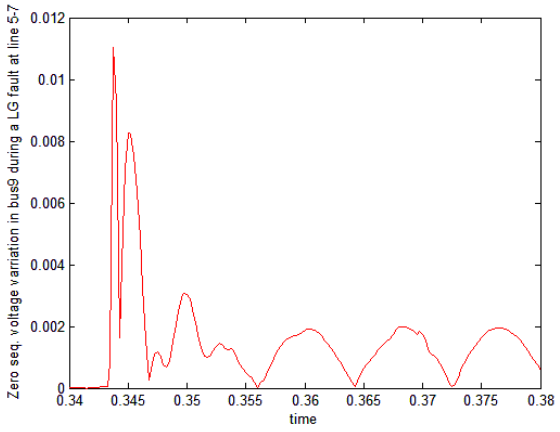

Fig.7(e). Zero Sequence Voltage Profile at bus9

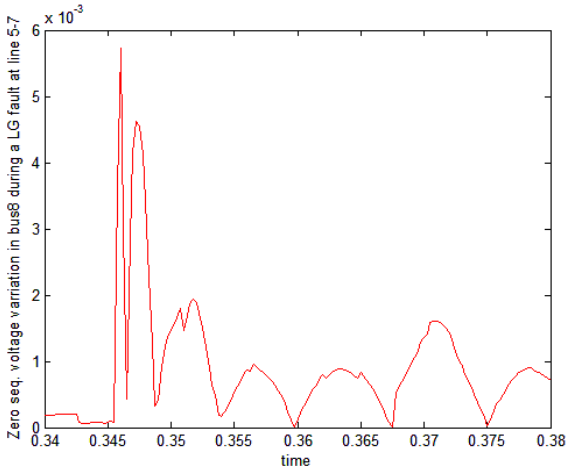

Fig.7(f). Zero Sequence Voltage Profile at bus8

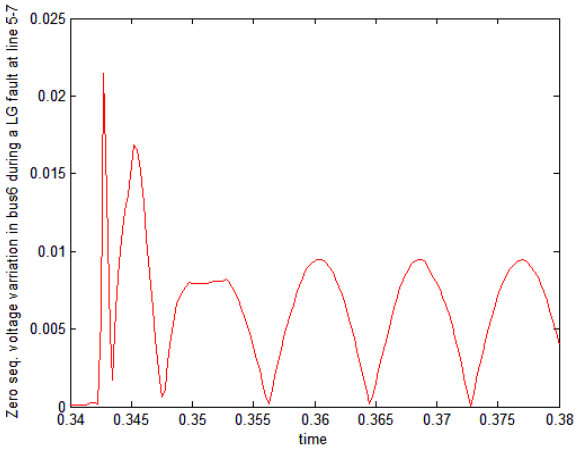

Fig.7(g). Zero Sequence Voltage Profile at bus6

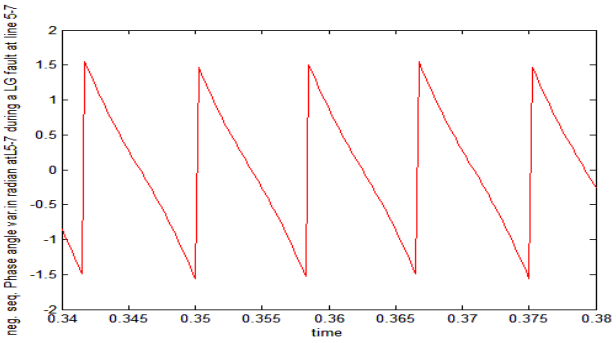

Fig.8(a). Phase Variation Line 5-7

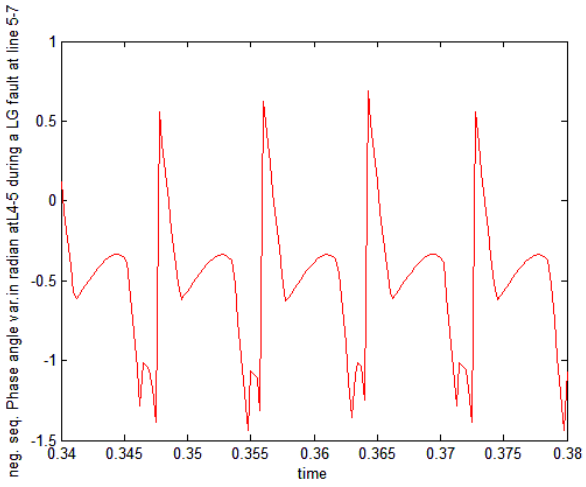

Fig.8(b). Phase Variation Line 4-5

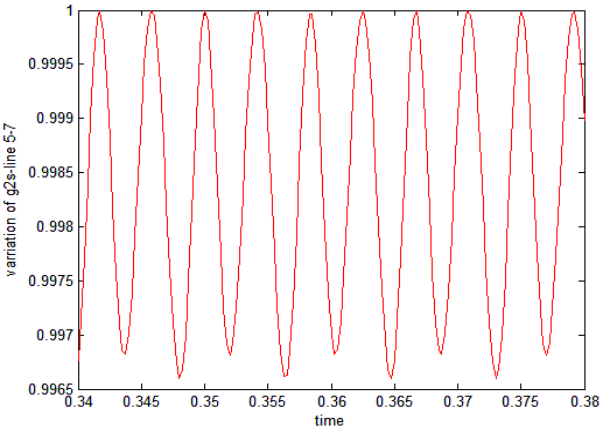

Fig.9(a). g_{2s} profile during LG fault

The observation of the figures 7(a), 7(b), 7(c), 7(d), 7(e), 7(f), 7(g) clearly shows it satisfies the equation (4), the pickup condition for unbalanced fault as:

$$K_2V_n = 40 \text{ KV} \qquad K_0V_n = 40 \text{ KV}$$

Bus 5 zero sequence voltage profile having maximum voltage magnitude among other buses in the network. So, the bus 5 data satisfy the criterion for an unbalanced fault and as bus 5 having maximum zero sequence magnitude, Bus5 is closest to the fault.

Two lines are adjacent to bus5.Line 5-7 and Line 4-5. The negative sequence phase variation is shown for those two lines are in figure 8(a), 8(b).The phase variation is expressed in radian. It is seen the variation of phase lies between - π/2 to +π/2 or -90degree to +90 degree.

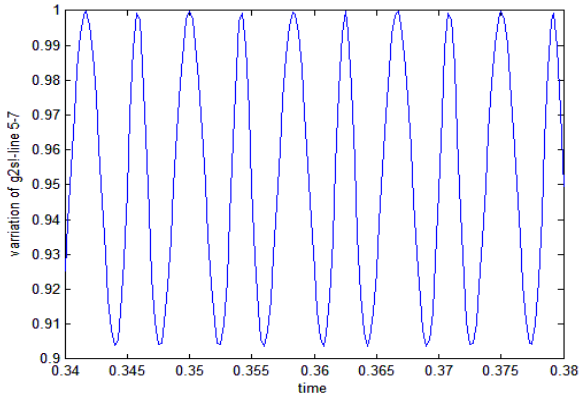

Fig.9(b). g_{2s} [1]profile during LG fault.

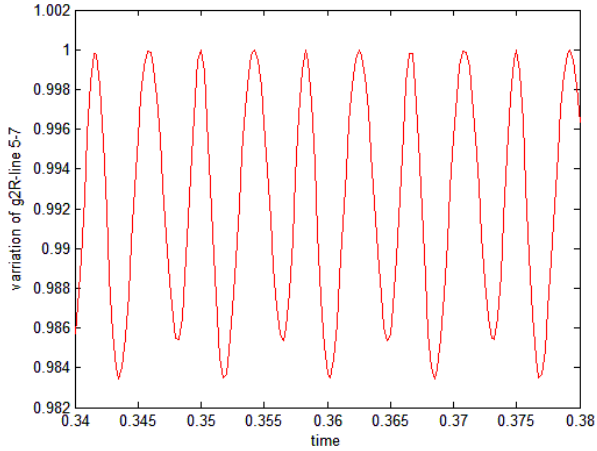

Fig.9(c). g_{2R} ` profile during LG fault

From the figures 8(a), 8(b) and 9(a), Fig.9(b), Fig.9(c),it is clear that line 5-7 is satisfying the equation (6), hence the criterion and authentication of an unbalanced fault .
So, line 5-7 is the faulted line.

B. Case-ii : LLL fault:

a 3-phase fault is created at 0.34 s on line 5-7 at a distance of 30km from bus-5 for 0.04 sec. After collecting all data, the following analysis has been done:

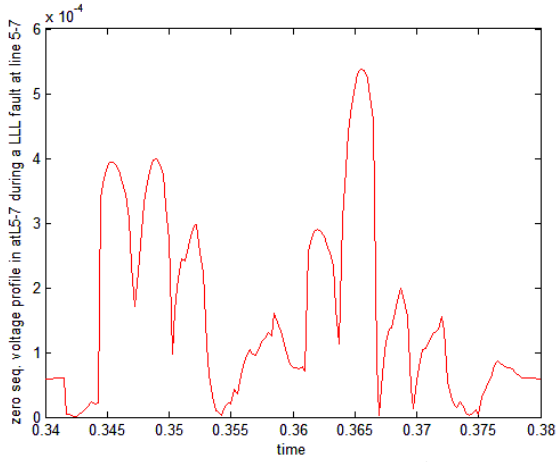

Fig.10(a). Zero Sequence Voltage Profile at bus5.

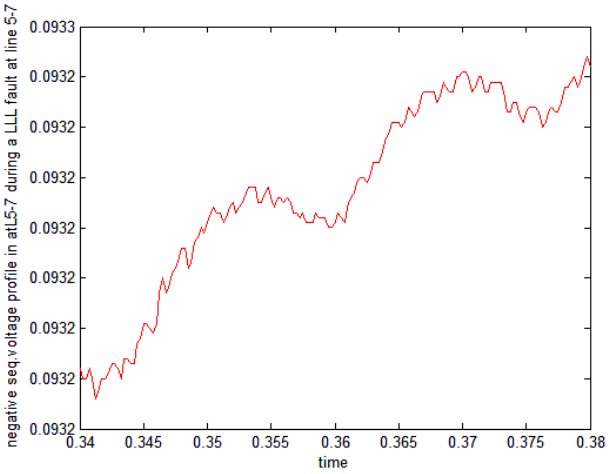

Fig.10(b). Negative Sequence Voltage Profile at bus5.

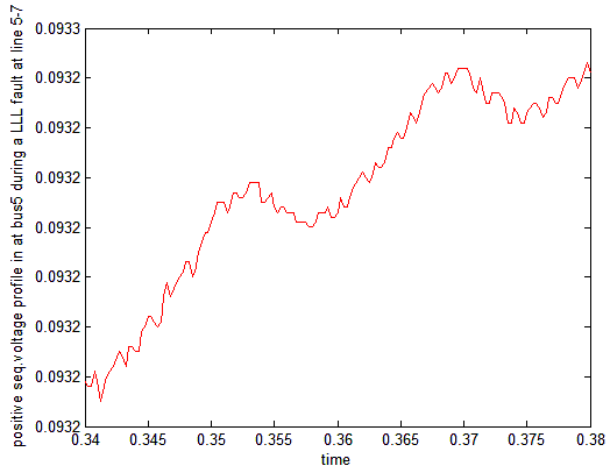

Fig.10(c). Positive Sequence Voltage Profile at bus5.

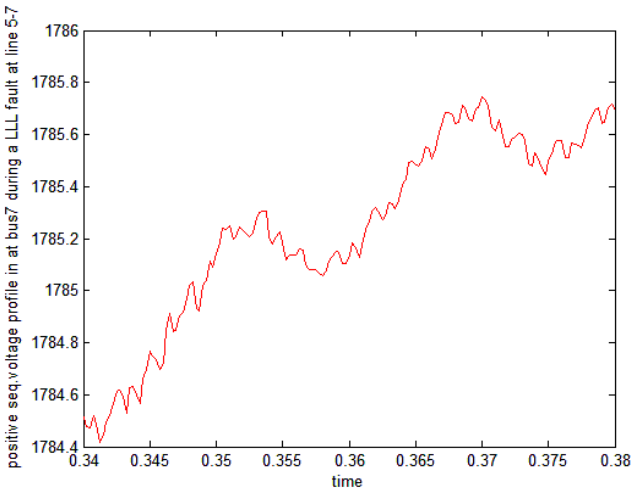

Fig.10(d). Positive Sequence Voltage Profile at bus7.

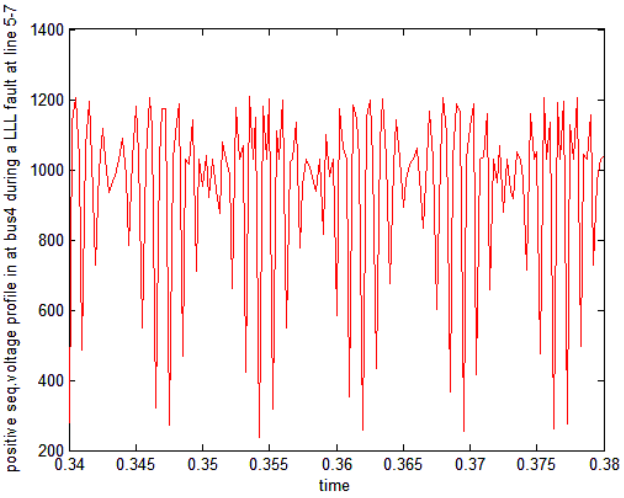

Fig.10(e). Positive Sequence Voltage Profile at bus4.

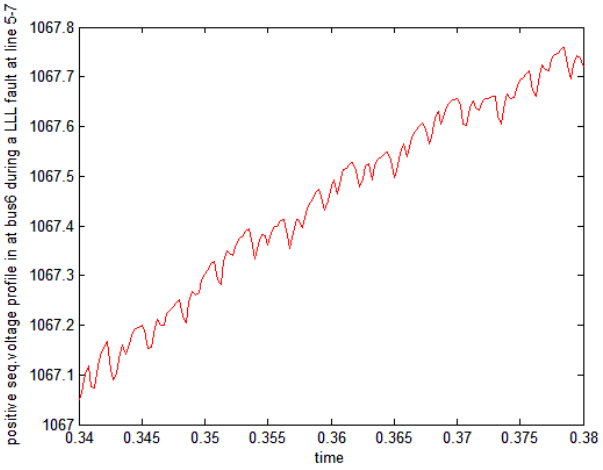

Fig.10(f). Positive Sequence Voltage Profile at bus6.

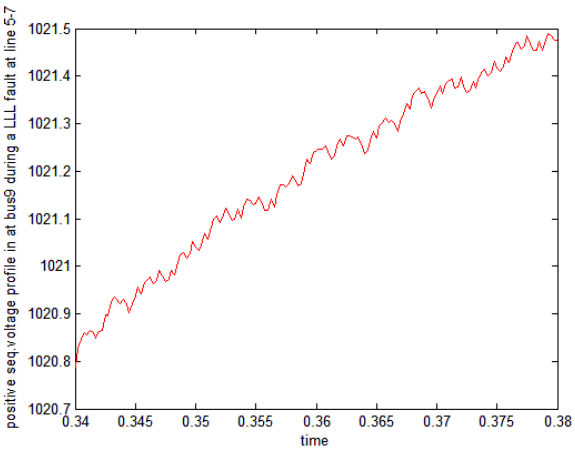

Fig.10(g). Positive Sequence Voltage Profile at bus9.

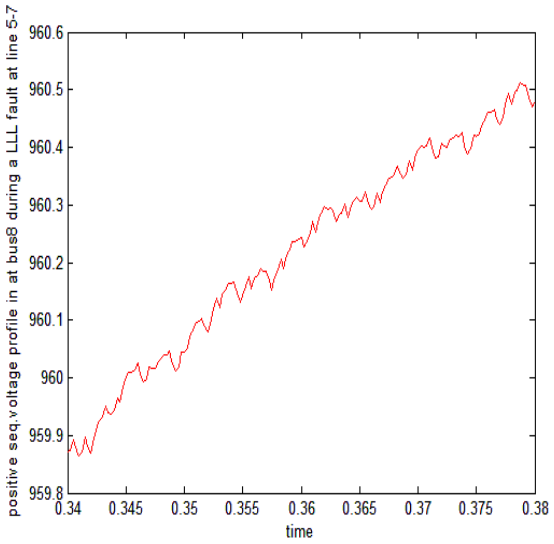

Fig.10(h). Positive Sequence Voltage Profile at bus8.

All the units of voltage are expressed in Kilo Volt (KV) here and time in second. The observation of the figure 10(a), 10(b), 10(c), 10(d), 10(e), 10(f), 10(g), 10(h) clearly shows it does not satisfy equation (4), the pickup condition for unbalanced fault.

as $V_{m2} \leq K_2V_n$ && $V_{m0} \leq K_0V_n$

$K_2V_n = 40KV$ $K_0V_n = 40$ KV

But it satisfies equation (5), the pickup criterion of a balanced fault as:

$K_1V_n = 240$ KV.

and minimum value of positive sequence voltage exist in bus5. So, bus 5 can be considered as bus nearest to the fault.

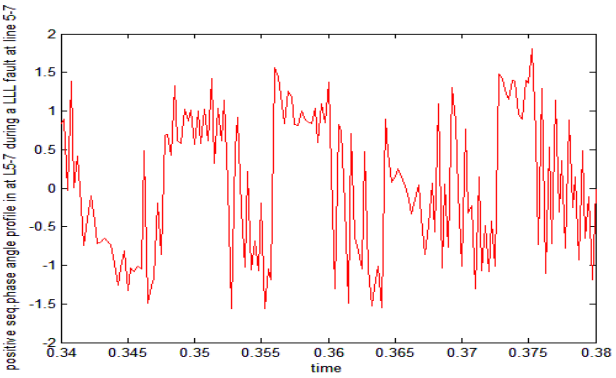

Fig.11(a). Phase Variation Line 5-7.

From the figures11(a), 11(b), 11(c) and 12(a), 12(b), 12(c) it is clear that line 5-7 is satisfying equation (7), and hence the criterion and authentication of a balanced fault. So, line 5-7 can be considered as the faulted line.

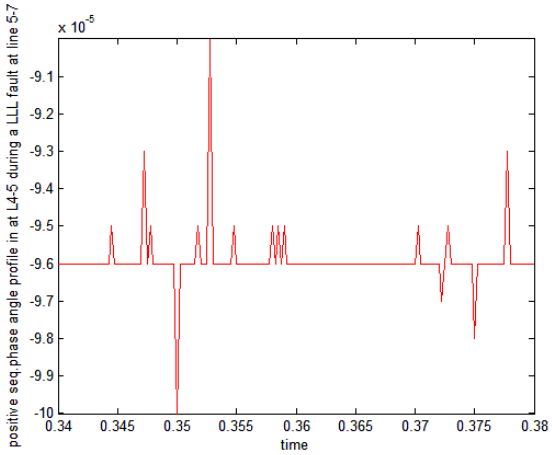

Fig.11(b).Phase Variation Line 4-5.

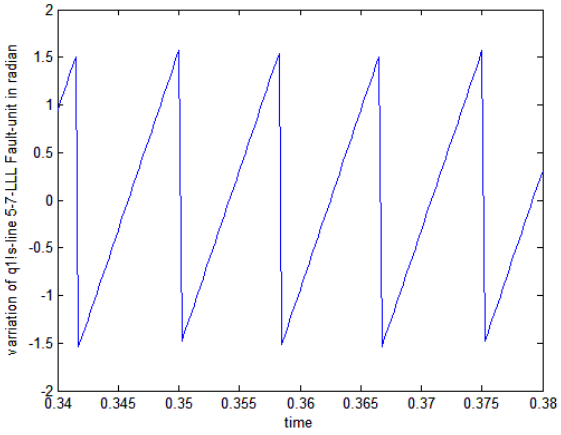

Fig.11(c).Variation of , $Ø_{1s}$ ' for Line 5-7

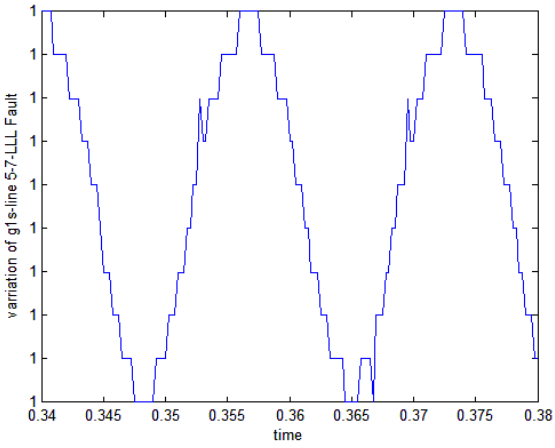

Fig.12(a). g_{1s} profile during LLL fault.

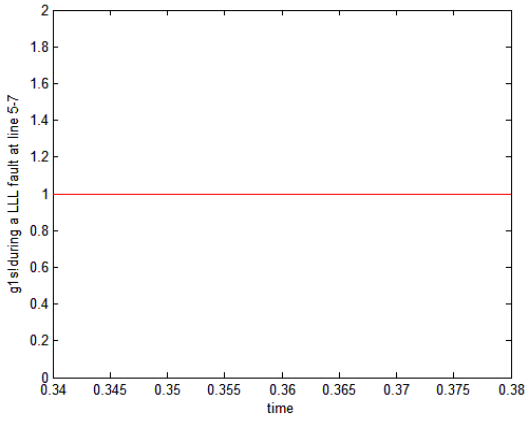

Fig.12(b). g_{1s}' profile during LLL fault.

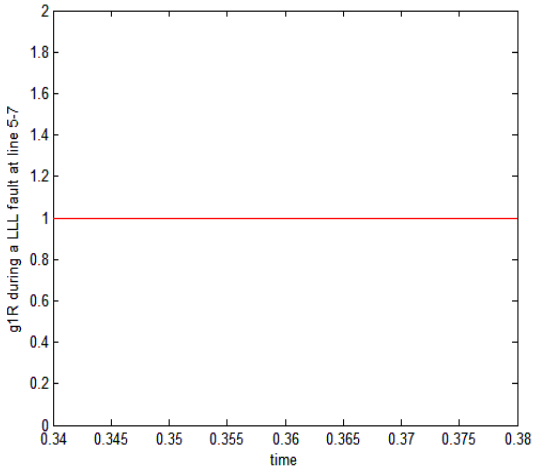

Fig.12(c). g_{1R} profile during LLL fault

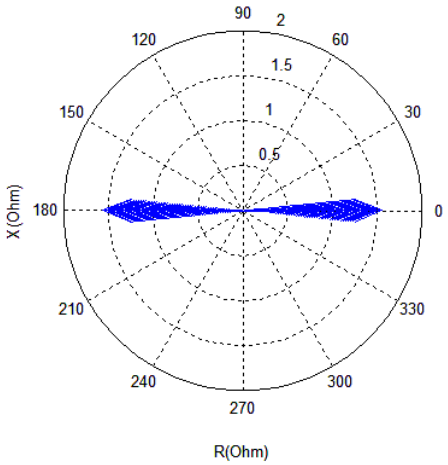

Fig.13(a). Positive Sequence Impedance Trajectory in Z-ø plane.

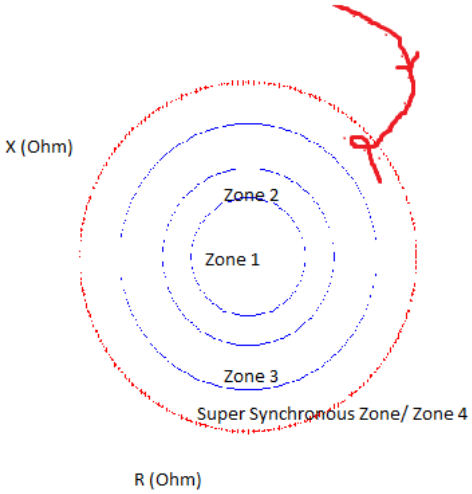

Fig.13(b). Positive Sequence Impedance Trajectory in Z-ø plane enters super synchronous zone (zone 4).

The positive sequence impedance of the test system seen by the relaying point during the fault is plotted in the impedance plane (Fig 13(a)). From the trajectory of the fault impedance, it can be concluded which zone the locus is confined and whether distance relay is going to generate any trip signal to circuit breaker or not and if there is any chance for evolving load encroachment problem or not. Fig.13(b) is showing another case of analysis of system behavior through analysis of impedance trajectory. Here we are considering another circle apart from 3 circles of 3-zone characteristics of relay, encircling zone 3 or relay characteristics. We are calling it as super synchronous zone or zone 4 of the relay. Zone 4 boundary is chosen very nearer to the boundary of zone 3 but greater than zone 3 circle boundary. If from the study of impedance characteristics of a system, we found that impedance trajectory entered in zone 4 or super synchronous zone of the relay characteristics then the system can be distinguished as prone to fault or prone to generate trip signal to the circuit breaker of the system. So, it can be said that, the system need precaution. This analysis can be used in case of condition based monitoring of the system to increase its reliability or security of operation. Thus the impedance trajectory is very helpful in judging several critical conditions of power systems including power swing or dynamic loading conditions (load encroachment etc.), fault prone conditions etc.

C. Case-iii: Simultaneous Faults:

Protection of power systems or occurrence of faults in a power network is not an isolated task. It may happen simultaneously. So, now the new WABP algorithm is tested under the condition of occurrence of simultaneous faults across the power network. And here also it is found that it is having immunity to support simultaneous occurrence of faults phenomena.

a) Bus5 and Bus9 both involved with LLL fault:

a LLL fault is created at 0.34 s on line 5-7 at a distance of 30km from bus-5 for 0.04sec and at the same time another LLL fault is created at line 8-9 at 0.35sec for 0.04 sec. The wave forms obtained from this case is studied below :

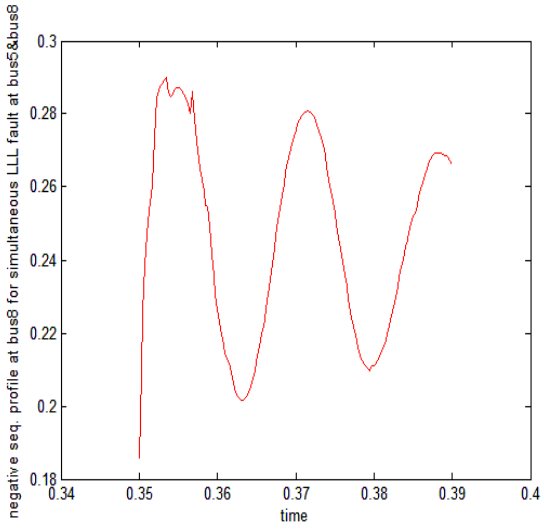

Fig.14(a). Negative Sequence Profile at bus8.

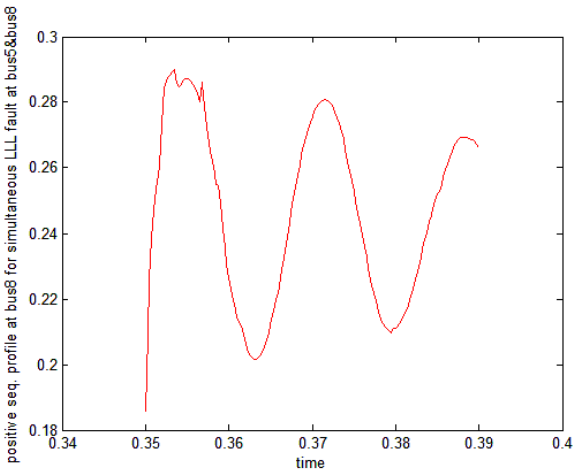

Fig.14(b). Positive Sequence Voltage Profile at bus8.

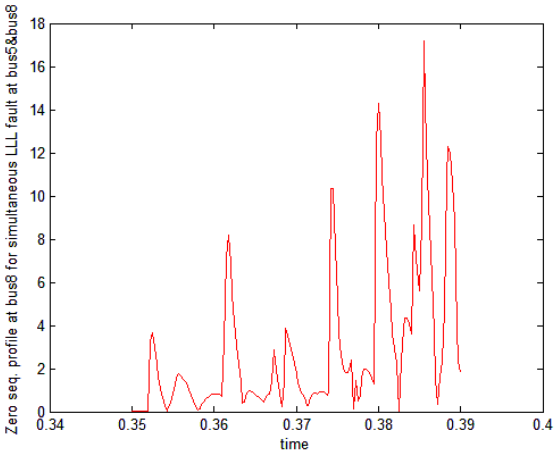

Fig.14(c). Zero Sequence Voltage Profile at bus8.

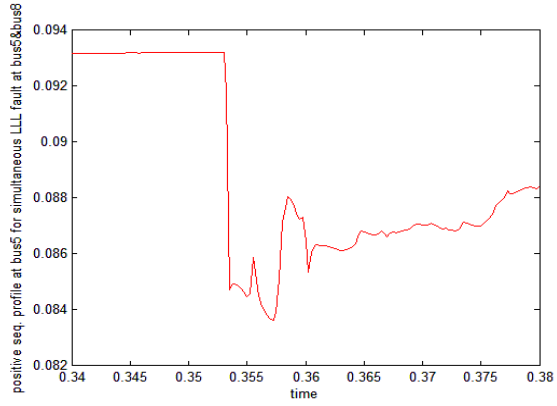

Fig.15(a). Positive Sequence Voltage Profile at bus5.

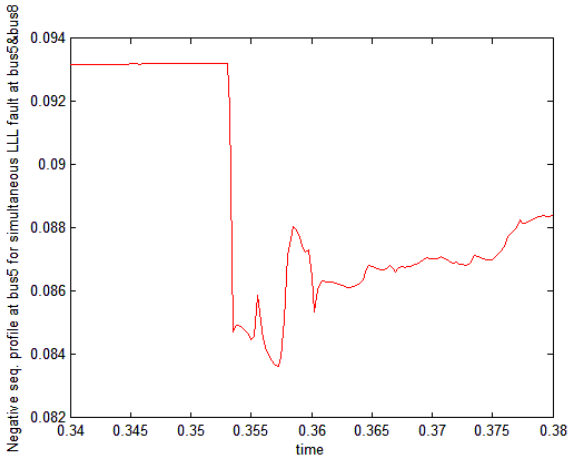

Fig.15(b). Negative Sequence Profile at bus5.

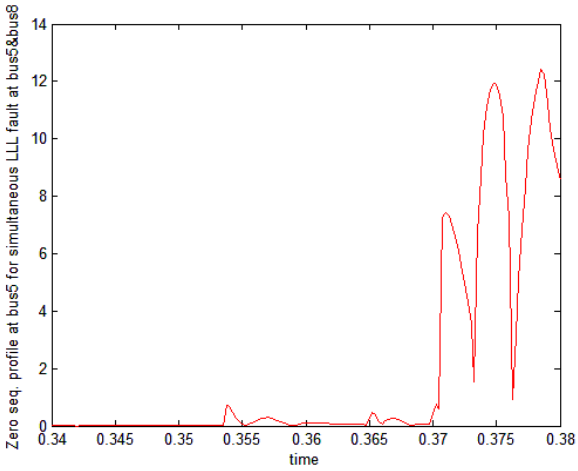

Fig.15(c). Zero Sequence Voltage Profile at bus5.

From the sequence voltage (positive, negative and zero) profiles at both the buses, it is evident both the buses individually satisfying the pickup criterion for a balanced fault.

b) Bus5 with LLL and Bus 9 with LLG Fault:

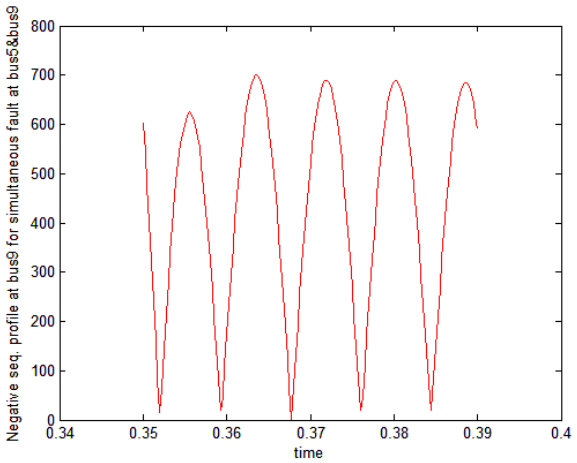

Fig.16(a). Negative Sequence Profile at bus9

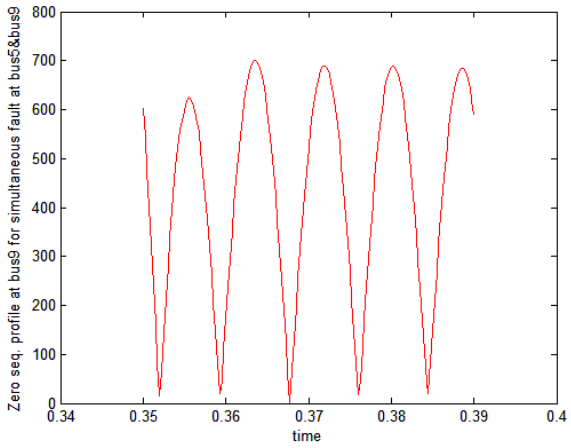

Fig.16(b). Zero Sequence Profile at bus9.

Here also both the sequence voltage profiles will satisfy their individual fault pick up criterion. However, depending on source, load and measurement errors in each substation and circumstances some samples may deviate from the pickup criteria. During critical conditions of power systems like- load encroachment and power swing conditions, the positive sequence impedance may enter zone3 of relay which can cause undesired tripping of lines. But in those cases FLI criterion will not satisfy and thus such events will declare as a non-fault situation by the scheme. Thus WABP Scheme mitigates the problem raised during critical conditions of power network (e.g-load encroachment and power swing conditions). So, this scheme works fine for Zone 3 protection support also.

D. Case-iv : Sources of error/ Limitation : Simultaneous Faults at different Lengths of the same Line :

A-G fault is created at Line 5-7 at 0.32 sec for 0.04 sec at 30KM distance from bus 5 and at the same time another fault is created on the same line and almost at the same distance (within 1km) for 0.34 sec for 0.04 sec which is a 3-phase fault. Now the fault voltage profile from 0.32 sec to 0.38 sec. for bus 5 is indicated as follows:

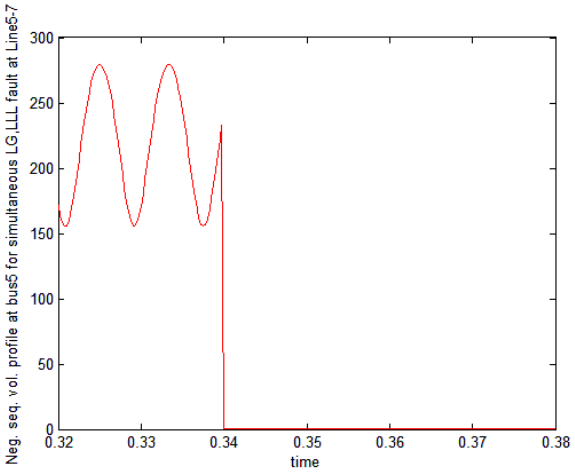

Fig.17(a). Negative Sequence Profile at bus5.

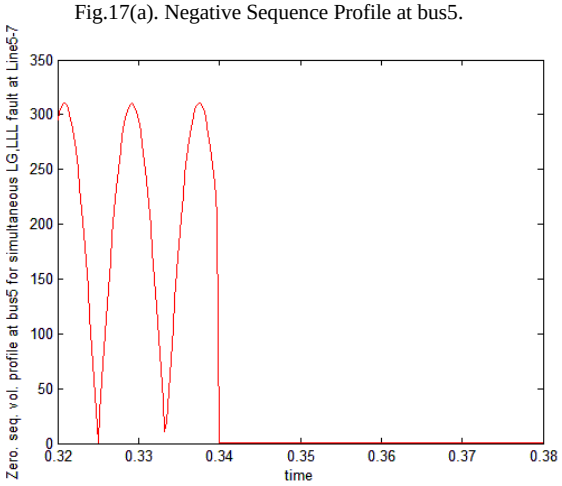

Fig.17(b). Zero Sequence Profile at bus5.

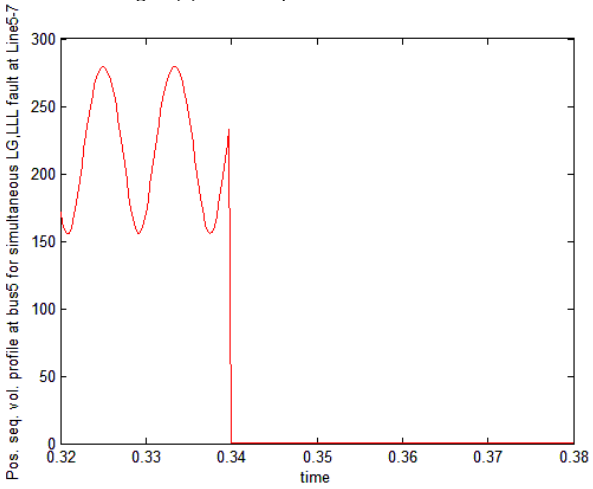

Fig.17(c). Positive Sequence Profile at bus5.

From the above figure no. 17(a), 17(b),17(c), it is clear that resultant waveforms having two parts.

i) up to 0.32-0.34 sec., it is obeying the pickup criterion of an unbalanced fault and

ii) 0.34-0.38 sec, the waveforms are obeying the pickup criterion for a balanced fault.

Theoretically, the wave should have three parts, 0.32-0.34 sec. unbalanced fault, 0.34-0.36 sec both balanced and unbalance fault exist in the line and 0.36-0.38 sec balanced fault exist in the line. Here the circuit is obeying superposition theorem of network. As 3-phase fault is the most severe fault in the circuit, it nullifies the effect of an unbalanced fault and predominates. So, with this scheme if some balanced fault is indicating, it may contain some percentage of simultaneous unbalanced faults also, in the line as faults in power system is not an isolated issue. This scheme is showing unbalanced fault means the line contains unbalanced faults only but in case of balanced fault, the line may contain some percentage of unbalanced faults also.

So, existence of Simultaneous faults in the same Line is confirmed with logic shown below.

i) Balanced + Unbalanced- Output Balanced
ii) Balanced+ Balanced- Output Balanced
iii) Unbalanced + Balanced- Output Balanced
iv) Unbalanced +Unbalanced –Output Unbalanced

With the existing scheme, it is difficult to distinguish the simultaneous faults in a same line. Moreover, depending on the several parameters and constraints of the power system like - source strength, demand of load and other errors in measurement and operation, some samples may deviate from their own pick up criterion sometimes.

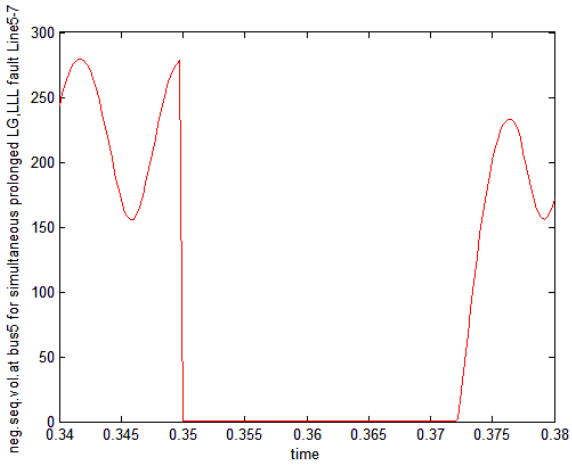

Fig.18. Negative Sequence Profile at bus5.

Fig.18 is another case study, where an A-G fault is created at 0.34 sec for 0.04 sec on Line 5-7 at 30KM distance, at the same time another close in fault which is a 3-phase fault by nature is created on the same line for 0.02sec. same as previous case between 0.35-0.37 sec., the balanced fault predominates and suppressed the effect of unbalanced A-G fault and once the balanced fault is cleared, between 0.37-0.38 sec, the effect of unbalanced fault is again seen. Thus output is a composite figure in nature. So, in the presence of a balanced fault, the effect of unbalanced fault cannot be distinguished as LLL fault predominates with respect to its degree of severity than LG fault. LLL is the most severe fault, however most occurred fault in power system is LG fault. Around over 70% fault occurred in the power systems are generally LG fault and

a perfect symmetrical fault occurred in a power system is seen to be very rare.

V. CONCLUSIONS

A Novel WABP scheme based on synchronized phasor measurements is proposed in this paper which can improve the operation of power system in several respects. The sequence components of voltage, phase angles and the sign of cosine of the angle between voltage and current at both ends of a line is used to identify the faulted area and faulted branch. Simulation results for the nine-bus power system show that the method performs accurately during several faults in systems, interconnected systems and simultaneous faults. Other than the simple setting principles, the scheme has the ability to distinguish the fault from load encroachment and power swing and can mitigate the shortcomings of the conventional backup protection scheme. It is helpful to prevent blackouts. Thus with the context of today's backup protection schemes, the scheme described here is commendable.

APPENDIX A

System data for 3-machine 9-bus configuration:

Gererators

Gen-1: 600 MVA,22KV,50HZ
Gen-2: 465 MVA,22KV,50HZ
Gen-3: 310 MVA,22KV,50HZ.

Transformers

T1: 600 MVA,22/400KV,50HZ,D/Y;
T2: 465 MVA,22/400KV,50HZ,D/Y;
T3: 310 MVA,22/400KV,50HZ,D/Y;

Transmission line:

Length of line 7-8=320Km.,line 8-9=400Km,line 7-5=310Km.,line 5-4=350Km,line 6-4=350Km,line 6-9=300km.

Loads

Load A=300MW+j100MVAr.
Load B=200MW+j75MVAr.
Load C=150MW+j75MVAr.
Other parameter used are same as used in Reference [11].

REFERENCES

[1] S. Horowitz and A. G. Phadke, "Third zone revisited", IEEE Transactions on Power Delivery, Vol.21, No.1, pp.23–29, Jan.2006.

[2] J.D. Ree, V. Centeno, J.S. Thorp, and A.G. Phadke, "Synchronized phasor measurement applications in Power systems, "IEEE Transactions on .Smart Grid, Vol.1, No.1, pp.20–27, June 2010.

[3] A.G. Phadke and J.S. Thorp, Synchronized Phasor Measurements and Their Applications. New York: Springer, 2008.

[4] M.M. Eissa, M. E. Masoud, and M.M.M. Elanwar, "A novel backup wide area protection technique for power transmission grids using phasor measurement unit, "IEEE Transactions on Power Delivery, Vol.25, No.1, pp. 270–278, Jan. 2010.

[5] P.V. Navalkar and S. A. Soman, "Secure remote backup protection of transmission lines using synchrophasors", IEEE Tranactions on Power Delivery, Vol.26, No.1, pp.87–96, Jan. 2011.

[6] H. Lin, S. Sambamoorthy, S. Shukla, J. Thorp, and L. Mili, "Ad-hoc vs. supervisory wide area backup relay protection validated on power/network co-simulation platform", presented at the 17th Power System Computation Conference., Stockholm, Sweden, Aug. 22–26, 2011.

[7] J. Ma, J. Li, J. S. Thorp, A. J. Arana, Q. Yang, and A. G. Phadke, "A fault steady state component-based wide area backup protection algorithm", IEEE Transactions on Smart Grid, Vol.2, No.3, pp.468–475, Sep.2011.

[8] Z.He, Z. Zhang,W. Chen,O. P.Malik, and X. Yin,"Wide-area backup protection algorithm based on fault component voltage distribution", IEEE Transactions on Power Delivery, Vol.26, No.4, pp.2752–2760, Oct. 2011.

[9] B. Kasztenny, "Distance protection of series-compensated lines:problems and solutions", presented at the 28th Annual Western Protective Relay Conference , Spokane, WA, USA, Oct. 22–25, 2001.

[10] D. Novosel, A. G. Phadke, M.M. Saha, and S. Lindahl, "Problems and solutions for microprocessor protection of series compensated lines", in Proceedings of Conference Development of Power System Protection, 1997, pp.18–23.

[11] Paresh Kumar Nayak, Ashok Kumar Pradhan, and Prabodh Bajpai, "A Fault Detection Technique for the Series compensated Line During Power Swing", IEEE Transactions on Power Delivery, Vol.28, No.2, April 2013, pp.714-722.

[12] S.N.Muneswar, R.Hasabe, D.Shelar, P.Kose, "A New Adaptive PMU based Protection Scheme for Interconnected Transmission Network System," 2014 International Conference on Circuit, Power and Computing Technologies [ICCPCT].

[13] P.K. Nayak, A.K. Pradhan, and P. Bajpai, "Wide-Area Measurement-Based Backup Protection for Power Network with Series Compensation", IEEE Transactions on Power Delivery, V.29, No.4, August 2014, pp.1970-1977.

[14] A.K. Pradhan, P. Jena, "Directional relaying in the presence of a thyristor-controlled series capacitor", PES General Meeting Conference & Exposition, 2014 IEEE, 27-31 July 2014.

[15] T. Routtenberg, Yao Xie, R.M. Willett, Lang Tong, "PMU Based Detection of Imbalance in Three-Phase Power Systems", IEEE Transactions on Power Systems ,Vol.30, No.4, July2015, pp.1966-1976.

[16] Ali.H.Al Mohammed, M.A. Abido, "A Fully Adaptive PMU-Based Fault Location Algorithm for Series compensated Lines", IEEE Transactions on Power Systems, Vol.29, No.5, September 2014, pp.2129-2137.

[17] I. Kamwa, S.R. Samantaray, G. Joos,"Wide Frequency Range Adaptive Phasor and Frequency PMU Algorithms", IEEE Transactions on Smart Grid,Vol.5, No.2, March 2014, pp.569-579.

[18] P. Kundu, A.K. Pradhan, "Online identification of Protection element failure using wide area measurements", IET Generation, Transmission and Distribution, 2015,Vol.9, No.2, pp.115-123.

[19] S. Roy, P.S. Babu, "Power swing protection of series compensated transmission line with novel fault detection technique", IEEE International Conference on Green Computing, Communication and Electrical Engineering [ICGCCEE], 6–8 March 2014, Coimbatore.

BIOGRAPHIES

SAPTARSHI ROY, received the B.E degree in Electrical Engineering from Jadavpur University, West Bengal, India in 2009.Received M.Tech degree from NIT WARANGAL in 2014. Currently he is pursuing PhD in Electrical Engineering in the department of Electrical Engineering, National Institute of Technology, Warangal, India. His areas of interest are power system protection, Phasor Measurement Unit applications in power systems, Synchro-phasors applications in power systems.

SURESH BABU PERLI, Currently he is working as an Assistant Professor in Department of Electrical Engineering, National Institute of Technology, Warangal. His areas of interest are Power System Protection with digital multifunction relays, Development of Adaptive protection schemes and Digital filtering algorithms.

Detection and Classification of Power Quality Disturbances in the Supply to Induction Motor Using Wavelet Transform and Neural Networks

Sridhar. S, K. Uma Rao and Sukrutha Jade

***Abstract*— This paper aims to represent a proposition of an innovative and novel methodology applicable in detecting and classifying the power quality disturbances present in the supply to the induction motor. In all practicality, considering circumstantial real world applications, induction motors are usually operated on load. If the supply voltage is varied in any way, it would adversely affect the normal operation of the motor. In the present work, a healthy induction motor is subjected to power quality disturbances like balanced voltage sag, balanced voltage swell, unbalanced voltage sag and unbalanced voltage swell. For the purpose of detecting these power quality disturbances, discrete wavelet transform is applied to the stator current of the induction motor. The stator current wavelet coefficients are fed as input to the neural network for the classification purpose. Radial basis neural network and feed forward neural network have been independently trained and tested. The observation about the feedforward network having higher performance efficiency as compared to the radial basis network, has been seen.**

Index Terms— **Induction motor, power quality disturbances, discrete wavelet transforms, feedforward neural network, radial basis neural network.**

I. INTRODUCTION

DESPITE espite several precautions taken, supply in the grid is never perfectly balanced. Due to this imbalance in the supply, a lot of harmonics are generated which will lead to increase in losses and decrease in efficiency of the machine which is directly connected to them. If an induction motor is subjected to power quality (PQ) disturbance repeatedly, when operating on critical loads, it leads to its malfunctioning and would also lead to internal failures in the machine. Along with unbalanced voltage, the other power quality (PQ) disturbances whose effect is detrimental to the operation of a healthy induction motor are voltage sag, swell, harmonics, short interruptions, impulse surges, overvoltage and under voltage [1-2].

Sridhar. S, is with Department of Electrical and Electronics Engineering, RNS Institute of Technology, VTU, Bangalore, India, (e-mail: prof_sridhar6@rediffmail.com).

K.Uma Rao, is with Department of Electrical and Electronics Engineering, R.V College of Engineering, VTU, Bangalore, India, (e-mail: umaraok@rvce.edu.in).

Sukrutha Jade, is with Robert Bosch Engineering and Business Solutions Bangalore, INDIA (e-mail: sukrutha.jade@gmail.com).

Identification and mitigation of PQ disturbances are of primary concern for power quality engineers. Since power quality disturbances are non-stationary in nature, it calls for advanced tools and techniques for its analysis. Though Fast Fourier Transforms (FFT), Short Time Fourier Transforms (STFT) are good signal processing techniques, they suffer from the fact that FFT provides only spectral information of the signal without time localization, and STFT provides fixed window width, which is more suitable for stationary signals. Wavelet transform is an excellent tool for the analysis of not-stationary signal as it employs a flexible window to obtain both time and spectral information of the signal. These signal processing techniques in conjunction with certain classification techniques like a neural network, fuzzy logic, neuro- fuzzy, support vector machine and expert systems have been used in the past for the classification of the power quality disturbances [3-14]. Chuah Heng Keow et al [15] has proposed a scheme for enhancing power quality problem classification based on wavelet transform and a rule-based method.

Primarily, this paper aims to categorize the balanced supply to the induction motor from balanced voltage sag, balanced voltage swell, unbalanced voltage sag and unbalanced voltage swell in the magnitude of the supply. A 3 phase, 3.2KW, 400V, 50Hz, 4 pole induction motor is selected to perform the simulation. The MATLAB SIMULINK software has been employed to carry out the entire simulation. Samples of the stator current of the induction motor are taken with a sampling frequency of 100 KHz and is processed by an 11^{th} level Daubechies-9 (DB9) wavelet for the efficient extraction of the signatories of the disturbances. Multilayer feedforward neural network (FFNN) and radial basis neural network (RBNN) are independently trained and tested for the identification of an optimal network for the classification of the disturbance. The classification accuracy of all the networks are compared and presented.

II. FEATURE EXTRACTION USING WAVELET TRANSFORM

The detection of PQ disturbance involves feature extraction, followed by classification. The discrete wavelet transform is applied to the stator current for extracting the signature of the fault. In each step, the wavelet transform applies the scaling function and wavelet function to the input data. Wavelet

decomposition is achieved by passing the input sampled signal through a high-pass filter g(n) and a low pass filter h(n) as seen in Fig 1. At each level, half of the signal samples are eliminated. At the end of first level of decomposition, the resultant approximate ($cA_1(n)$) and detail coefficients($cD_1(n)$) are obtained, which are given by

$$cA_i(n) = \sum kf(n) * h_d(-k+2n) \quad (1)$$

$$cD_i(n) = \sum kf(n) * g_d(-k+2n) \quad (2)$$

The second level approximate ($cA_2(n)$) and detail coefficients($cD_2(n)$) are based on level 1 approximate coefficients($cA_1(n)$). The iteration of this process continues till 'n' levels and ends when all the wavelet coefficients are known. Fig 2 gives a three level wavelet decomposition tree. The wavelet coefficients determine whether there is a discontinuity in the function or not. These coefficients are fed as input to neural networks for training.

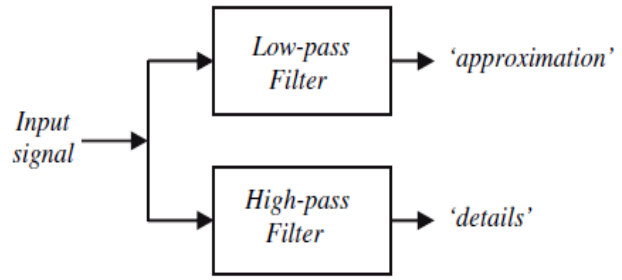

Fig. 1. one level decomposition

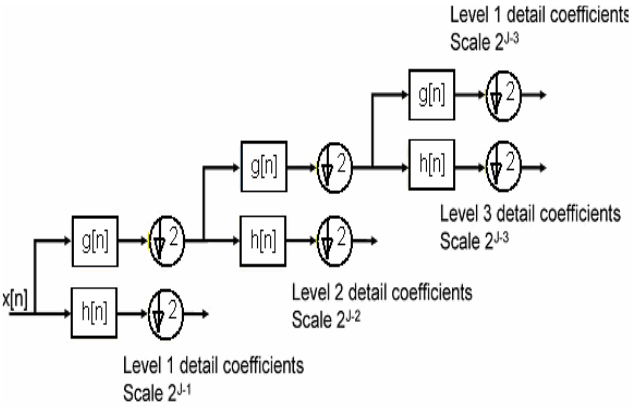

Fig. 2. 3 leveled wavelet tree.

III. CLASSIFICATION USING NEURAL NETWORK

Neural networks have been extensively used for the classification because of their large data handling capability. They are used to recognize and classify complex fault patterns without much knowledge about the system they deal with. The neural networks are described by the transfer function of their neurons, by training algorithm and by the connecting formula. Two different neural networks are considered in this paper.

1. Feed forward neural network
2. Radial basis neural network

A. Feed Forward Neural Network

Fig. 3 shows the network architecture of the feed forward neural network whose overall input-output behavior is determined by a collection of changeable parameters. Given the inputs $x = [x_1, x_2, x_3, \ldots, x_n]^T$ and weights w, the neural network computes the output $y = [y_1, y_2, y_3, \ldots, y_n]^T$. The network contains a set of source nodes that comprise of the input layer, 1 or more hidden layers, and an output layer. The propagation of the flow of the input signal through the network occurs in the forward direction on a layer-by-layer basis. There is no link between nodes in the same layer. The output of the *j*th node o_f in layer *l*, for $j = 1, 2, \ldots, k$ can be found from the quantity expressed as,

$$o_j = f\left(\sum_{i=1}^{k} w_{ji} v_i + b_j\right) = f\left(w_j^T V + b_j\right) \quad (3)$$

Where b_j is the bias of the j^{th} neuron, w_{ji} are weighted; v_i are inputs and f is the activation function. The sigmoid function is the most popular activation function because of its similarity to the behavioral property of many biological neurons. The sigmoid function can be expressed as,

$$o_j = \frac{1}{1+e^{-\left(w_j^T V + b_j\right)}} \quad (4)$$

During the feed-forward computation, the neural network weights *w* is fixed. This network is usually preferred because of its modularity, i.e., nodes in the same layer have the same functionality about input vectors. The mapping between input and output nodes may be either a linear or highly nonlinear relationship depending upon the activation function used in the network. Back propagation algorithm is a very commonly used training algorithm for training the neural networks.

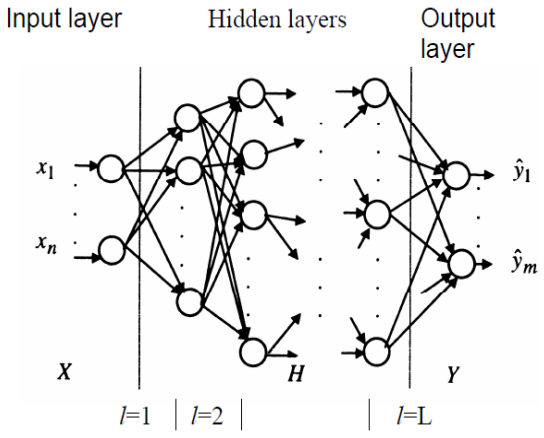

Fig. 3. Multilayer feeds forward network

B. Radial basis neural network

The block diagram of a version of an RBF classifier with one hidden layer is shown in Fig. 4. Each unit in the hidden layer of the RBF network has its centroid, and for each input

$x= (x_1,x_2,\ldots, x_r)$, it computes the distance between x and its centroid. Its output is a nonlinear function of the distance. Thus, each kernel node in the RBF network computes an output that depends on a radially symmetric function, and usually, the strongest output is obtained when the input is near the centroid of the node. For r input nodes and m output nodes, the overall response function without considering nonlinearity in an output node has the following form:

$$\sum_{i=1}^{M} w_i \cdot K\left(\frac{x - Z_i}{\sigma_i}\right) = \sum_{i=1}^{M} w_i \cdot g\left(\frac{\|x - Z_i\|}{\sigma_i}\right) \quad (5)$$

where M ϵ N the set of natural numbers is the number of kernel nodes in the hidden layer, w_i ϵ R^m is the vector of weights from the i^{th} kernel node to the output nodes, *x* is an input vector ,K is a radially symmetric kernel function of a unit in the hidden layer, z_i and σ_i, are the centroid and smoothing factor (or width) of the i^{th} kernel node, respectively, and g: $[0,\infty) \rightarrow R$ is a function called the activation function, which characterizes the kernel shape.

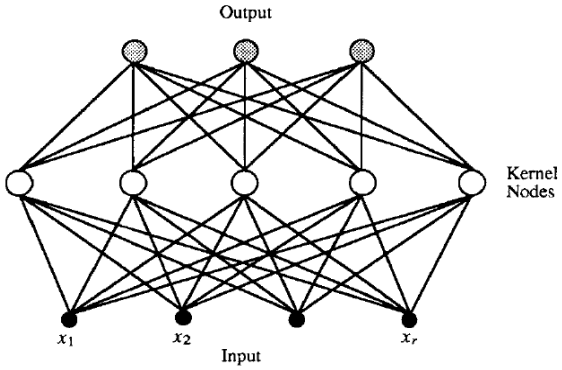

Fig. 4. A radial basis function network

The commonly used radial basis activation functions are multiquardratic and Gaussian. The multiquardratic function is given by

$$p(\gamma) = \frac{1}{\left(c^2 + \gamma^2\right)^{\alpha}}, \ \alpha>0 \quad (6)$$

and Gaussian function is given by,

$$p(\gamma) = \exp(-\gamma^2) \quad (7)$$

IV. PROPOSED METHODOLOGY

In identifying the PQ disturbance, extracting features, and characteristics is the primary step. When the machine is normally running on load. The sample of stator currents are taken with a sampling frequency of 100 KHz for the extraction of signature of the fault and is processed by Ann 11^{th} level DWT. The methodology proposed in this paper is designed to recognize

- Balanced sag and unbalanced sag as seen in Fig. 5
- Balanced swell and unbalanced swell as seen in Fig. 6

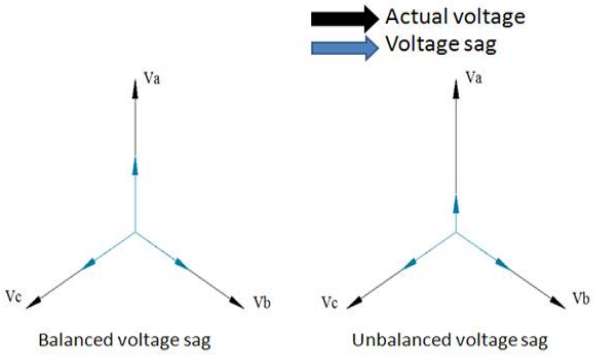

Fig. 5. Pictorial representation of balanced and unbalanced sag.

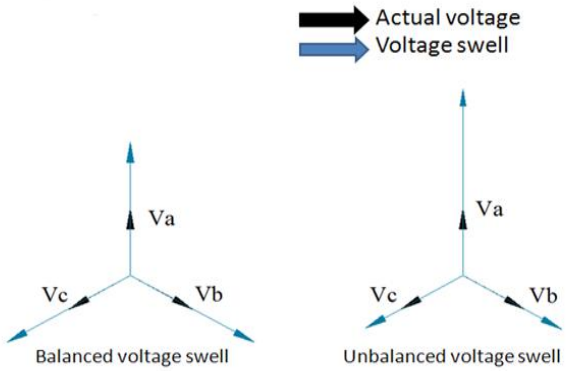

Fig. 6. Pictorial representation of balanced and unbalanced swell.

The final classification of PQ disturbances is obtained using neural networks, which takes wavelet coefficients as input. Fig. 7 shows the generalized block diagram of the neural network. The target vector consists of 3 columns.

- The first column (y_1) indicates the health of the supply (1for balance or 0 for unbalancing).
- The second column (y_2) indicates sag/ swell if any in present in the supply voltage (-1 indicates sag and +1 indicates swell). If the supply is balanced with no sag and swell, then this column indicates 0.
- The third column (y_3) provides the percentage of sag or swells present if any.

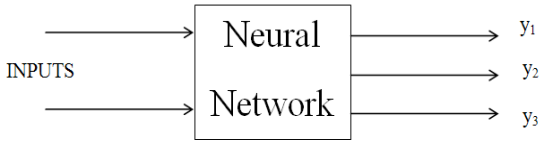

Fig. 7. Generalized block diagram of neural network

Before its utilization in the classification process, the neural network is thoroughly trained. The proposed methodology is implemented using the following steps.

Step 1. Sample the stator current of the induction motor.

Step 2. Computation of the wavelet coefficient of the stator current is done.

Step 3. The so obtained wavelet coefficients are given as input to the neural network.

Step 4. Classification of the type of existing voltage variation is done.

Step 5. The type of voltage variation is displayed if found to exists.

Step 6. Display the percentage of voltage variation if any.

These steps are executed for both FFNN and RBNN. The neural network which gives the best classification is finally considered. The Simulink block diagram used for the creation of the PQ disturbances in the supply of the induction motor is given by Fig.8. The three phase programmable voltage source in varied for obtaining different types of PQ disturbances. The three phase VI measurement block is used to observe the variations in the supply voltage. A 3 phase, 3.2KW, 400V, 50Hz, 4 pole induction motor is selected to perform the simulation. The induction motor is operated at full load, with a full load torque of 30.25 N-m. The novelty of the proposed methodology is that one phase stator current (phase A) in alone used for obtaining the signature of the PQ disturbances, unlike other cases where all the 3 phase currents are used for obtaining the signature of the PQ disturbances.

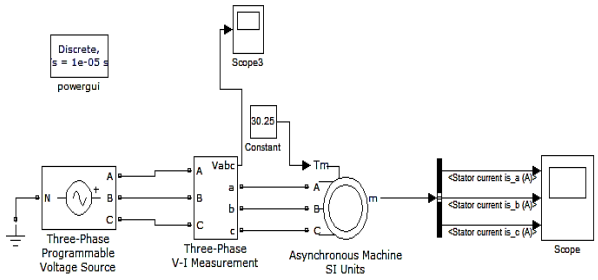

Fig. 8: Matlab/ Simulink block diagram.

V. RESULTS AND DISCUSSION

The stator current of phase A corresponding to balanced supply, supply with balanced sag and unbalanced sag, supply with balanced swell and unbalanced swell are as given in Fig. 9 to Fig 13.

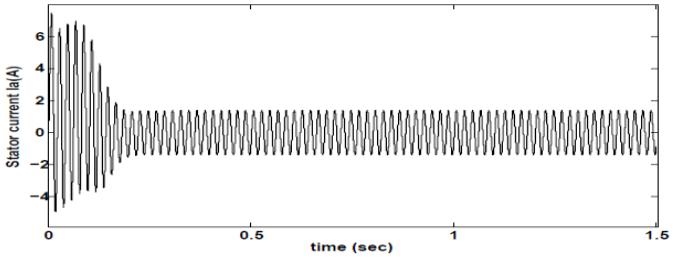

Fig.9. Stator current of healthy machine with balanced supply

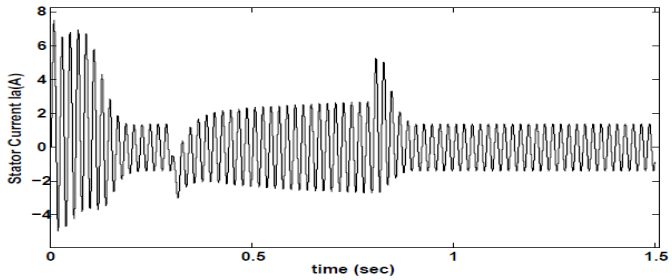

Fig.10. Stator current of healthy machine supplied with 40% sag in the supply

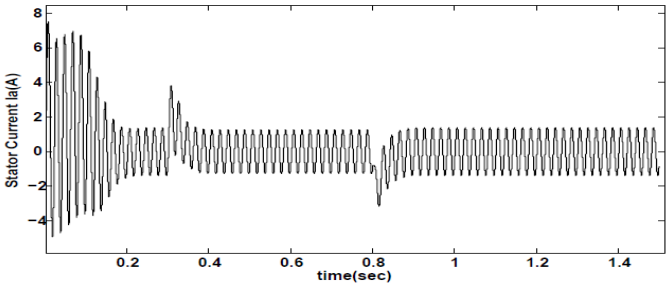

Fig.11. Stator current of healthy machine supplied with 40% swell in the supply

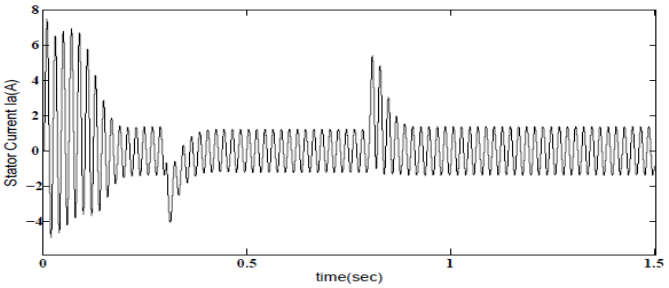

Fig.12. Stator current of healthy machine supplied with 40% unbalanced sag in the supply

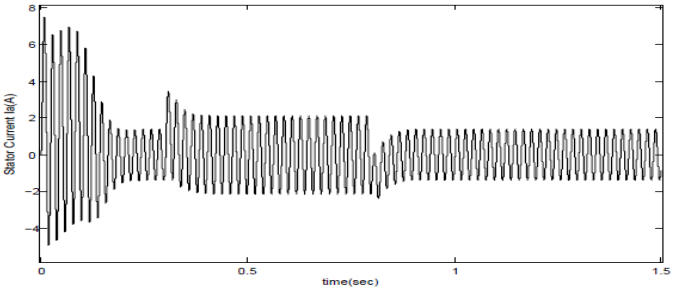

Fig.13.Stator current of healthy machine supplied with 40% unbalanced swell in the supply

The sample of the stator currents are taken with a sampling frequency of 100 KHz. The type of the mother wavelet chosen, the order of the wavelet and the number of decomposition levels are crucial for obtaining an effective output. In the present work, the suitability of the Daubechies wavelet-9 (DB9) has been ascertained, after several comparative studies between different wavelets. The number of levels of decomposition L is calculated according to the following formula [16].

$$L \geq \text{int}\left[\frac{\log\left(\frac{f_s}{f}\right)}{\log 2}\right] \quad (8)$$

Where f_s is the sampling frequency and f is the supply frequency of the stator current. For a 50Hz signal with a sampling frequency of 100 KHz, the number of levels of decomposition is found to be 11 as calculated from equation (8). The 11th level detailed coefficients are feed as inputs for further classification using neural networks. The final stage involves classification of the PQ disturbances using suitable network architecture

A. Classification using feedforward neural networks

The training of the neural network has been performed taking 37 inputs (1 balanced supply and 36 cases of PQ disturbance in the supply voltage), each containing 114 wavelet coefficients. During the training procedure, observation has been made regarding the fact that the selection of the neural network architecture, i.e., the number of layers, the number of neurons in each layer and the activation function play an essential role towards successful classification. Hence considering all these parameters, a feed forward neural network was created using Conjugate gradient backpropagation with Powell-Beale restarts as training function. Table 1 shows the number of hidden layers, number of neurons in the hidden layer with its transfer function, number of iterations, execution time, gradient, performance and classification accuracy of the proposed network.

Though faster performance with reduced number of the epoch, and faster convergence with accurate classification is always preferable, in practice a compromise has to be made with few of these parameters, as an ideal neural network is never realizable. The ultimate aim of the FFNN is always to obtain good classification accuracy. The corresponding parameters of the network for the highest accuracy are highlighted in Table-I. The network contains 1 input layer, 2 hidden layers with 750 neurons and 600 neurons respective layers, and 1 output layer with 3 neurons. *The tan-sigmoid* transfer function is used for training the hidden layers while *purelin* transfer function is used for training the output layer. Fig. 14 shows the performance plot of the proposed network. Linear regression between the output of the neural network and the target is performed. The regression coefficients show that the target and ANN output values match very closely as seen in Fig. 15.

TABLE I
FEEDFORWARD NEURAL NETWORK WITH CONJUGATE GRADIENT BACKPROPAGATION WITH POWELL-BEALE RESTARTS AS TRAINING FUNCTION

NUMBER OF HIDDEN LAYERS	NUMBER OF NEURONS IN EACH LAYER AND ITS TRANSFER FUNCTION	NUMBER OF ITERATIONS	EXECUTION TIME (IN MIN)	GRADIENT	PERFORMANCE	CLASSIFICATION ACCURACY
2	600 500 TAN TAN	293	0:40	5.60	0.005	80%
	600 500 TAN LOG	184	0:24	0.48	0.000417	50%
	750 600 TAN TAN	**277**	**0:54**	**6.87**	**0.00836**	**98.5%**
	700 600 TAN TAN	247	0:43	10.4	0.024	88%
	700 600 TAN LOG	289	0:48	0.311	$5.2E^{-5}$	60%

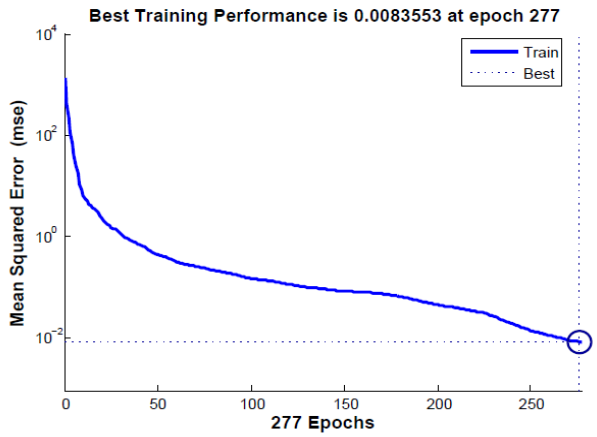

Fig. 14: performance plot of FFNN

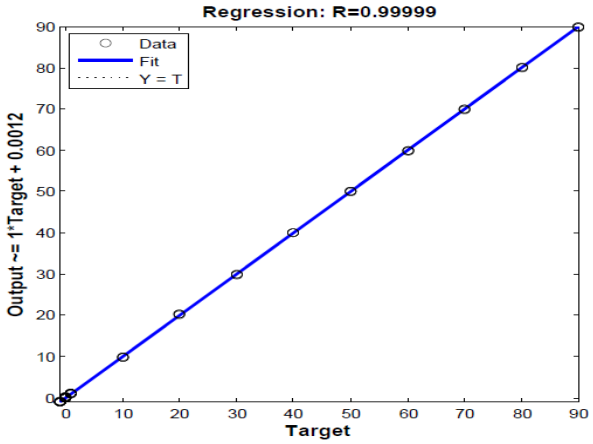

Fig. 15: Regression plot of FFNN

25 additional test data corresponding to each case of the disturbance were generated For the purpose of evaluating the proposed FFNN. Table II gives the classification results for different types of disturbance for FFNN. The accuracy of the classification is 94.1% for balanced sag, 100% for balanced swell, unbalanced sag and unbalanced swell as seen in Fig 16. Further prediction accuracy was 100% for trained data, 98% of test data and overall accuracy being 98.53% as seen in Fig 17.

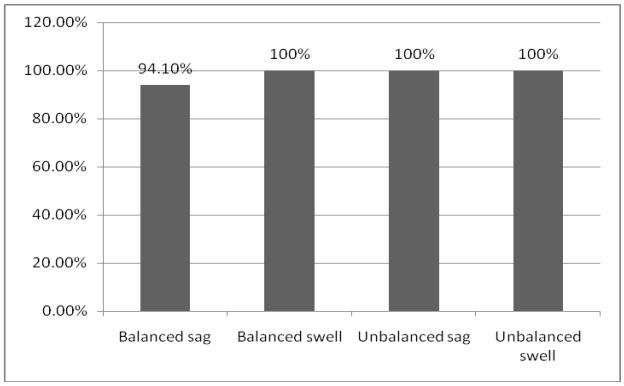

Fig. 16: The accuracy of classification for different types of disturbance

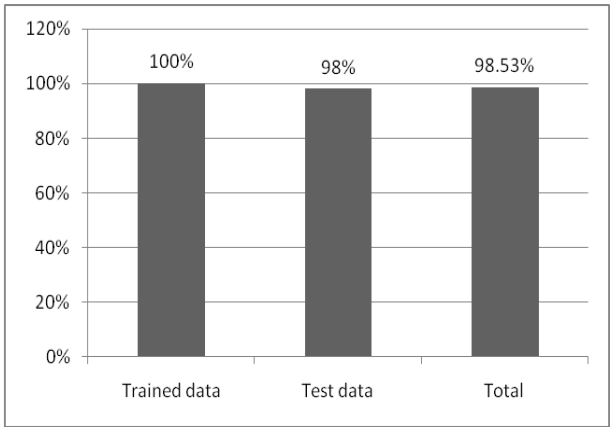

Fig. 17: The accuracy of classification for trained data, testing data, and total data.

TABLE II
THE RESULT OF CLASSIFICATION FOR DIFFERENT TYPES OF DISTURBANCE USING FFNN

Sl. No.	Type of disturbance	Trained data	Testing data	Total	Accuracy
1	Balanced sag	9/9	23/25	32/34	94.1%
2	Balanced swell	9/9	25/25	34/34	100%
3	Unbalanced sag	9/9	25/25	34/34	100%
4	Unbalanced swell	9/9	25/25	34/34	100%
Grand total		36/36	98/100	134/136	98.53%
Percentage column wise		100%	98%	98.53%	--

B. Classification using radial basis neural network

Table III shows the goal, spread, epoch, performance, gradient, validation check, step size and classification accuracy for RBNN. The training function for training the RBNN employs the use of Conjugate gradient backpropagation with Powell-Beale restarts. It is observed that the radial basis network is sensitive to spread but highly sensitive to variation in goal. Hence to obtain an optimal network for good classification, both goal and spread are varied, and the results are tabulated in Table 3. The network with highest classification accuracy is highlighted in Table 3 and is used for the classification purpose. Fig. 18 shows regression plot for the chosen network. From Fig. 18 it is seen that the target and ANN output values match closely to each other.

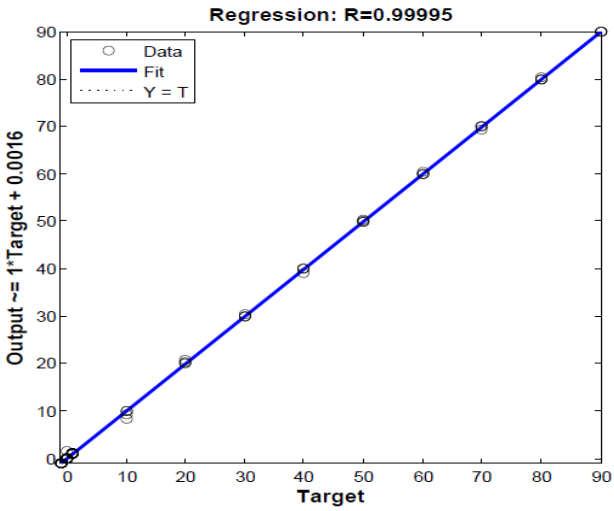

Fig. 18. Regression plot for RBNN

TABLE III
RADIAL BASIS NEURAL NETWORK (RBNN) WITH CONJUGATE GRADIENT BACKPROPAGATION WITH POWELL-BEALE RESTARTS AS TRAINING FUNCTION

GOAL	SPREAD	EPOCH	PERFORMANCE	GRADIENT	VALIDATION CHECK	STEP SIZE	CLASSIFICATION ACCURACY
0	30	0	$8.22E^{-28}$	$1.19E^{-11}$	0	1	55%
0	35	0	$2.2E^{-27}$	$2.52E^{-11}$	0	1	64%
0	40	0	$1.6E^{-27}$	$2.91E^{-11}$	0	1	78%
0	45	1	$4.98E^{-27}$	$1.68E^{-10}$	0	0	48%
0	50	1	$1.25E^{-27}$	$1.02E^{-10}$	0	0	40%
0.2	65	1	0.169	108	0	0	55%
0.1	**68**	**1**	**0.0746**	**178**	**0**	**0**	**89.7%**
0.01	68	1	0.0035	6.24	0	0	35%
0.3	68	1	0.266	82.2	0	0	67%
0.2	68	1	0.0746	178	0	0	89%

Table IV gives the classification results for different types of disturbance for RBNN. The accuracy of classification is 79.41% for balanced sag and swell, 100% for unbalanced sag and swell as seen in Fig 19. Further prediction accuracy was 94.4% for trained data, 88% of test data and overall accuracy being 89.7% as seen in Fig 20. From Fig 21, it is found that the overall performance of RBNN is 89.7%, and FFNN is 98.53%.

TABLE IV
CLASSIFICATION RESULT FOR DIFFERENT TYPES OF DISTURBANCE USING RBNN

Sl. No.	TYPE OF DISTURBANCE	TRAINED DATA	TEST DATA	TOTAL	ACCURACY
1	Balanced sag	8/9	19/25	27/34	79.41%
2	Balanced swell	8/9	19/25	27/34	79.41%
3	Unbalanced sag	9/9	25/25	34/34	100%
4	Unbalanced swell	9/9	25/25	34/34	100%
Grand total		34/36	88/100	122/136	89.7%
Percentage column wise		94.4%	88%	89.7%	--

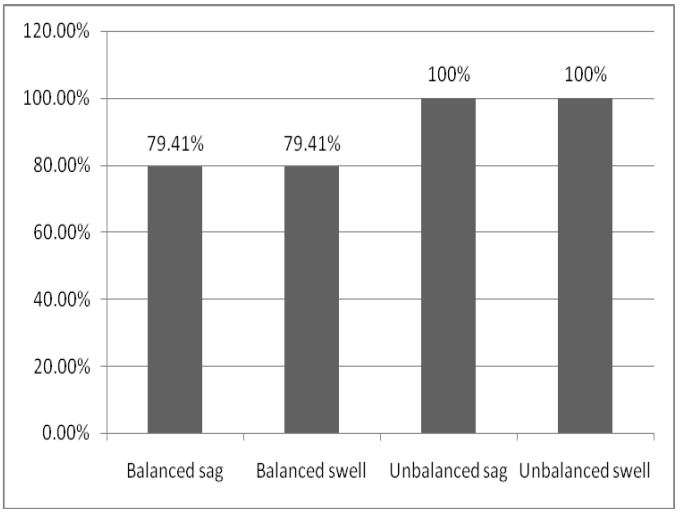

Fig. 19. Classification accuracy for different type of disturbance

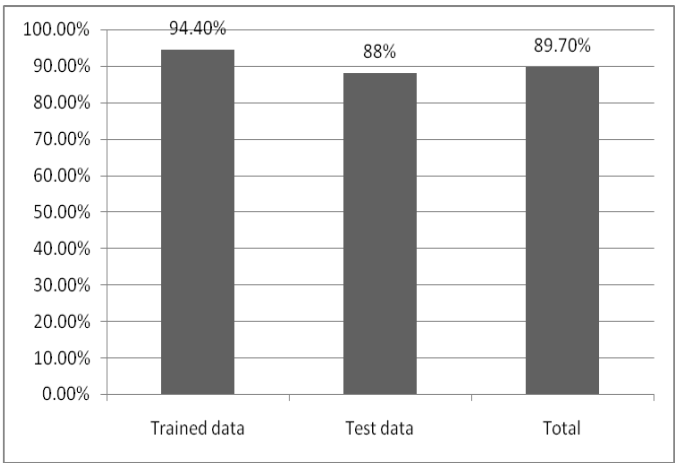

Fig. 20. Classification accuracy for trained data, testing data, and total data for RBNN.

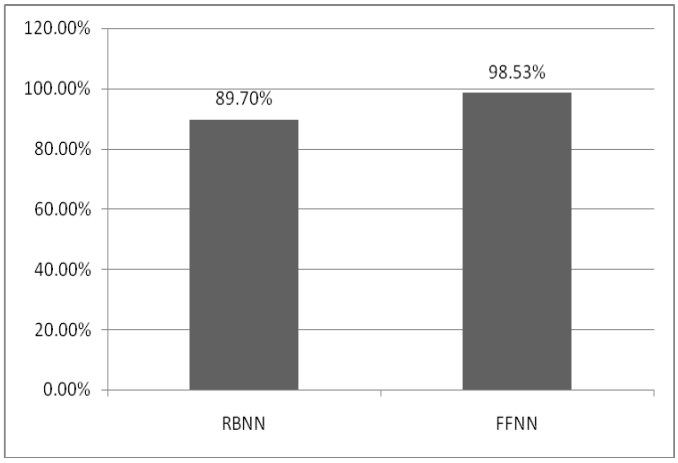

Fig. 21. Classification accuracy of RBNN and FFNN

VI. CONCLUSION

This paper presents a resourceful new technique for the automatic classification of PQ disturbance in the supply to the induction motor. Supply voltage was varied from 10% to 90% for sag, swell, unbalanced sag and unbalanced swell. The wavelet coefficients bear sufficient information regarding the type and percentage of variation in the supply voltage compared to the balanced supply. These wavelet coefficients are fed as input to both RBNN and FFNN and the results are presented in this paper. The FFNN is not only able to detect the PQ disturbances but is also able to determine the percentage of the disturbance more accurately than RBNN. The overall performance evaluation of FFNN is found to be good compared to RBNN.

REFERENCES

[1] A. Domijan, G. T. Heydt, A. P. S Meliopoulos, S. S. Venakata and S. west, "Directions of research on power quality", IEEE Transaction on power delivery, 8(1) (1993), pp. 429- 436.

[2] J. Douglas, "Solving power quality problems", EPRI Journal, 18(8) (1993), pp. 6-15.

[3] W. R. A. Ibrahim and M. M. Morcos, "Aritificial intelligence and advanced mathematical tools for power quality applications: A survey", IEEE Trans. power delivery, 17(2) (2002), pp. 668- 673.

[4] J. Huang, M. Negnevitsky and D.T. Nguyen, "A neural- fuzzy classifier for recognition of power quality disturbances", IEEE Trans. power delivery, 17(4) (2002), pp. 609- 616.

[5] Mamun Bin Ibne Reaz, Florence Choong, Mohd Shahiman Sulaiman, Faisal Mohd. Yasin and Masaru Kamada, "Expert system for power quality disturbance classifier", IEEE Trans. on power delivery, 22(3)(2007), pp. 1979- 1988.

[6] Rajiv Kapoor & Rashmi Gupta, "Statistically matched wavelet-based method for detection of power quality events," International Journal of Electronics, 98(1) (2011), pp. 109-127.

[7] Valdomiro VEGA, cesar DUARTE and Gabriel ORDONEZ, "Automatic power quality disturbances detection and classification based on discrete wavelet transform and support vector machine", 19th international conference on electricity distribution (CIRED), Vienna, 21-24 May 2007, paper ID 0827.

[8] Ali Asheibi, David Stirling, Sarath Perera and Duane Robinson, "Power quality data analysis using unsupervised data mining", Australasian universities power engineering conference (AUPEC 2004), 26-29 September 2004, Brisbane, Australia.

[9] Whei-Min Lin, Chien-Hsien Wu, Chia-Hung Lin, and Fu-Sheng Cheng," Detection and Classification of Multiple Power-Quality Disturbances with Wavelet Multiclass SVM", IEEE Transactions on power delivery, 23(4)(2008), pp. 2575- 2582.

[10] Murat Uyar, Selcuk Yildiri, Muhsin Tunay Gencoglu, "An expert system based on S-transform and neural network for automatic classification of power quality disturbances", Expert Systems with Applications, 36 (2009), pp. 5962–5975.

[11] Abdel-Galil T.K., Kamel M., Youssef A.M., El-Saadany E.F., and Salama M.M.A.,"Power quality disturbance classification using the inductive inference approach", IEEE Trans. on Power Delivery, 19 (2004), pp. 1812 – 1818.

[12] Harapajan Singh, Manjeevan Seera, and Ahmad Puad Ismail, "Condition monitoring of electrical supply voltage quality to electrical machines using RBF neural network," 2010 IEEE International conference on power and energy (PECon 2010), Nov 29th – Dec 1st , Kuala Lumpur, Malaysia, pp. 312- 317.

[13] Bizjak Boris. and Planinsic Peter., "Classification of power disturbances using fuzzy logic", Proc. of IEEE Power Electronics and Motion Control Conference, EPE-PEMC 2006, Portoroz, Slovenia.

[14] B. Biswal, M. Biswal, S. Mishra and R. Jalaja, "Automatic classification of power quality events using balanced neural tree," IEEE Trans. on industrial electronics, 61(1) (2014), pp. 521- 530.

[15] Bollen M.H.J., Gu I.Y.H., Axelberg P.G.V. and Styvaktakis E., "Classification of underlying causes of power quality disturbances: deterministic versus statistical methods", EURASIP Journal on Advances in Signal Processing, 2007, pp.1-17.

[16] Chah keow, P. Nallagownden, K.S. Rama Rao, "Denoising scheme for enhancing power quality problem classification based on wavelet transform and a rule based method", International conference on electrical, control and computer engineering, Malaysia, June 21st - 22nd 2011.

[17] M. Riera-Guasp, Jose A. Antonino-Daviu, M. Pineda- Sanchez, R. Puche- Panadero and J. Perez- Cruz, "A general approach for the transient detection of slip-dependent fault componenets based on the discrete wavelet transform," *IEEE transactions on Industrial electronics*, 55(12) (2008), pp. 4167-4180.

BIOGRAPHIES

Sridhar. S received his B.E. degree in Electrical and Electronics Engineering from Bangalore University in 2003 and M.Tech from Visvesvaraya Technological University in 2006. Currently, he is working as assistant professor in the Department of Electrical and Electronics Engineering at RNS Institute of Technology, Bengaluru, India. His research area includes power quality, digital signal processing and intelligent monitoring of electrical machines.

Dr. K. Uma Rao is a professor in the Department of Electrical Engineering, at RV College of Engineering, Bengaluru, India. She completed her Ph.D. from Indian Institute of Science (IISc), Bengaluru. She has over 28 years of teaching and research experience. She has authored 11 technical books in different areas of electrical engineering. She has over 150 technical publications. Her research areas include Power system dynamics, Power Quality, FACTS and Custom power devices.

Sukrutha Jade, completed B.E in Electrical and Electronics Engineering from RNS Institute of Technology, Visvesvaraya Technological University. Currently, she is working as an Associate Software Engineer in Robert Bosch Engineering and Business Solutions (RBEI). Her research areas include Automation, Machine learning, and embedded systems.

An alternative image quality assessment method for blurred images

H. Boztoprak

Abstract: This study proposes a no-reference image quality assessment method for blurred images. In this approach, first, a discrete wavelet transform was applied to the sample images and then the results were decomposed into four subbands. This was followed by the calculation of the spatial frequencies of high-high (HH_2) and low-low (LL_2) subbands. Then the ratio of spatial frequencies of HH_2 and LL_2 subbands was calculated. Information about the image quality was obtained by using this ratio, with lower values indicative of better image quality. The study aims to investigate whether the proposed method is capable of measuring the image quality. The proposed technique was tested on the standard images. Three different images were used, of which each one was distorted with the same type and amount of noise. Motion noise, blurring and sharpening was applied to distort the images. The performance of the proposed method was evaluated and compared with eight representative image quality measures. This provides a meaningful comparison across different types of image distortions. Then, the cameraman image was also blurred with two different noises: Gaussian and disk-shaped blur. The varying amount of blur was compared with Universal Image Quality Index (UIQI) values of the cameraman image. The method gives good results in different resolutions as well. Its computation is easy, independent of viewing conditions.

Index Terms— **Blurring, Image Quality, Spatial Frequency, Wavelet Transform**

1. INTRODUCTION

IMAGE quality is a characteristic of an image that measures the detected image corruption. The quality assessment is an important part of image processing and vision algorithms. For measure amount of degradation in compressed image, filtering and quality enhancement systems are often used. Image compression reduces the quality of the image and some measure to quantify this image degradation is required.

Image quality assessment can be done subjectively or objectively. Objective image visual quality analysis can be into no-reference (NR), reduced-reference (RF) and full-reference (FR) based on the availability of the reference image. In FR metrics, the quality of a test image is measured by comparing it with a reference image. RR methods have partial information from the reference image. However, NR methods try to estimate the quality of an image without any reference. The aim of objective quality assessment research is to provide quality metrics that can predict video and image quality automatically [1].

H. Boztoprak, is with Department Computer Program, Alaaddin Keykubat University, Akseki Vocational School, Antalya, Turkey, (e-mail: halimeboz@yahoo.com).

Subjective methods are impractical for real time implementation, because there are costly and time consuming [2]. In human vision system (HSV) based metrics, difference between the test and the reference images is standardized according to its visibility, as determined by psychophysics of human perception.

There are many objective image quality measure methods in the literature. The MSE (Mean Squared Error) and the PSNR (Peak Signal-to-Noise Ratio) are the two most common objective assessment methods [3]. The MSE, SNR and PSNR are computed quickly. However, these assessment methods are not always the best choice, especially if a comparison will be performed against the human perception of the image quality [4]. A mathematically defined universal image quality index is proposed [5]. This approach does not depend on the images being tested, the individual observers or the viewing conditions. It must be convenient to different image processing applications and supply significant comparison across various types of image distortions. UIQI and SSIM are more correct and consistent than PSNR and MSE despite they cost more [6]. De-noising performances are quantitatively measured by the PSNR, MSE, RMSE, IEF (Measure of Enhancement Factor) [7-9].

Blurring is one of the most common distortions encountered in image processing applications. It can be caused by lot of reasons like camera shake, defocus, motion etc. Extreme blur in an image creates problem for user to classify and identify objects in an image. Numerous design strategies have been utilized by different researchers in developing image quality assessment techniques for blurred images [10]. Calculation of edge-width [11], histogram based assessment [12, 13], power spectrum based assessment [14], wavelet based techniques [15, 16], and neural network-based methods [4] are among these approaches. A no reference blur image quality metric was introduced in [17]. This approach was based on wavelet transform. It was examined edges through a multiresolution decomposition. In [18] study, the input image is decomposed via a three-level separable discrete wavelet transforms (DWT). The log-energies of the DWT subbands are estimated. A scalar index is calculated using a weighted average of these log-energies.

This study proposes a no-reference image quality assessment method for blurred images. The approach is independent from the images being tested, the individual observers or the viewing conditions. We present a simple and effective method. Its computation is easy, independent of viewing conditions. This supplies a meaning comparison across various types of image distortions. The achievement of the proposed method was estimated and compared with the other representative quality assessment.

2. MATERIAL AND METHODS

2.1. Image Quality Measures

In the objective approach, the image quality is assessed by using a mathematical formula that attempts to quantify the amount of image distortion.

2.1.1. The signal to noise ratio (SNR) and Peak Signal to Noise Ratio

SNR and PSNR are a mathematical measure of image quality based on the pixel differences between two images [19, 20]. The SNR measure is a calculation of the quality of a reconstructed image compared with the original image. The whole idea is to obtain a single number that reflects the quality of the image by computing the ratio of the signal power to the noise power. The PSNR is the rate between the maximum possible power of a signal and the power of corrupting noise. The PSNR is expressed in logarithmic level. The mathematical term for it is:

$$\text{PSNR}=20\log_{10}\left(\frac{\text{MAX}_f}{\sqrt{\text{MSE}}}\right) \quad (1)$$

MAX_f: The maximum signal value that exists in the original image

2.1.2. Mean Squared Error (MSE)

MSE is a measure of control and quality. The MSE is defined as follows

$$\text{MSE}=\frac{1}{\text{M*N}}\sum_a\sum_b [A(a,b)-W(a,b)]^2 \quad (2)$$

where A(a, b) is the original image and W(a, b) is the distorted image that contain M x N pixels.

2.1.3. Universal Image Quality Index (UIQI)

The UIQI is a mathematically defined measurement, that is easy to compute and independent of viewing conditions. In 2002, Wang and Bovik proposed this measure [5], it breaks the comparison between distorted and original image into three comparisons: contrast, structural, luminance and comparisons as in (3), (4), and (5). The dynamic range for the quality index is [-1; 1], where 1 represents a perfect image quality.

$$\text{l}(x,y)=\frac{2\mu_x\mu_y}{\mu_x^2+\mu_y^2} \quad (3)$$

$$\text{c}(x,y)=\frac{2\sigma_x\sigma_y}{\sigma_x^2+\sigma_y^2} \quad (4)$$

$$\text{s}(x,y)=\frac{2\sigma_{xy}}{\sigma_x+\sigma_y} \quad (5)$$

where $\mu_x\mu_y$ represents the mean values of distorted and original images. And $\sigma_y\sigma_x$ represents the standard deviation of distorted and original images, and σ_{xy} is the covariance of both images. The UIQI is given in (6).

$$\text{UIQI}(x,y)=\text{I}(x,y).\text{c}(x,y).\text{s}(x,y)=\frac{4\mu_x\mu_y\mu_{xy}}{(\mu_x^2+\mu_y^2)(\sigma_x^2+\sigma_y^2)} \quad (6)$$

2.1.4. Root Mean Squared Error (RMSE)

MSE is a tool to quantify the difference between a copy and the true value of the amount being calculated. In statistic it is defined as a risk function [4]. Mathematically it is expressed as:

$$\text{RMSE}=\sqrt{\frac{1}{\text{XY}}\sum_{x=0}^{\text{X}}\sum_{y=1}^{\text{Y}}[\text{I}(x,y)-\text{I}_c(x,y)]^2} \quad (7)$$

where I (x, y) is the original image and $\text{I}_c(x,y)$ is the distorted image. X and Y are the sizes of the image.

2.1.5. Structural Similarity (SSIM)

The distorted and original images are divided into blocks of size 8 x 8 and then the blocks are converted into vectors. Then, two standard derivations, two means and one covariance value are computed as in (8), (9), and (10) [5].

$$\mu_x=\frac{1}{T}\sum_{i=1}^{T}x_i \quad \mu_y=\frac{1}{T}\sum_{i=1}^{T}y_i \quad (8)$$

$$\sigma_x^2=\frac{1}{T-1}\sum_{i=1}^{T}(x_i-\bar{x})^2 \quad \sigma_y^2=\frac{1}{T-1}\sum_{i=1}^{T}(y_i-\bar{y})^2 \quad (9)$$

$$\sigma_{xy}^2=\frac{1}{T-1}\sum_{i=1}^{T}(x_i-\bar{x})\,(y_i-\bar{y}) \quad (10)$$

Structural similarity index measure between images x and y is given by (11).

$$\text{SSIM}(x,y)=\frac{(2\mu_x\mu_y+c_1)(2\sigma_{xy}+c_2)}{(\mu_x^2+\mu_y^2+c_1)(\sigma_x^2+\sigma_y^2+c_2)} \quad (11)$$

where c_1 and c_2 are constants.

Like in UIQI, SSIM is applied locally using sliding window of size B x B that moves pixel by pixel horizontally and vertically covering all the rows and columns of the image, starting from top left corner of the image [6].

2.1.6. The measure of enhancement (EME) and measure of enhancement factor (EMF)

EME and EMF are defined in equation (4) and (5) respectively. EME (measure of enhancement) has been developed by Agaian *et. al*. [21].

$$\mathrm{EME(e)} = \frac{1}{k_1 k_2} \sum_{m=1}^{k_1} \sum_{l=1}^{k_2} 20 \ln \left(\frac{I_{max}^{l,m}}{I_{min}^{l,m}} \right) \qquad (12)$$

where, the image is divided into k_1k_2 blocks, α is a constant, $I_{max}^{l,m}$ and $I_{min}^{l,m}$ are the maximum and minimum values of the pixels in each block of the enhanced image. EMF between input image and output image is described as:

$$\mathrm{EMF} = \frac{\mathrm{EME}_{output}}{\mathrm{EME}_{input}} \qquad (13)$$

2.1.7. Mean absolute error (MAE)

MAE is described as below [22];

$$MAE(r,e) = \frac{1}{MN} \sum_{i=0}^{M-1} \sum_{j=0}^{N-1} [n(i,j)] \qquad (14)$$

2.2. Proposed Method

In this study, first, a discrete wavelet transform (DWT) was applied to the sample images. Multi-resolution filter banks and particular wavelet filters are used in this transform for the analysis and reconstruction of signals. The different output signals of the decomposition filter bank are called as sub-bands. A filter bank consists of filters that separate a signal from the frequency bands [23]. Two-level 2D transform operations were computed by using filter banks. The high-high (HH_1), high-low (HL_1), low-high (LH_1), and low-low (LL_1) subbands are one level decomposition of 2D-DWT. After finishing the first level decomposition, second level decomposition was performed [24].

And, as a result of this transform, it was decomposed into four sub-bands: HH_2, HL_2, LH_2 and LL_2. This was followed by the calculation of the spatial frequencies of HH_2 and LL_2 sub-bands using equation (5)-(7). For an M × N sized image, the spatial frequency is calculated as follows: where, RF is the row frequency, and CF is the column frequency. Spatial frequency indicates the overall information level in an image and measures the variation of pixels [25]. It is usually used with wavelet transform in image fusion studies [26, 27]. In [28], wavelet transform and spatial frequency was used to calculate iterative value of cellular neural network. The spatial frequency needs to be decreased if the images are blurred more. And, a higher value of spatial frequency indicates higher quality and contrast of the image.

$$SF = \sqrt{(CF)^2 + (RF)^2} \qquad (15)$$

$$CF = \sqrt{\frac{1}{MN} \sum_{n=1}^{N} \sum_{m=2}^{M} [F(m;n) - F(m-1,n)]^2} \qquad (16)$$

$$RF = \sqrt{\frac{1}{MN} \sum_{m=1}^{M} \sum_{n=2}^{N} [F(m;n) - F(m,n-1)]^2} \qquad (17)$$

Then the ratio of spatial frequencies of HH_2 and LL_2 subbands was calculated. Information about the image quality was obtained by using this ratio. And, the value was compared with known image sharpness/blur measures.

3. EXPERIMENTAL RESULTS

The test images used for our analysis shown were in Fig. 1 (a) Cameraman, (b) Lena and (c) Peppers. Three different images were used, of which each one was distorted with the same type and amount of noise. Motion noise, blurring and sharpening was applied to distort the images. Fig. 2 shows (a) original cameraman image, (b) motion noise, (c) blurring and (d) sharpening image.

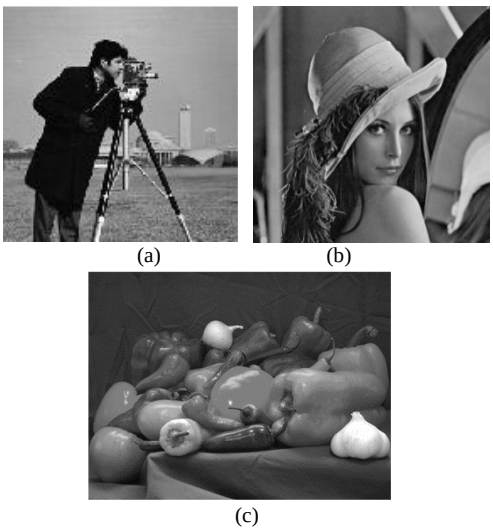

Fig. 1. Examples of test images used for our analysis (a) Cameraman, (b) Lena and (c) Peppers

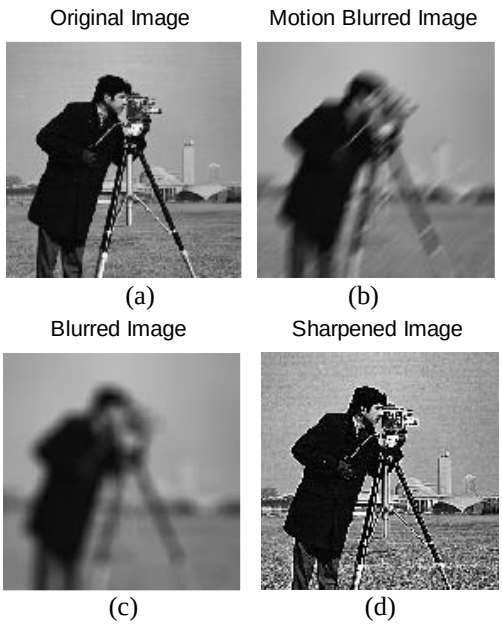

Fig. 2. (a) Original cameraman image, 256x256, 8 bits/pixel, (b) motion, (c) blurring and (d) sharpened image

First image used was the 8 bit 256x256 grayscale cameraman image. After applying some distortion to the original images, the image quality assessments were performed on these distorted images and the results were compared.

The image quality assessment for the cameraman image is shown in the results in Table 1. Table 1 shows the UIQI, PSNR, MSE, RMSE, EME, EMF, MAE, SNR and SIMM values, calculated between original and distorted images, respectively. Proposed methodology utilizes a no-reference image approach.

TABLE 1.
COMPARISON OF CAMERAMAN IMAGE QUALITY MEASURES

Cameraman	motion	blurred	sharpened
Proposed	3.5203	14.1384	1.1646
UIQI	0.2100	0.1097	0.5678
PSNR	19.8642	18.9878	19.5906
MSE	676.1797	827.3670	720.1431
RMSE	26.0035	28.7640	26.8355
EMF	0.42	0.28	0.58
MAE	14.0620	16.344	15.4276
SNR	-4.5376	-5.413	-4.8111
SIMM	0.6069	0.5508	0.6987

The proposed algorithm was also tested on the Lena image. Lena image was an 8 bit 256x256 grayscale image. Assessment values are shown in Table 2.

TABLE 2.
COMPARISON OF LENA IMAGE QUALITY MEASURES

Lena(256x256)	motion	blurred	sharpened
Proposed	3.8160	15.3463	1.2064
UIQI	0.4214	0.2290	0.6718
PSNR	21.1862	19.6975	20.7449
MSE	498.7276	702.6348	552.0695
RMSE	22.3322	26.5073	23.4962
EMF	0.44	0.28	0.53
MAE	14.1988	18.1324	14.2617
SNR	-2.9832	-4.4718	-3.4245
SIMM	0.6034	0.4889	0.7026

Some processing was applied to the Peppers Image. The Peppers image was 8 bit and 1200x1200 grayscale image. Assessment values are shown in Table 3.

TABLE 3.
COMPARISON OF PEPPERS IMAGE QUALITY MEASURES

Peppers (1200x1200)	motion	blurred	Sharpened
Proposed	10.3359	17.2360	3.0954
UIQI	0.4176	0.3801	0.6593
PSNR	33.6666	34.0125	41.5911
MSE	28.1720	26.0151	4.5433
RMSE	5.3077	5.1005	2.1315
EMF	0.44	0.32	0.62
MAE	1.8506	1.8128	1.2749
SNR	5.3962	5.7421	13.3207
SIMM	0.9679	0.9712	0.9988

For good metric, the values of PSNR, SNR, UQI, EMF and SSIM should be high. Also, the values of MSE, RMSE, and MAE should be low. RMS is obtained by the square root of the MSE. The small is preferred. The MSE, SNR and PSNR are fast to compute, and hence widely used. However, this measures are not always the best choice, especially if a comparison against human perception of the image quality is done. Although there is a clear visual difference between these images, the difference is not very good reflected in the quality score given by the PSNR and the MSE. The SSIM and UIQI are visually more consistent with the image quality scores, according to the results presented in the Tables. The dynamic range for UIQI is [-1; 1], where 1 represents a perfect image quality.

The clarity of image is expected to decrease when a motion or blur distortion is applied. And, the clarity of image is expected to increase when a sharpening is applied. Accordingly, the SIMM and UIQI parameters provide the scores in each of the Tables. The proposed method may give information about the clarity, inversely proportional to these two parameters. Proposed value decreases with increasing clarity. A lower proposed value indicates a better quality image. So, it can give information about the image. The higher this value is so much noise.

The cameraman image was also blurred with two different noises: Gaussian and disk-shaped blur. First, the cameraman image was blurred with Gaussian blur at different values of sigma = 0.5, 1.0, 2.0, 2.5. Then, the image was further blurred with disk-blur with se = 5, 10, 12, 15. The blurred images and respective proposed values changed depending on the noise levels are shown in Fig.3 (a). Fig.3 (a) indicates the relationship between the proposed image quality assessment and the amount of blurring applied to the cameraman image for different values of sigma.

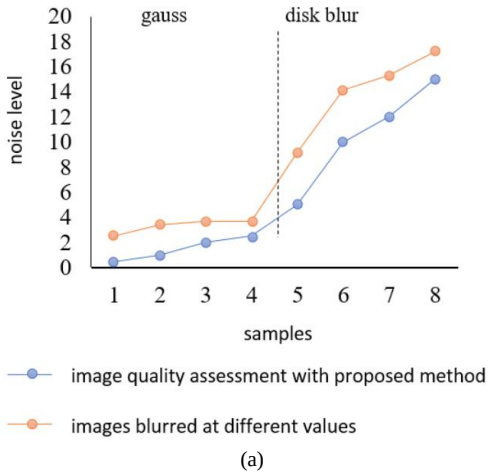

(a)

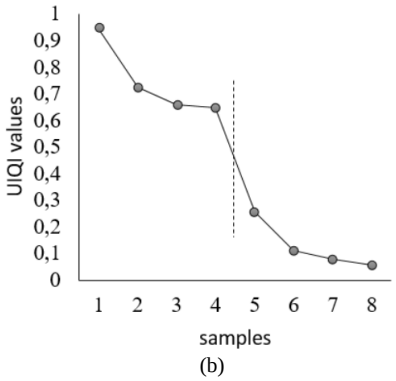

(b)

Fig. 3. (a) Shown that changed proposed value with noise, b) shown that changed UIQI value with noise.

The value of proposed value increases as the quality of image decreases in all cases. This trend is also seen in the images blurred with different disk-shape blur values. The proposed values increase with increasing noise. Fig. 3 (b) shows UIQI values of the cameraman image with varying amount of blur. An important observation is that the proposed value increases with the amount of blur in an image.

4. CONCLUSIONS

It is hard to get the same quality score even if the same level of distortion is applied to different images. Most of the image quality metrics are based on the difference between the distorted and the original image. In this study, we have discussed an objective quality assessment approach that requires no reference image. This method was tested on three different grayscale images. Test images were generated from the original images by distorting with noise. The proposed values obtained without reference images were compared with other image quality assessment parameters. It has a low computational complexity, that is, it is fast and easy to implement. This assessment method gives good results in variable quality of input images as well. And also, it is capable of giving information about the blurred images. The method has been shown to provide information about the quality of the image in a simple way without reference image. The method enables us to measure the noise level. Further studies, using this information about the quality of the image, image enhancement / repair operations can be done.

REFERENCES

[1] Z. Wang, A. C. Bovik, & L. Lu, "Why is image quality assessment so difficult?" Acoustics, Speech, and Signal Processing (ICASSP), 2002 IEEE International Conference on. Vol. 4. IEEE, 2002.

[2] A. Zaric, et al. "Image quality assessment-comparison of objective assessment with results of subjective test", pp 113-118, Sep. 2010.

[3] M. Jiang, Digital Image Processing. Department of Information Science, School of Mathematics, Peking University, 2003.

[4] A. Havstad, Image quality assessment using artificial neural networks. MSc, Engineering and Mathematics, Edith Cowan University, 2004.

[5] Z. Wang & A.C. Bovik, "A universal image quality index." Signal Processing Letters, IEEE 9.3 (2002): 81-84.

[6] Al-Najjar, Yusra AY. Dr. Der Chen Soong, "Comparison of Image Quality Assessment: PSNR, HVS, SSIM, UIQI"." International Journal of Scientific & Engineering Research 3.8 (2012): 1.

[7] N. Ramanaiah & S. Kumar, (2013). Removal of hıgh density salt and pepper noise in images and videos using denoising methods.

[8]R. Arumugham, K. Vellingiri, W. F. Habeebrakuman, & K. Mohan, (2012). A New Denoising Approach for the Removal of Impulse Noise from Color Images and Video Sequences. Image Analysis & Stereology, 31(3), 185-191.

[9] Om, H., & Biswas, M. (2015). A generalized image denoising method using neighbouring wavelet coefficients. Signal, Image and Video Processing, 9(1), 191-200.

[10] De, Kanjar, and V. Masilamani. "Image Sharpness Measure for Blurred Images in Frequency Domain." Procedia Engineering 64 (2013): 149-158.

[11] Ong EePing, et al. "A no-reference quality metric for measuring image blur." Signal Processing and Its Applications, 2003. Proceedings. Seventh International Symposium on. Vol. 1. Ieee, 2003.

[12] N.K. Chern, N.P.A. Neow, M.H. Ang Jr, "Blur determination in the compressed domain using DCT information", In Proc. IEEE Int. Conf. Robotics and Automation, 3, pp. 2791-96, 2001.

[13] Y. Yildiray. "A histogram based image quality index." Przegl Ą Elektrotechniczny Electr. Rev. NR 7a 88 (2012): 126-129.

[14] Nill, Norman B., and Brian Bouzas. "Objective image quality measure derived from digital image power spectra." Optical engineering 31.4 (1992): 813-825.

[15] Ferzli, Rony, and Lina J. Karam. "No-reference objective wavelet based noise immune image sharpness metric." Image Processing, 2005. ICIP 2005. IEEE International Conference on. Vol. 1. IEEE, 2005.

[16] Dumic, Emil, Sonja Grgic, and Mislav Grgic. "New image-quality measure based on wavelets." Journal of Electronic Imaging 19.1 (2010): 011018-011018.

[17] Kerouh, F., A. Serir. "A No Reference Quality Metric for Measuring Image Blur In Wavelet Domain." International journal of Digital Information and Wireless Communication 1.4 (2012): 767-776.

[18] Vu, Phong V., and Damon M. Chandler. "A fast wavelet-based algorithm for global and local image sharpness estimation." Signal Processing Letters, IEEE19.7 (2012): 423-426.

[19] Avcybab, Y., Image quality statistics and their use in stange analysis and compression, Ph.D, Bogazici University, İstanbul, Turkey, 2001.

[20] Rafael, C., Gonzalez Woods and Richard, E., Digital Image Processing, Addison-Wesley Publishing Company, 1992.

[21] Lal, Shyam, and Rahul Kumar. "Enhancement of Hyperspectral Real World Images Using Hybrid Domain Approach." International Journal of Image, Graphics and Signal Processing (IJIGSP) 5.5 (2013): 29.

[22] Planitz, B., and A. Maeder. "Medical image watermarking: A study on image degradation." Proc. Australian Pattern Recognition Society Workshop on Digital Image Computing, WDIC. 2005.

[23] R.J.E. Merry, Steinbuch M., van de Molengraft M.J.G., Wavelet theory and applications literature study, Eindhoven University of Technology, Department of Mechanical Engineering, Control Systems Technology Group, 2005.

[24] Dia, Dhaha, et al. "Multi-level discrete wavelet transform architecture design." Proceedings of the world congress on engineering. Vol. 1. 2009.

[25] A. Eskicioglu, M., and Paul S. Fisher. "Image quality measures and their performance." Communications, IEEE Transactions on 43.12 (1995): 2959-2965.

[26] Maddali R., Prasad K.S., Bindu C.H., Discrete wavelet transform based medical image fusion using spatial frequency technique, Int J of Sys Alg & App (IJSAA) 2012; 2: 2277-2677.

[27] Jain, Atika, P. M. Kanjalkar, and J. V. Kulkarni. "Estimation of image focus measure and restoration by Wavelet." Intelligent Networks and Intelligent Systems (ICINIS), 2011 4th International Conference on. IEEE, 2011.

[28] H. Boztoprak, Y. Özbay, A new method for segmentation of microscopic images on activated sludge. Turk J Elec Eng & Comp Sci, 23.Sup. 1 (2015): 2253-2266.

BIOGRAPHY

Halime BOZTOPRAK was born in Konya, Turkey in 1982. She received B.Sc. degree in 2004 and the M.Sc. degree in 2007 from the University of Süleyman Demirel, Isparta, and the Ph.D. degree in 2014 from the University of Selçuk, Konya, Turkey. Her current research interests are digital image processing, artificial neural networks, cellular neural network.

BAJECE
Balkan Journal of Electrical & Computer Engineering
An International Peer Reviewed, Indexed and Open Access Journal

ISSN: 2147- 284X
Vol: 4
No:1
Year: March 2016

CONTENTS

K.Lenin, B.RavindhranathReddy, and M.Suryakalavathi; Reduction of Real Power Loss by Nature Inspired Algorithm, ……..…….. **1-4**

A. Ates, and C. Yeroglu; Online Tuning of Two Degrees of Freedom Fractional Order Control Loops, …….....……..... **5-11**

T. Pala and A.Y. Camurcu; Design of Decision Support System in the Metastatic Colorectal Cancer Data Set and Its Application, …… **12-16**

A. Darwish, I. Morsi, and A. El Zawawi; Complete Combustion Control for a Steam Boiler Plant, ……...…….. **17-23**

S. Roy and Dr. P.S. Babu; An Advanced Fault Locating Technique with WAMS based Backup Protection Scheme for Power System with Simultaneous Faults, ……. **24-36**

Sridhar. S, K. Uma Rao and Sukrutha Jade; Detection and Classification of Power Quality Disturbances in the Supply to Induction Motor Using Wavelet Transform and Neural Networks, ……...…….. **37-45**

H. Boztoprak; An alternative image quality assessment method for blurred images, **46-50**

BALKAN JOURNAL OF
ELECTRICAL & COMPUTER ENGINEERING
(An International Peer Reviewed, Indexed and Open Access Journal**)**

Contact
Istanbul Technical University
Department of Electrical Engineering,
Ayazaga Campus, Maslak, Istanbul-Turkey

Web: https://www.bajece.com
http://dergipark.ulakbim.gov.tr/bajece/
e-mail: editor@bajece.com
bajece.editor@gmail.com